

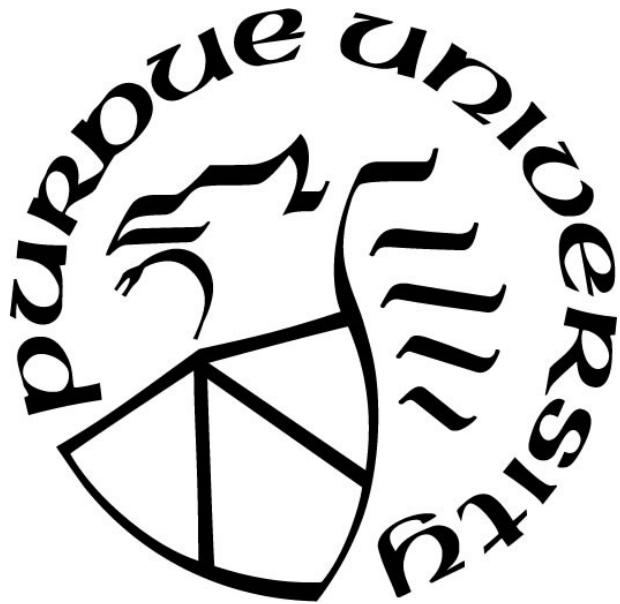
**MODELING AND MEASUREMENT OF DUST DISPERSION PATTERNS
IN CONFINED SPACES**

by
Yumeng Zhao

A Dissertation

*Submitted to the Faculty of Purdue University
In Partial Fulfillment of the Requirements for the degree of*

Doctor of Philosophy



School of Agricultural and Biological Engineering

West Lafayette, Indiana

August 2020

**THE PURDUE UNIVERSITY GRADUATE SCHOOL
STATEMENT OF COMMITTEE APPROVAL**

Dr. R.P. Kingsly Ambrose, Chair

School of Agricultural and Biological Engineering

Dr. Richard L. Stroshine

School of Agricultural and Biological Engineering

Dr. Albert J. Heber

School of Agricultural and Biological Engineering

Dr. Carl R Wassgren

School of Mechanical Engineering

Approved by:

Dr. Nathan S. Mosier

To My Parents

ACKNOWLEDGMENTS

First of all, I express my deep sense of gratitude to Dr. Kingsly Ambrose for offering me the opportunities for graduate research. During my research, he offered me valuable guidance, encouraging me throughout the program, and helping me with all the paperwork. I appreciate the great opportunities that he provided me to mentor undergraduate students.

Sincere thanks to Dr. Richard Stroshine, Dr. Albert Heber, and Dr. Carl Wassgren for serving on my Committee. I am grateful to Dr. Stroshine for his help and advice for conducting my experiments. The discussion with Dr. Heber broadened my understanding of dust dispersion and suspension and the suggestions from Dr. Wassgren helped me to understand the focus of scientific research.

I acknowledge Dr. Dhananjay Pai for arranging the space for my experiments in the lab and Dr. Jae Hong Park for guiding me in understanding aerosol technology.

I would like to show my gratitude to my past and current research group members: Karthik Salish, Abhay Patwa, Achint Sanghi, Benjamin Plumier, Camila Jange, Mavis Owureku-Asare, Zhengpu Chen, Pranav Vashisht and Qi Bian for their support. My special thanks to Camila, Karthik, and Zhengpu, for their help.

I greatly appreciate the help of ABE Department staff, Scott Brand for the chamber built-up, and Stanley Harlow for Computing support, and Administrative, Clerical, and Business office staff and Flexlab building manager for their official and personal help during my program of study.

Special thanks to my friends, Bi Yaping, Zhou Huiwen, Jia Jingnan, Tank and Ruohan for encouraging me during my Ph.D. I'm also deeply indebted thanks to Dr. Ke Bian for his support.

I acknowledge the Purdue Process Safety and Assurance Center for funding my study.

In the end, I would like to thank my parents for being there for me without a doubt. I love you.

STABLE OF CONTENTS

TABLE OF CONTENTS.....	5
LIST OF TABLES.....	8
LIST OF FIGURES	9
LIST OF SYMBOLS	11
ABSTRACT.....	13
1. INTRODUCTION.....	15
1.1 Problem Statement: Dust Hazards	15
1.2 Research Hypotheses and Goals.....	17
1.2.1 Research objectives	18
1.2.2 Dissertation outline.....	18
1.3 References.....	19
2. LITERATURE REVIEW: DUST DISPERSION AND EXPLOSION.....	21
2.1 Dust Hazards.....	21
2.1.1 Primary and secondary explosions	22
2.1.2 Dust explosion factors	23
2.1.3 Determining dust explosibility	28
2.1.4 OSHA regulations and NFPA standards.....	29
2.2 Dust Dispersion Mechanism.....	31
2.2.1 Particle-fluid interaction	31
2.2.2 Particle-particle interaction.....	33
2.2.3 Modeling particle dispersion process	34
2.3 Optical Properties of Dust.....	38
2.3.1 Particle scattering theory	38
2.3.2 Light extinction coefficient.....	40
2.4 References.....	41
3. MODELING DUST DISPERSION AND SUSPENSION PATTERN UNDER TURBULENCE.....	49
Abstract.....	49
3.1 Introduction.....	50

3.2	Materials and Methods.....	52
3.2.1	CFD-DPM model development.....	52
3.2.2	Experimental validation.....	58
3.2.3	Data analysis.....	60
3.3	Results and Discussion	60
3.3.1	Simulated dust concentration.....	60
3.3.2	Dust cloud spread and distribution pattern	64
3.3.3	Dust particle transport.....	67
3.4	Conclusions.....	69
3.5	References.....	70
4.	SIMULATION OF CONTINUOUS DUST DISPERSION.....	74
	Abstract.....	74
4.1	Introduction.....	74
4.2	Materials and Methods.....	76
4.2.1	CFD-DPM model development.....	76
4.2.2	Experiment validation.....	80
4.2.3	Statistical analysis.....	81
4.3	Results and Discussion	81
4.4	Conclusions.....	88
4.5	References.....	89
5.	EFFECT OF SUSPENDED DUST CONCENTRATION ON THE LIGHT EXTINCTION COEFFICIENT	92
5.1	Introduction.....	92
5.2	Theoretical Background.....	94
5.3	Materials and Methods.....	96
5.3.1	Experimental dust dispersion.....	96
5.3.2	Measurement of the actual suspended dust concentration during dispersion.....	96
5.3.3	Dust concentration measured using Two-target method	97
5.3.4	Dust particle properties.....	99
5.3.5	Statistical analysis.....	99
5.4	Results and Discussion	99

5.4.1	Dust concentration and extinction coefficient during dispersion	99
5.4.2	Mass extinction coefficient.....	102
5.4.3	Dust particle properties and mass extinction coefficient (K)	103
5.5	Conclusions.....	104
5.6	References.....	105
6.	SUMMARY OF CONCLUSIONS AND DISCUSSION	109
6.1	Restatement of Dissertation Goals.....	109
6.2	Project Overview	109
6.3	Discussion of Major Findings.....	110
6.3.1	CFD-DPM model with particle–wall interaction to predict suspended dust concentration.....	110
6.3.2	CFD-DPM with particle–wall interaction to predict continued dust dispersion and dust deposition.....	111
6.3.3	Light extinction property of suspended dust	111
6.4	Future Work.....	112
6.4.1	Prediction of dust dispersion and deposition using CFD-DPM.....	112
6.4.2	Sensitivity analysis of particle properties used in the simulations	113
6.4.3	Inclusion of particle properties in understanding light extinction coefficient of suspended dust.....	113
APPENDIX A. SUSPENDED DUST CONCENTRATIONS AT 0.1S INTERVALS FOR 0.5 S OF DISPERSION FOR VARIOUS COMBINATION OF AIR VELOCITY AND DUST CONCENTRATION.....		114
VITA.....		115

LIST OF TABLES

Table 2.1 List of OSHA regulations related to dust explosion prevention.....	30
Table 2.2 List of NFPA standards related to dust explosion prevention	31
Table 2.3 Atmospheric particle sizes of different forms of water particles in the atmosphere (Source: Kaushal and Kaddoum, 2017).....	39
Table 3.1. Summary of particle properties and simulation parameters used in this study	58
Table 3.2 Comparison criteria between the predicted and experimental dust concentrations at 0.5, 5 and 10 s after dispersion	63
Table 4.1 Summary of particle properties and simulation parameters used in this study	79
Table 4.2 Mean square prediction error (MSPE; $(g/m^2)^2$) of the settled dust within the confined chamber.....	85
Table 5.1 Dust particle properties	104

LIST OF FIGURES

Figure 1.1 Dust explosion pentagon (Source: Sanghi and Ambrose, 2016).....	16
Figure 2.1 The explosion pressure rise under venting conditions (Source: Tamanini and Valiulis, 1996)	25
Figure 2.2 Measured minimum explosion concentration for polyethylene (Source: Eckhoff, 2003)	26
Figure 2.3 Schematic of 20 L Dust explosion chamber (ASTM E 1226).....	28
Figure 2.4 PUMPF model of total dispersion (Source: Weiler et al., 2010).....	34
Figure 2.5 Particle light scattering process (Source: Bohren, 2004)	39
Figure 2.6 Relation between extinction efficiency and particle size (Source: Louedec and Urban, 2012)	41
Figure 3.1 Schematic representation of the simulation approach	56
Figure 3.2 Dust dispersion chamber and mesh construction	56
Figure 3.3 Simulated dust concentration using the stick-rebound model at various air velocities	61
Figure 3.4 Simulated dust cloud spread and distribution pattern during dispersion (scale bar in kg/m ³).....	65
Figure 3.5 Experimental dust cloud spread and distribution pattern during dispersion	66
Figure 3.6 Model prediction of kinetic energy of dust particles at (a) 2 m/s and (b) 10 m/s inlet air velocity (scale bar in m ² /s ²).....	67
Figure 3.7 Model predictions for explosive dust cloud at 1.0s of (a) 2 m/s 0.05 kg/m ³ , (b) 10 m/s 0.05 kg/m ³ , (c) 2 m/s 0.10 kg/m ³ and (d) 10 m/s 0.10 kg/m ³	68
Figure 4.1 Cumulative particle size distribution.....	78
Figure 4.2 The dust chamber and mesh constructed for the simulation	79
Figure 4.3 Picture of experimental set-up.....	81
Figure 4.4 Predicted dust concentrations during continued dispersion	82
Figure 4.5 Total deposited dust at the bottom of the chamber.....	83
Figure 4.6 Amount of dust settled at the selected three locations within the confined chamber (the solid lines represent the simulated results and the dots represent the experimental values)	85
Figure 4.7 Simulated particle size distribution at three locations after 30 s of dispersion	87
Figure 4.8 Cornstarch particles deposited on the glass slide after 10 s of dispersion at 4 g/min dispersion rate. (Slides were taken from location 1, 2 and 3 (left to right))	88

Figure 5.1 Calibration curve for measuring dust concentration using a laser.	97
Figure 5.2 Schematic representation of measuring light extinction coefficient	98
Figure 5.3 Extinction coefficient of cornstarch during dispersion.	100
Figure 5.4 Extinction coefficient of sawdust during dispersion.	100
Figure 5.5 Extinction coefficient of corn dust during dispersion.	101
Figure 5.6 Extinction coefficient of dusts at different concentrations.....	102
Figure 5.7 Extinction coefficient for cornstarch up to 100 g/m ³ of suspended concentration....	103

LIST OF SYMBOLS

A	: Hamaker constant
A_{vent}	: Venting area
C_c	: Cunningham correction
C_D	: Drag coefficient
C	: Particle concentration
dP/dt	: Rate of pressure rise
D	: Brownian diffusivity of particles
d_{agg}	: Diameter of agglomerates
d_p	: Particle diameter
E_{ad}	: Particle-wall adhesion energy
E_L	: Energy lost due to elastic deformation.
F_{ad}	: Adhesion force
F_D	: Drag force
F_{diff}	: Diffusion force
F_x	: Additional force from fluid phase to particle
g	: Gravitational acceleration
G	: Intensity value obtained from a CCD sensor
I	: Light intensities
J_A	: Ambient light intensity
J	: Real light intensity
k	: Turbulence kinetic energy
K	: Mass extinction coefficient
K_{st}	: Deflagration index
Ke	: Kinetic energy
L	: Path length of the light
m	: Mass
P_{max}	: Maximum explosion pressure
R	: Distance

R_{ep} : Particle Reynolds number
 t : Time
 u : Air velocity
 u_p : Particle velocities
 V : Vessel volume
 ν_p : Particle turbulent diffusion coefficient
 V_T : Terminal velocity
 Y_d : The particle mass fraction with diameter greater than d
 ϵ : Turbulence dissipation rate
 λ_p : Air free path
 μ : Air viscosity
 ρ : Air density
 ρ_p : Particle density
 σ_e : Extinction coefficient
 σ_e^α : Extinction efficiency of particle
 σ_{disp} : Dispersion strength
 τ_a : Aerodynamic response time
 Γ : Effective particle diffusivity
 Γ_v : Normalized vent parameter

ABSTRACT

In the grain handling and processing industry, dust emission and accumulation are major concerns for the safety of workers and for explosion risks. Dust emission and accumulation locations highly depend on the facility design and equipment used for handling and processing. To prevent an explosive atmosphere, monitoring the amount of dust accumulated or dispersed is extremely important. However, methods of measuring the dust concentration require the installation of equipment. The Occupational Safety and Health Administration (OSHA) regulations and National Fire Protection Association (NFPA) standards restrict the thickness of dust layers on floors for fine powder materials such as starch. The objective of this dissertation was to better understand the rate of dust layer accumulation, dust suspension patterns, and the optical properties of suspended dust. For this purpose, The Discrete Phase Model (DPM) was combined with a Computational Fluid Dynamics Model (CFD) and the hybrid model was used to model dust dispersion. Dust dispersion patterns under pressure, such as primary explosions or leakage from equipment, were simulated using the unsteady CFD-DPM approach. The particle-wall interaction based on energy conservation was also introduced in this model. Both one-time and continuous dust dispersion in an enclosed chamber were simulated to mimic secondary explosions and the dust emission from processing equipment. In addition, the light extinction property of suspended dust was studied as a method of measuring suspended dust concentration.

For a one-time dust dispersion incident, the predicted dust concentration agreed with the simulation result for the trial conducted at a dust injection velocity of 2 m/s with injection rates of 0.05 and 0.10 kg/m³ and at a dust injection velocity of 10 m/s with an injection rate of 0.05 kg/m³. The dust concentration in the entire chamber increased with dust injection velocity and the mass of injected dust. As dust injection velocity increased, dust spread out and formed a larger explosive dust cloud. However, the dust concentration inside the chamber was non-uniform. Considering the minimum explosive concentration, the largest explosive cloud was created at a dust injection velocity of 10 m/s with an injection rate of 0.10 kg/m³. Explosive concentrations of dust were found somewhere in the chamber for all dispersion rates. At an injection velocity of 10 m/s with an injection rate of 0.10 kg/m³, the predicted dust concentration was 10% more than the measured dust concentration. Thus, this model is suitable for dilute dust particle dispersion flows, where the volume fraction of particles is less and only a single particle layer settles.

Continuous dispersion was simulated to determine the suspended dust concentration and particle deposition patterns. Dust was dispersed for 30 s at dispersion rates of 2, 4 and 6 g/min at a dust injection velocity of 2 m/s. The dust concentration increased at a constant rate after a few seconds of dispersion, regardless of the dust dispersion rate. Most dust particles were deposited near the dust dispersion nozzle. Large particles were more affected by gravitational force and inertia compared with small particles, which traveled with airflow and settled behind the nozzle. The dust accumulated close to the dispersion nozzle faster than behind the nozzle location. However, specific attention must be paid to small particles, because they are more likely to cause an explosion, as their minimum explosive concentration is lower than that of large particles.

The light extinction coefficients of cornstarch, grain dust, and sawdust were measured using a two-target method. The suspended dust concentration was measured using a calibrated laser instrument. The light extinction coefficient was linearly related to the suspended dust concentration. The correlation coefficient between the light extinction coefficient and suspended dust concentration depended on particle size, particle shape, and chemical properties.

Controlling dust cloud generation and minimizing the concentration and volume of dust clouds are some key measures to prevent dust explosions. The mathematical models developed in this study to predict dust dispersion, suspension, and rate of settling will help solve a few of the challenges in the particulate material handling and processing industry. This method of measuring the light extinction coefficient can be applied development of a dust safety monitoring system. The result presented in this dissertation will help the industry prevent the formation of an explosive atmosphere.

1. INTRODUCTION

This dissertation presents an investigation of the mechanisms of dust dispersion during grain handling and processing. The study involves mathematical modeling of dust dispersion and settling patterns, Computational fluid dynamics – Discrete phase model (CFD-DPM) simulation of dust dispersion, and light extinction properties of the suspended dust cloud. Almost all industries involving size reduction, conveying, drying, storage, and packaging generate dust, thus causing an increased hazard to the health and safety of workers who are exposed to it. Therefore, understanding the dust dispersion pattern would help develop better sensing mechanisms and strategies for efficient dust collection.

This chapter gives an overview of the various dust dispersion scenarios, which is the primary focus of this dissertation. In Section 1.1 dust hazards, as well as the dust dispersion measurement methods in processing industries are enumerated. The hypothesis, goals, and objectives of this study are given in Section 1.2. Section 1.3 provides an overview of the remainder of the dissertation.

1.1 Problem Statement: Dust Hazards

With the increasing demand for food, energy, and chemicals, the number and volume of powder processing industries have also risen. Most of the dusts generated in the processing industry are explosive (Ebadat, 2010). Inhaling dust particles will also cause various respirable diseases.

The presence of five factors that lead to dust explosions, which are commonly known as the explosion pentagon (Fig 1.1), are confined space, combustible dust, dispersion, oxidants, and ignition. Controlling any one of these factors can prevent an explosion (Eckhoff, 2003). Although dust explosions have been studied since the 19th century, the only clear guidelines for prevention provided by the Occupational Safety and Health Administration (OSHA) are good housekeeping and maintaining the dust layer below 1/32 of an inch (OSHA 29 CFR Part 1910). The National Fire Protection Association (NFPA) has developed standards to follow to prevent dust explosions, which include suggestions such as implementing a proper design of an exhaust system with knowledge of the physical and chemical properties of the materials (NFPA Standards 68, NFPA

Standards 654, NFPA Standards 61). Due to varied processing environments, the establishment of a universal standard for preventing dust explosions is difficult.

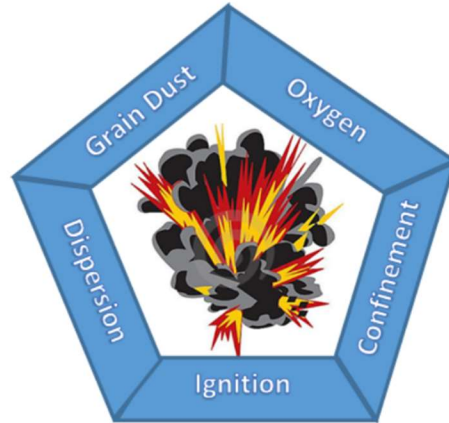


Figure 1.1 Dust explosion pentagon (Source: Sanghi and Ambrose, 2016)

Suspended dust concentration is one of the most important factors when aiming for preventing dust explosions, as the dust does not explode when the dust concentration is below the minimum explosive concentration (MEC). MEC depends on material combustion properties, particle size, and morphology (Eckhoff, 2009). Some materials reach the maximum explosion pressure at a concentration of only 0.2–0.3 kg/m³, such as coal and polyethylene (Cashdollar, 2000). Therefore, ensuring that the dust cloud is below the minimum explosive limit is necessary to prevent dust explosions. The measurement and characterization of the spread of the dust cloud during particulate material processing are essential to predicting dust cloud generation and explosion risk levels. However, the dispersion process is highly dependent upon the actual industrial situation and differs between various kinds of equipment, such as bucket elevators, pneumatic transport systems, and silos. In addition to the processing conditions, particle size and shape, which affect burning speed and hence explosion pressure, also affect the dust cloud dispersion properties (Eckhoff, 2009). The current methods to minimize the dispersed dust cloud concentration has limited practical applicability, and the technical measures adopted are often expensive (Eckhoff, 2003).

Real-time suspended dust concentration monitoring systems are always expensive, and the industry continuously strives to develop more cost-effective safety measures (Eckhoff, 2005).

Currently, dust concentration is calculated either by the gravitational method or by the laser scattering method. The gravitational method requires the sampling of air, which introduces bias when particles are diffused onto the sampler's wall boundaries, and high-accuracy filters are always needed for proper measurements. The laser scattering method, on the other hand, measures with a default particle density of 1000 kg/m^3 (Hinds, 1999). The dust explosive concentration is expressed in mass per volume; therefore, it fails to consider the particle's true density, which leads to misjudgment of suspended dust concentration. For example, the explosive dust concentration measurement method proposed by Conti et al. (1981), uses a laser method and does not require sampling but needs to be calibrated before every use. Furthermore, the probe can only measure the concentration at a particular point, rather than a concentration in a specified volume, owing to its narrow measurement area. In summary, the development of dust concentration sensors must be economically efficient, easy to use and maintain, and highly mobile, with a relatively large test area. The bias during the sampling of air should also be minimized.

1.2 Research Hypotheses and Goals

Controlling both dust dispersion and deposition, within confined spaces, is important to prevent dust explosions. Due to the uncertainty of environmental conditions and material properties, and with the complexities in the facility design, using a computational method to predict the dust cloud condition will be valuable. Furthermore, mathematical prediction can give more detailed information such as particle movement, dust suspension and deposition patterns. Several simulation approaches have been adopted to simulate explosive dust dispersion. But, most of these approaches do not include both discrete and fluid phases when predicting dispersed dusts.

Particle–solid and particle–fluid interactions must be considered when the particle volume fraction is high. As the dust particle drag force caused by the fluid phase is significantly affected by the particle size, the simulation of real operational conditions is essential. However, scaling up simulations is time-consuming and computationally inefficient. The number of particles is also a significant driver of increased computational time. Simulations with computational efficiency and accurate predictive power are the practical goal of model development. The discrete phase model (DPM) with the concept of “parcel” saves calculation time by tracking a group of particles as one parcel (Fluent, 2019). Therefore, the DPM was used in this study to take advantage of both computational efficiency and accuracy for dust dispersion under the explosive concentration limit.

The process of developing and validating the model had the additional benefit of helping to identify factors that have a major influence on dust dispersion and deposition.

Dust suspended in the air produces a visual effect, therefore the effects of the dust cloud concentration on the atmospheric optical properties will be used as the principle to quantify dust concentration. Suspended dust in the path of light will either scatter or absorb the light waves, which causes light extinction. The light extinction properties of particles depend on their particle size, shape and chemical components (Hinds, 1999). In a particulate material handling and processing plant, most often the suspended particles are generated from the same source, thus those suspended particles will have similar properties. The relationships between the light extinction and the suspended dust cloud concentration were studied in this dissertation, which can be applied to develop a dust concentration monitoring system.

The working hypothesis of this study is that particle properties influence dust dispersion and deposition under confined conditions. The research objectives are listed below:

1.2.1 Research objectives

The overall goals of this project are to develop a model to understand the dust dispersion pattern under confined conditions and to study the light extinction properties of dust clouds. This will be pursued by fundamental studies, broken down into two primary objectives, with their sub-objectives listed below:

1. Develop a CFD-DPM model to predict the dust dispersion pattern in confined conditions
 - 1.1. Develop a model that includes interaction of the suspended particles with the wall and predicts the dust dispersion when there is air turbulence.
 - 1.2. Develop a continuous dust dispersion model using the CFD-DPM approach to predict dust dispersion and deposition.
2. To study the change in light extinction as influenced by suspended dust clouds

1.2.2 Dissertation outline

The remainder of this dissertation is divided into four chapters. In Chapter 2, the published literature on dust dispersion simulation is described. In Chapter 3, development of a dust dispersion

CFD-DPM model using that includes the particle-wall model is presented along with validation experiments. Chapter 4 describes the continuous dust dispersion simulation and deposition of dust layers. In Chapter 5, the relationship between dust extinction coefficient and dust concentration is presented. Chapter 6 summarizes the findings of this dissertation and includes some suggestions for future work based on the understandings gained from this dissertation work.

1.3 References

- Hinds, W. C. (1999). *Aerosol technology: properties, behavior, and measurement of airborne particles*. John Wiley & Sons. New York, NY.
- Cashdollar, K. L. (2000). Overview of dust explosibility characteristics. *Journal of Loss Prevention in the Process Industries*, 13(3-5), 183-199.
- Conti, M., Geremia, R., Adamo, S., & Stefanini, M. (1981). Regulation of Sertoli cell cyclic adenosine 3': 5' monophosphate phosphodiesterase activity by follicle stimulating hormone and dibutyryl cyclic AMP. *Biochemical and Biophysical Research Communications*, 98(4), 1044-1050.
- Eckhoff, R. K. (2003). *Dust explosions in the process industries: identification, assessment and control of dust hazards*. Elsevier. New York, NY.
- Eckhoff, R. K. (2005). Current status and expected future trends in dust explosion research. *Journal of loss prevention in the process industries*, 18(4-6), 225-237.
- Eckhoff, R. K. (2009). Understanding dust explosions. The role of powder science and technology. *Journal of Loss Prevention in the Process Industries*, 22(1), 105-116.
- National Fire Protection Association. (2005). *NFPA 654: Standard for the Prevention of Fire and Dust Explosions from the Manufacturing, Processing, and Handling of Combustible Particulate Solids*. National Fire Protection Association. Quincy, MA.
- National Fire Protection Association. (2007). *NFPA 68: Standard on explosion protection by deflagration venting*. National Fire Protection Association. Quincy, MA
- National Fire Protection Association. *NFPA 850. Recommended Practice for Fire Protection for Electric Generating Plants and High Voltage Direct Current Converter Stations*. National Fire Protection Association. Quincy, MA.

National Fire Protection Association. (2008). NFPA 61. Standard for the Prevention of Fires and Dust Explosions in Agricultural and Food Processing Facilities. National Fire Protection Association. Quincy, MA.

Occupational Safety and Health Administration. (2003) OSHA Standard 29 CFR 1910.272, Grain Handling Facilities, Department of Labor, Washington D.C.

Sanghi, A., & Ambrose, R. K. (2016). Analysis of the effect of prevailing weather conditions on the occurrence of grain dust explosions. *Journal of Agricultural Safety and Health*, 22(3), 187-197.

2. LITERATURE REVIEW: DUST DISPERSION AND EXPLOSION

The aim of this Chapter is to summarize in detail the published experimental and theoretical approaches in order to gain a better understanding of the perils of dust explosions. Since the focus of this dissertation is on grain dust particles, most of the examples presented in this Chapter are based on published literature on grain dust. The factors that influence dust s and the parameters for assessing the risks are presented. The Chapter includes a review on dust explosion factors and their effects on explosion severity, and the published work on the effect of dust particle properties on dust explosion (Section 2.1). In Section 2.2, some of the reported modeling approaches to predict the dust dispersion are discussed. Section 2.3 gives a broad overview of the optical properties of particles, including light scattering and absorption.

2.1 Dust Hazards

More than 70% of the powders processed in the industry are combustible (Sun et al., 2001). According to the chemical safety and hazard investigation board (CSB, 2006; CSB, 2017), there have been 392 dust explosions from 1980 to 2017, which caused 185 fatalities and 1055 injuries. Among these, 24% of the incidents occurred in the food industry. In addition, there were 85 dust explosions from 2010 to 2019 in the grain industries (Ambrose, 2019). Grain dust is generated by the abrasion of kernels during the handling of grains. Farant and Moore (1980) estimated that 3–4 pounds of dust can be generated for each ton of grain when passing through a grain elevator. The physical and chemical compositions of grain dust vary depending on the type of grain and the location of generation. The grain dust is mainly composed of fractured grain kernels, weed seed, husks, storage mites, insects, bacteria, molds, inorganic matter, and chemicals (Chan et al., 1992). Martin and Sauer (1976) observed that the majority of grain dust was generated during the second handling, where the grain was cleaned. In addition, they determined the wheat bin transfer and car unloading had similar dust generation rates, i.e., 0.007 and 0.009% of total grain weight. This was much lower than the rate for corn.

A dust explosion is an energy release when combustible dust particles are ignited. As opposed to gas explosions, dust explosion requires the presence of an oxidant, fuel, and ignition, as well as suspended dust particles above a specific concentration. Figure 1.1 presents the

explosion pentagon, a well-known concept used to describe the dust explosion, listing all necessary conditions for a dust explosion to occur.

The following section describes the dust explosion process, the key explosibility parameters and their relation to the explosion pentagon, and common prevention and mitigation methods.

2.1.1 Primary and secondary explosions

Dust is considered explosive if, after igniting the dust/air mixture with a suitable source, there is flame propagation in combination with a rise in pressure. Dust explosions originate from a fire or a primary explosion from the ignition of dust. This primary explosion disperses the dust collected on surfaces as a dust cloud or disperses within the confined space. The ignition from the primary source then ignites the dust cloud and leads to the major secondary explosion.

The explosion may transmit through tubes, pipes, and conveyors from one vessel (equipment or storage bin) to another. The secondary explosion in a connected vessel has a much higher pressure rise rate and peak pressure than those in single closed vessels (Phylaktou and Andrews, 1993). The secondary explosion causes severe damage to infrastructure, environment and can result in human fatalities and injuries (Maremonti et al., 1999; Yuan et al., 2016). In most dust explosions, one or more secondary explosions have been reported as a consequence of a primary dust explosion. Yuan et al. (2016) referred to these chains of dust explosions as a dust explosion domino effect.

The parameters used to assess the severity of a dust explosion are the maximum explosion pressure (P_{max}), rate of pressure rise (dP/dt), and the deflagration index (K_{st}) (Cao, et al., 2012). K_{st} is related to the maximum pressure rise rate, defined as $K_{st} = \left(\frac{dP}{dt}\right)_{max} V^{1/3}$, where V is the vessel volume (Bartknecht, 1979). Coal dust has been tested to have a P_{max} of 7.2 bar and dP/dt of 179 bar/s at a concentration of up to 700–800 g/m³ in a 20-L explosion chamber (Pilao et al., 2006). P_{max} for a vessel is usually 7–10 times greater than the operating pressure (Holbrow et al., 1999). P_{max} of a primary explosion can range from 1 to 10 bars. Holbrow et al. (1996) reported that the primary explosion as tested in a linked vessel has a P_{max} of approximately 2 bar, whereas the secondary explosion has a P_{max} of 6.2 bar. CSB (2005) also reported a P_{max} of 7.59 bar during a secondary explosion of resuspended resin dust. The magnitude of the secondary explosion depends

on the amount of resuspended dust, pressure from the primary explosion, and flame propagation. However, a secondary explosion is always more severe than the primary explosion. Furthermore, there can be more than one secondary explosion owing to the domino effect.

2.1.2 Dust explosion factors

As presented in Figure 1.1, the presence of an ignition source, confined space, combustible dust (fuel), dispersed dust, and oxygen leads to an explosive environment. The explosion factors such as dust ignition and dust dispersion have primarily been studied to prevent and mitigate dust explosions, while the effect of confined space and oxygen is less studied as these factors are nearly always presented. In this section, the effect of dust properties and ignition conditions on dust explosions are reviewed in detail.

2.1.2.1 Ignition

Several different potential contributing factors could provide the spark or heat needed for an explosion. Some examples are friction sparks, and welding sparks, etc. Dust ignition energy is a key factor determining the explosive risk of different materials. The minimum ignition energy (MIE) and minimum ignition temperature (MIT) are commonly used tests to determine the ignitability of different dust particles. The MIE and MIT are the minimum energy and temperature, respectively, required to ignite a dust cloud and cause an explosion. There are mainly two experimental methods to determine the MIE; the Hartmann tube with capacitor spark generator, and a commercially available MIKE3 device (EN [13821:2002](#), 2002; Cesana and Siwek, 2001). Janes et al (2008) reported that the MIKE3 apparatus generally provides lower MIE values than the Hartmann tube for dust MIE between 1 and 10 mJ and over 100 mJ (Janes et al., 2008). The MIE is mostly determined experimentally, while researchers have also studied statistical methods to predict the MIE (Marmo and Cavallero, 2008; Bernard et al., 2010; Yuan et al., 2014). Mitsui and Tanaka (1973) developed a mathematical model to estimate the MIT by factoring particle size and material properties and by calculating the rates of heat generation and heat loss in the dust cloud. Hosseinzadeh et al. (2019) modeled the MIT using the lumped-capacitance thermal balance of a particle, and found that the model well predicted the MIE considering 40-60% energy loss from ignition. Di Benedetto et al. (2010) developed a thermo-kinetic model to predict the MIT based on the mass and energy balance of the explosion reaction.

The MIE and MIT of dust particles depend on their chemical composition, size, and morphology, as well as on the environmental conditions such as turbulence, humidity. Both the MIE and MIT decrease with a decrease in the particle size (Huang et al., 2006; Bouillard et al., 2010). Thomas et al. (1991) studied the effect of morphology of lycopodium dust particles on the MIE and concluded that the MIE could be affected by the surface-area-to-volume ratio. A similar result was found in a study on aluminum dust ignition, where irregular aluminum dust had a lower MIE than spherical aluminum dust due to more efficient heat transfer from the irregular particles (Bagaria et al., 2019). Other than the powder properties, the oxidant concentration, initial pressure, and turbulence have also been found to affect the MIE (Kauffman et al., 1985; Cashdollar, 2000; Kuai et al., 2013).

2.1.2.2 Oxygen concentration

Oxygen is the most common oxidant for dust explosion incidents and makes up 21% of the atmosphere. The P_{max} and dP/dt are expected to increase linearly with oxygen concentration both theoretically and experimentally (Cashdollar, 2000). Oxygen concentrations greater than 21% tend to increase the burning velocity, and concentrations less than 21% reduce the burning velocity. The oxygen level that can no longer support combustion is known as the limit oxygen level. Near the limit oxygen level, the pressure decreases very rapidly with decreasing oxygen concentration, until the mixture is no longer explosive (Cashdollar, 2000).

2.1.2.3 Confined space

Confined space is an area with a limited or restricted exchange of air and energy. The confined space can be fully or partially confined. A partially confined space has openings that allow pressure release, which is called a vent, wherein the explosion overpressure will decrease to the operating pressure after the release (Edri et al., 2011).

The venting area required to release the explosion pressure is influenced by K_{St} and the confined space volume. The normalized vent parameter Γ_v can be determined as follows:

$$\Gamma_v = a \frac{A_{vent} P_{max}}{V^{2/3} K_{St}} \quad 2.1$$

where a is 'a' constant that depends on the vent flow coefficient, A_{vent} is the venting area, V is the confined space volume, and P_{max} is the maximum pressure rise without any venting system (Tamanini and Valiulis, 1996). Using the vent parameter, the overpressure after venting can be calculated as shown in Figure 2.1. Bartknecht (1989) and Wiemann (1987) also reported that, in

confined spaces, the initial pressure affects the P_{max} and K_{st} , and that these values increase with an increase in the initial pressure.

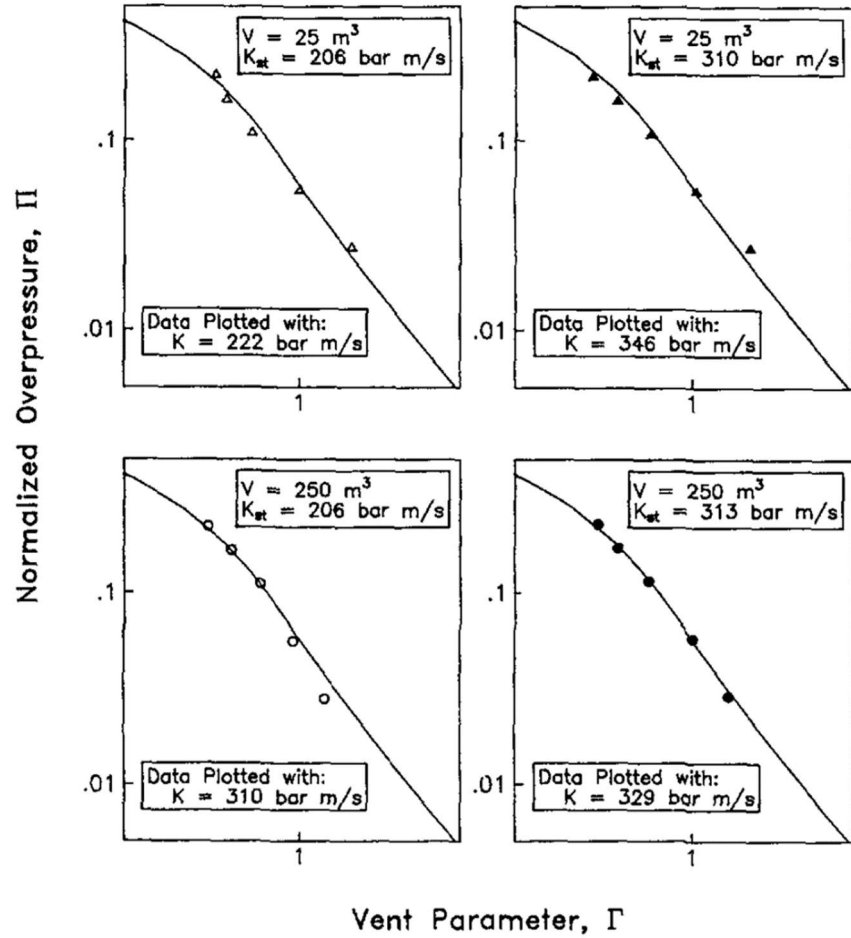


Figure 2.1 The explosion pressure rise under venting conditions (Source: Tamanini and Valiulis, 1996)

2.1.2.4 Combustible dust (fuel)

Dust is always present in a particulate material handling and processing facility. For example., one metric ton of grain contains about 1-5 kg of dust that is brought into a grain handling facility. According to the Occupational Safety and Health Administration (OSHA), a fine powder that is less than 420 microns (particles that passthrough a US 40 sieve) is a dust particle. The magnitude of the dust explosion depends on chemical and physical characteristics, especially the particle size distribution (Cashdollar, 2000). Particle shape and porosity are also important

properties that influence dust explosibility. In general, a higher specific surface area will have a faster reaction rate and generate a more severe explosion. The majority of the grain dust particles had a size lower than 125 μm . Furthermore, 52% of the grain dust produced during the on-farm handling had a diameter lower than 21 μm , and the geometric mean diameter of grain dust collected from the grain elevator was 12.3 μm (Boac et al., 2009).

Cashdollar (1994) studied the effect of particle size on the explosibility of iron dust. He found that P_{max} and dP/dt decreased with an increase in dust particle size, while the minimum explosion concentration increased with the particle size increase until the particle size reached a size that could not be ignited. According to the author, a dust cloud cannot be ignited when the coal dust particle is between 200 and 300 μm . The author also found that the P_{max} and dP/dt data for the broad size distributions were slightly higher than those in the narrow size distributions. K_{St} also decreased with an increase in particle size, as demonstrated by Addai et al. (2016). Similar results were reported by Eckhoff (2012) for P_{max} and dP/dt for nanoparticles; however, the K_{St} values did not show differences between the nanoparticle dust and particle powders.

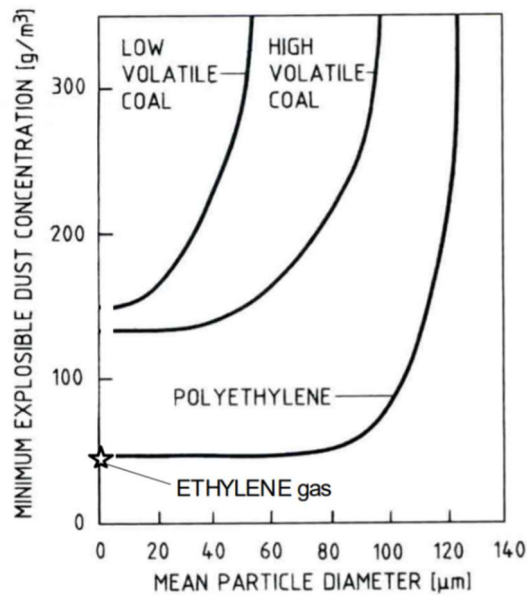


Figure 2.2 Measured minimum explosion concentration for polyethylene (Source: Eckhoff, 2003)

Particle size also affects the minimum explosive concentration (MEC) (Figure 2.2). The MEC decreases with a decrease in the dust particle size (Dobashi, 2009). Increasing particle size

may reduce explosion risks in the process industries, where MEC is increased and the explosion parameters P_{max} , dP/dt , and K_{st} are decreased. But, practical application limits don't allow for increasing the particle size. So, most industries rely on explosion suppression devices rather than on altering the particles.

2.1.2.5 Dust dispersion

Dust dispersion is one of the most important factors that leads to secondary explosions. In some situations, such as air jet mills, the explosive dusts are dispersed by the equipment, but in most cases, the dusts are resuspended from the external surfaces of process equipment, walls and floors in the building (Eckhoff, 2009). Dust dispersion is affected by particle properties and airflow, and both the suspended dust concentration and air turbulence affect the dust explosion. The relation between dust properties, turbulent flow, and dust suspension and deposition are reviewed in Section 2.2. This section only reviews dust concentration and its effect on dust explosion.

As the dust particle is the only fuel in the explosion, the concentration is the most important factor for the combustion process. When dust concentration is below a specific threshold concentration, explosions cannot occur. This concentration is called MEC or lean flammable limit (LFL). MEC varies based on their particle size, moisture content, relative humidity, distance from ignition source, etc. Kuai et al. (2013) found that the minimum explosion concentration is significantly affected by ignition energy for magnesium dust and sweet potato starch particles. If the dust particles size is large or if the moisture content and relative humidity is high, then the MEC will be high. i.e. the threshold level to start an explosion will be high. There has been considerable effort in determining the MEC of different materials to provide a reference for dust explosion prevention. The American Society for Testing and Materials (ASTM) has a standard method to test the MEC in a 20-L sphere apparatus (ASTM E 1515). The National Fire Protection Association provides guidance on MEC for all combustible dusts and non-combustible dusts. For example, the MEC of both food powders (corn starch, sugar) and metal dust (aluminum) are 30 g/m^3 , and some polymers is 15 g/m^3 in.

During dust dispersion, the turbulence of a dust cloud also has a strong influence on both its ignitability and explosibility. The initial turbulence before ignition can remove heat from the ignition zone due to rapid convection. Thus, dust dispersed by higher initial turbulence has a higher MIE (Glarner, 1984). On the other hand, the turbulence generated by the primary explosion can affect P_{max} , dP/dt , and K_{st} by accelerating the flame propagation.

2.1.3 Determining dust explosibility

Standard methods to determine dust explosibility are described in ASTM E1226 (ASTM test, 1978) which describes how to estimate P_{max} , dP/dt , and K_{st} using the pressure and time curves from a dust explosion in a closed chamber. In this method, the 1-m³ apparatus is considered the best standard equipment, but it requires a large amount of dust and is large for a standard laboratory. Therefore, Siwek (1977) developed a “Siwek 20-L Apparatus”, which can reproduce approximately the same dust dispersion degree and turbulence of a 1-m³ vessel described by International Organization for Standardization (ISO). This apparatus is the chamber most often used for recent explosion experiments.

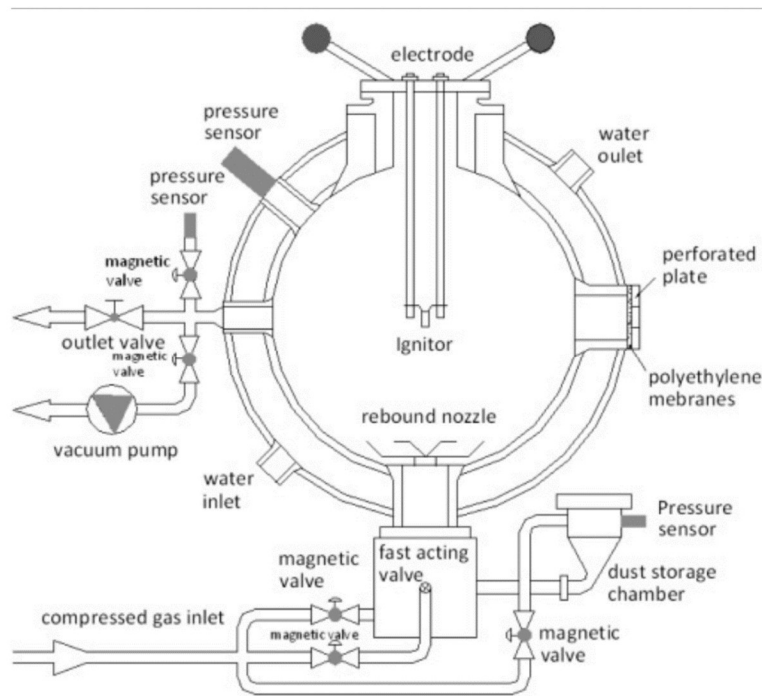


Figure 2.3 Schematic of 20 L Dust explosion chamber (ASTM E 1226)

Besides the standard explosion chamber, researchers also use tube-shaped containers to study the flame and explosion propagation rate as well as the primary and secondary explosion parameters (Kauffman et al., 1985; Razus et al., 2003, Liu et al., 2010). These experiments were also performed under real processing conditions such as coal mines and grain silos to determine explosion parameters in large-scale explosions (Eckhoff, et al., 1987; Hauert, et al., 1996; Sapko et al., 2000).

Studies have shown that with increasing dust concentration, the P_{max} in the combustion vessel increases to a peak value, and at higher dust concentrations, the pressure remains constant with an increased amount of dust, as dP/dt and K_{st} (Cashdollar and Chatrathi, 1993). Cashdollar and Chatrathi (1993) tested coal dust for concentrations up to 4000 g/m^3 and found a decrease in P_{max} and K_{st} when the concentration exceeds 800 g/m^3 . This phenomenon was attributed to the increased heat sink effect or to the possible decrease in turbulence due to the large mass of dust. Some materials are found to have a maximum concentration limit, where the dust cannot explode due to an excessive amount of dust and limited available oxygen (Mintz, 1993). It may also be because the large mass of excess fuel becomes a huge heat sink and as such, the flame temperature is reduced below its MIT. However, most dusts can be considered to have no maximum concentration limit of explosibility.

Turbulence plays an important role in dust explosions. In industry, turbulence occurs due to the operation of fans, mechanical movements, and primary explosions, as mentioned in Section 2.1.1. Turbulence can lead to the formation of a dust cloud and keeps the dust mixed with air. This makes it a perfect condition for the secondary explosion. Besides the effect on the particle movement, turbulence can also affect the burning velocity, ignition energy, P_{max} , and dP/dt (Kauffman et al., 1985). In an explosion testing chamber, when turbulence was increased to disperse the dust, the resultant flame speed increased, and a better suspension of dust was observed (Amyotte et al., 1988). Kauffman et al. (1985) used a 1-m^3 premixed turbulent combustion bomb with grain dust, cornstarch, and polyethylene, and found that the burning velocity increased with an increase in turbulence intensity for the same concentration level. Although dust suspension and deposition can affect turbulence after a primary explosion, the effects of suspended dust concentration and turbulence have not been studied independently by researchers.

2.1.4 OSHA regulations and NFPA standards

In the early 1980s, OSHA formulated regulations to prevent dust explosions. In addition, the nonprofit organization, NFPA has developed industry safety standards for the including dust explosions. Both OSHA and NFPA have specified the reference values for various dust explosion parameters, including MEC, MIE, and MIT. Thus far, OSHA does not have a comprehensive regulation for preventing dust explosions. However, OSHA has formulated regulations that are specific to dust explosion hazards; for example, OSHA (29 CFR 1910.272) has classified the areas

that contain combustible dust with the aim of achieving good housekeeping and preventing dust accumulation in grain facilities. The complete list of OSHA regulations is provided in Table 2.1.

Table 2.1 List of OSHA regulations related to dust explosion prevention

OSHA 1910 Occupational Safety and Health Standards:
1910.22 Walking-working surfaces
1910.269 Electric power generation, transmission and distribution
1910.271 Grain handling facilities)
1910.307 Hazardous (classified) locations.
1910.1200 Hazard communication.

Explosive dust clouds are formed by re-entrainment and redispersion of powders and by dust produced at an earlier stage during processing or that has accumulated intentionally or unintentionally. Silos, cyclones, and filters may remove dust during processing; however, the accumulated dust inside the equipment is a potential fuel for a dust explosion. There is a high possibility that the dust may accumulate on the external surfaces of process equipment and floors of the factory building. To prevent an explosion, NFPA standard 654 (Standard for the Prevention of Fire and Dust Explosions from the Manufacturing, Processing, and Handling of Combustible Particulate Solids) specifies that the accumulated dust layer must be less than 0.8 mm.

NFPA has developed comprehensive standards for controlling various aspects of dust explosions, which include regulating size reduction, dust separation, dust collection, fire protection, equipment and building venting, employee training, ignition control, and housekeeping (Table 2.2). These standards have helped to reduce dust explosions by utilizing inherently safe methods, which are achieved by minimizing the combustible dust using good housekeeping standards and dust collection systems.

Table 2.2 List of NFPA standards related to dust explosion prevention

NFPA 484 Standard for combustible metals
NFPA 61 Standard for the prevention of fires and dust explosions in agricultural and food processing facilities.
NFPA 654 Standard for the prevention of fire and dust explosions from the manufacturing, processing, and handling of combustible particulate solids
NFPA 68 Standard on explosion protection by deflagration venting
NFPA 850 Recommended practice for fire protection for electric generating plants and high voltage direct current converter stations

From the review of properties of dust, it is inferred that studying dust dispersion is important for the development of dust explosion prevention strategies. Containing dust dispersion could give an important understanding of preventing secondary explosions from occurring. The dust dispersion and suspension theory and dust dispersion models are reviewed in Section 2.2.

2.2 Dust Dispersion Mechanism

During an explosion, the dust particles are suspended by the air blast. The suspended particles move under the drag force from the air and spread out to form a dust cloud. The dispersion motion of dust particles in the presence of airflow follows Newton's law, and the efficiency of dust dispersion depends on the bulk properties of the dust (Hinds, 1999). In this section, the interaction of particles with air is described, and the simulation of two-phase flow is reviewed.

2.2.1 Particle-fluid interaction

During turbulent flow, the particle motion depends on the effects of the turbulent flow field, particle inertia, and gravity (Wells and Stock, 1983). Because the particles have a much higher density than that of the fluid in most of the particulate material handling processes, the movement of dense particles in the turbulent flow is significantly affected by their inertia and body force (typically gravity). For a single small spherical particle with a mass m , the motion is represented as per equation 2.2. This equation balances the particle inertia and acceleration with the fluid drag force, an additional force related to the fluid involved, and gravity (Maxey, 1987).

$$m \frac{du_p}{dt} = F_D (u - u_p) + mg + F_x \quad 2.2$$

where u and u_p are the air and particle velocities, respectively; F_D is the drag force; m is the particle mass; g is gravitational force; and F_x is the additional force.

Drag force is the major force acting over a particle moving in the fluid phase. It depends on the fluid viscosity, particle aerodynamic diameter, and density.

$$F_D = \frac{C_D R_{ep}}{\tau_a 24} \quad 2.3$$

where τ_a , R_{ep} , and C_D are the aerodynamic response time, particle Reynolds number, and drag coefficient, respectively.

The aerodynamic response time, τ_a , is the characteristic timescale by which a particle responds to the velocity changes in the flow field. This was also defined by Wang and Stocks (1993) as the time required for the velocity of a particle injected into a quiescent fluid to reach 1/e of its initial value if the drag on a particle is in the Stokes range. τ_a can be calculated using the following equation:

$$\tau_a = \frac{\rho_p d_p^2}{6\pi\mu} \quad 2.4$$

where μ is the air viscosity, d_p and ρ_p are the particle diameter and density, respectively.

The drag coefficient, C_D , has to be estimated using an empirical equation. Some empirical C_D values for differently shaped particles can be found in the literature (Hinds, 1999). The particle shape affects particle aerodynamic properties. Crosswise sphericity was introduced for non-sphere-shaped particles by Leith (1987). However, a good estimation equation for a spherical particle in the Stokes region was introduced by Cheng (2009) as:

$$C_d = \frac{24}{R_e} (1 + 0.27R_{ep})^{0.43} + 0.47[1 - \exp(-0.004R_e)^{0.38}] \quad 2.5$$

The particle Reynolds number is defined as per the following equation:

$$R_{ep} = \frac{\rho d_p |u_p - u|}{\mu} \quad 2.6$$

For dense particles, where the particles have a much higher density than that of the fluid, gravity could be the governing force that affects the particles' trajectories.

Brownian motion and diffusion are the particle random motion resulting from their collision with fast-moving air atoms or molecules. The diffusion force is calculated as:

$$F_{diff} = \frac{3\pi\mu u_p d_p}{C_c} \quad 2.7$$

where C_c is the Cunningham correction factor. This factor is defined as follows:

$$C_c = 1 + \frac{2.52\lambda}{d_p} \quad 2.8$$

where λ is the air free path. The mean free path for air at 1 atm and 20 °C is 0.066 μm .

The smaller particles move under Brownian motion, where particles collide with the fast-moving molecules in the air. In the grain handling process, the generated dust or product particle sizes are higher than 10 μm (Boac et al., 2009). In addition, the particles are considered to be much larger than the air molecules, and the dispersion motion is mainly governed by the turbulent motion of eddies, which have a typical size of 2–5 cm (Snyder and Lumkey, 1971). Therefore, the Brownian force can be neglected.

2.2.2 Particle-particle interaction

The interaction between dust and the surrounding fluid medium and the dispersion of dust from an aggregated powder have not been well understood (Calvert et al., 2009). The complete separation of fine cohesive powder during dispersion is considered difficult, especially for the powder with a particle size lower than 20 μm , owing to the relatively large inter-particle attraction force compared to the separation force (Geldart, 1973). The dispersed motion of a particle cluster in turbulent flow depends on its particle size, which is significantly affected by the inter-particle attraction and separation forces. Calvert et al. (2009) reported that larger agglomerates tend to disintegrate during dispersion due to surface erosion. The bulk tensile strength and shear strength are the two intrinsic bulk powder properties that could help in understanding powder dispersion. When mechanical stress is larger than the inter-particle forces between the particles within the primary agglomerates, the powder gets dispersed easily.

The most common interparticle forces include inter-particle locking, the van der Waals force, liquid bridge force and solid bridge force. These forces depend on the particle surface chemical composition, surface roughness, particle size and shape, and moisture content (Jange and Ambrose, 2019). There are published models that describe the breaking of interparticle forces and the de-agglomeration of particles. The planar fracture model of RUMPF is one of the widely accepted models that uses a two-particle approach (Rumpf, 1958) (Figure 2.4). Further, Weiler et

al (2010) summarize three main de-agglomerate stresses that a cluster experiences during dispersion and developed a total dispersion model for de-agglomerates during dispersion:

$$\sigma_{disp} = \frac{n\bar{F}}{\pi d_{agg}^2} \quad 2.9$$

where the dispersion strength σ_{disp} is calculated from the diameter of agglomerates (d_{agg}) with n number of primary particles, and the mean particle cohesion force \bar{F} .

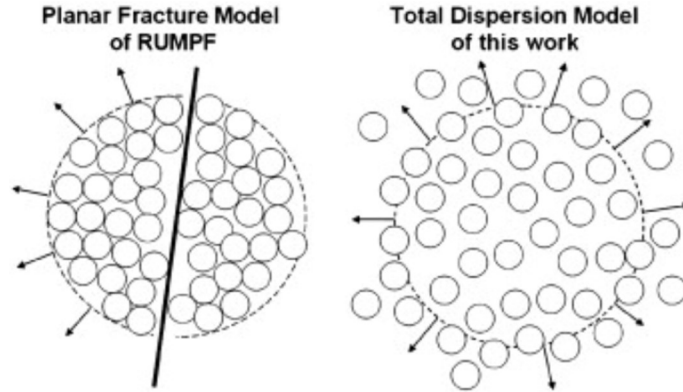


Figure 2.4 PUMPF model of total dispersion (Source: Weiler et al., 2010)

2.2.3 Modeling particle dispersion process

The particle dispersion modeling can be performed using three approaches. The first is to simulate the particle using the discrete element method (DEM) and then couple it with the fluid phase model using computational fluid dynamics (CFD). The second is the Eulerian model, which treats the particle as a continuous phase. The third is the statistical method, which uses Gaussian models.

Tong et al. (2010) modeled dust dispersion with particle translational and rotational movements in a system and observed that the momentum of a particle depended on its interactions with neighboring particles, walls, and surrounding fluid. The interparticle forces considered were the gravitational force, normal and tangential contact forces, viscous damping forces, van der Waals force, and particle-fluid interaction force. They introduced an index based on the cohesive energy and the particle-wall impact energy and demonstrated that the dispersion efficiency correlated well with the index.

The DEM simulates the discrete phase by equating the force balance of the particle (equation 2.2) and gravitational force as shown in the following:

$$-\frac{du_p}{dt} = F_D(u - u_p) + \frac{g_x(\rho_p - \rho)}{\rho_p} + F_x \quad 2.10$$

where ρ and ρ_p are the densities of fluid and particle, respectively.

The DEM tracks the movement of individual particles based on Newton's law. Therefore, this method is able to locate each particle and its particle concentration and trajectory.

The Lagrangian stochastic model is similar to the DEM model, which treats the particle as a discrete phase. This model simulates the dust dispersion by tracking particles as a group that is released continuously or instantaneously from the source (Wilson, 2000). The Lagrangian formulation for particle dispersion assumes that the particle's trajectory is affected both by the fluid phase and the particle velocity. The particle velocity is governed by the inertia and drift velocity of particles. The particle location is an unknown nonlinear function related to its velocity. Snyder and Lumley (1971) indicated that the Lagrangian particle velocity correlation, which describes the time evolution of particle velocity obtained by solving the dynamic equations of motion, does not have a general exact solution. However, using particle velocity correlation, this model can monitor the overall dust cloud concentration and deposition status.

The Eulerian method uses the single-fluid model by coupling momentum and turbulence equations into the particle concentration equations. This model treated the particle phase as a modified scalar species, and the particle phase transport equation is defined as:

$$\frac{d\rho C}{dt} + \frac{d\rho u_i C - \Gamma \frac{dC}{dx_i}}{dx_i} = S_c \quad 2.11$$

where C is the particle concentration; x_i are the three coordinates for $i=1, 2,$ and 3 ; u_i is the air velocity in three directions; S_c is the particle source term; and Γ is the effective particle diffusivity. Γ is defined as follows:

$$\Gamma = \rho(D + v_p) \quad 2.12$$

where D and v_p are the Brownian diffusivity of particles and the particle turbulent diffusion coefficient, respectively.

The selection of either the DEM or the Eulerian method depends significantly on the type of problem. The Eulerian method is better for studying suspended particle concentrations in indoor

environments. Zhang and Chen (2007) reported that for an unsteady particle dispersion and transport with a limited number of particles, it is difficult for the Eulerian method to converge and the result is longer simulation times. The DEM simulation offers the advantage of monitoring the motion of individual particles (Liu et al., 2013). The DEM model can deal with various particle attributes, such as, dense particles and a wide range of particle sizes. In the last couple of decades, the DEM modeling approach has been improved extensively; however, it is still the most computational expensive approach to simulate particle concentrations.

Other models that have been developed to study environmental air quality include numerical regional-scale air-quality models (such as the three-dimensional numerical photochemical air quality simulation models) and Gaussian dispersion models.

Numerical air-quality models are based on the mass balance during particle transport and are also called box models. Switzer and Ott (1992) derived the general mass balance equation for particles in an indoor environment with a known particle emission rate (g), effective air exchange rate (∂_e) and ventilatory air exchange rate (∂_v) of particles, dimensionless penetration factor (p), and volume of the indoor environment (V), as follows:

$$\frac{\Delta x}{T \partial_e} + \bar{x} = \frac{p \partial_v}{\partial_e} * \bar{x} \bar{o} + \frac{g}{V \partial_e} \quad 2.13$$

where the left-hand side is the mass inside the microenvironment and the right-hand side is the emission particle mass (Switzer and Ott, 1992). This modeling method requires immense information on the emission such as the exact effective and ventilatory air exchange rate; therefore, it is not accurate when there are changes in airflow and rate of emission.

Gaussian models mostly use plume and puff dispersion models, which are always nested within the Lagrangian and Eulerian models (Crowl and Louvar, 2001). The puff model is used for the instantaneous emission and the plume model is used to describe the continuous release of materials. These models are generally used for gas; however, they can also be used for studying dust emission under certain conditions, similar to the Eulerian model. The limitations of the Gaussian models are that they are not accurate when the dispersion occurs under low wind conditions or for the dispersion at sites close to the source, i.e., distances less than 100 m. Therefore, this method is a simplified treatment of turbulence and meteorology, and it is used for predicting the overall dust cloud location.

The Eulerian–Lagrangian approach is mostly used to predict the dust dispersion in standard explosion testing vessels. Murillo et al., (2013) simulated the Aluminum dust dispersion in a modified Hartmann tube using the Eulerian–Lagrangian approach. They used the Reynolds Stress Model to describe the fluid phase and the DPM to describe the particle size distribution. They concluded that the geometry and air injection are important characteristics that influence the airflow development during dust dispersion. Di et al., (2013, 2014) simulated dust dispersion in a 20 L standard explosion vessel, and found out that the larger sized dust particles are more likely concentrated at the vessel wall and move independent from airflow, and with the increase in concentration, the deposition prevails and the dust is mainly concentrated at the vessel walls. Particle density and shape also affect the particle distribution significantly in a confined space (Portarapillo, 2020). Cuervo et al., (2014) used the Euler-Lagrange simulation to optimize the dust explosion test. Their model gave a good prediction of the particle velocities and turbulence levels compared with values measured by Particle Image Velocimetry. Using this model, the author described the effect of initial turbulence on the homogeneity of the dust dispersion within the vessel.

The low computational intensity and high accuracy of the Lagrangian approach has helped with simulating the particle phase in dispersion of dust from shockwaves. However, the Eulerian-Lagrangian approach is still not used very much for predicting behavior of the fluid and particle phases from shockwave dust dispersion. Shimura and Matsuo (2019) used the two-dimensional CFD-DEM to predict the dispersion of the settled dust layer and combustion resulting from a shock wave in a narrow channel and found that the dispersed particles tend to attenuate the shock waves that are generated by the reaction front. Kosinski and Hoffman (2007) applied Eulerian–Lagrangian methods and showed that the particle-particle collisions and particle-wall (the value of coefficient of restitution) are important in determining dust re-suspended by shock waves.

In actual conditions of dust dispersion in an industry, the environmental conditions are complex. Therefore, the numerical air quality model and Eulerian model are not suitable for predicting the particle movement. The Lagrangian model has advantages of coupling the air and particle phase, and it is able to predict detailed particle movement. Instead of single-particle tracking, using a group of particles to calculate the trajectory can further save computational time. Therefore, the Lagrangian model is used in this dissertation work.

2.3 Optical Properties of Dust

Real-time monitoring systems for suspended dust concentration measurement are expensive, and the industry has constantly been attempting to develop more cost-effective safety measures (Eckhoff, 2005). Economically efficient real-time monitoring systems are the desired solution for dust explosion control. Currently, dust concentration measurements are calculated either by using the gravitational method or the laser scattering method. The gravitational method requires the sampling of air, which introduces bias when particles are diffused onto the sampler's wall boundaries. Filters are also required for accuracy. The laser scattering method provides mass distribution with a default particle density of 1000 kg/m^3 (Hinds, 1999). The dust explosive concentration is expressed as mass per volume; therefore, it fails to consider the particle's true density, which leads to inaccuracy. The explosive concentration measurement method proposed by Conti et al. (1981), which uses, for example, a laser method, does not require sampling; however, it must be calibrated before every use. Furthermore, owing to its narrow measurement area, the probe can only measure the concentration at a particular point, rather than the space concentration in a large space. In summary, dust concentration sensors that are economically efficient, easy to use and maintain, and highly mobile, capable of sensing a relatively large test area, must be developed. The bias caused by the sampling of air should also be minimized. In this section, background information on suspended dust concentration measurement, and particle light scattering properties are reviewed.

2.3.1 Particle scattering theory

The scattering of electromagnetic waves by any system depends on the heterogeneity of that system. Regardless of heterogeneity, the principle of scattering is similar in all the systems. For example, when a particle composed of electrons and protons is illuminated by an electromagnetic wave, the incident light will set the electric charge into oscillatory motion. The oscillatory motion of the electric charges on the particles surface will then radiate electromagnetic energy in all directions, as shown in figure 2.3. This is called particle scattering (scattering = excitation + reradiation). In addition to reradiating electromagnetic energy, some incident light may be transformed into other forms (such as thermal energy) and this process is called absorption.

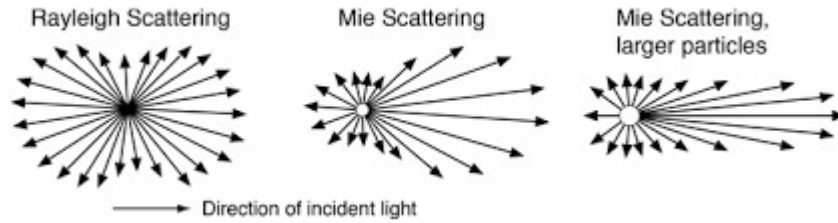


Figure 2.5 Particle light scattering process (Source: Bohren, 2004)

In light scattering theory, scattering due to density fluctuations in optically dense media is not considered. This review focuses on the interaction of light with a single particle and the dust cloud. Further, the effects of particle morphology and surface roughness on light scattering is presented. The scattered light depends on the geometrical factors such as scattering direction, size, and shape. The particle composition also affects light absorption and scattering.

The factors that affect the absorption and scattering of light by a particle are the wavelength of the incident radiation (λ), the particle size, and refractive index of the particle. In scattering theory, particle size (α) is given as $\alpha = \frac{\pi D}{\lambda}$, where D is the particle diameter. Scattering depends on the ratio of particle size to the light wavelength. The theoretical particle sizes and corresponding type of scattering are listed in Table 2.3 and the scattering process is shown in Figure 2.5.

Table 2.3 Atmospheric particle sizes of different forms of water particles in the atmosphere (Source: Kaushal and Kaddoum, 2017)

Type	Radius (μm)	Scattering Process
Air Molecules	0.0001	Rayleigh
Haze	0.01 – 1	Rayleigh – Mie
Fog	1 – 20	Mie - Geometrical
Rain	100-10000	Mie - Geometrical
Snow	1000-5000	Geometrical
Hail	5000-50000	Geometrical

If the molecules are not spherical, orientation fluctuations will occur. Radney et al. (2014) found that mass-specific absorption is independent of morphology; however, mass-specific extinction depends on the morphology. Thus, the particle shape affects light scattering, but the absorption depends more on the chemical composition and size. For example, sulfate, organic

carbon (OC), and nitrate species are usually considered the most important species for particulate light scattering (Omar et al., 1999).

The surface roughness also affects particle light scattering. Fan et al., (2014) found that smaller particles are less affected by the surface roughness; however, for a particle with $\alpha > 15$, the roughness will change the particle's light scattering properties.

2.3.2 Light extinction coefficient

Incident light energy decreases when passing through one or more dust particles, which results in the extinction of the incident beam. Light is either scattered or absorbed by the particles (Extinction = Absorption + Scattering).

The relationship between the extinction coefficient and light intensity is described by the Lambert-Beer law:

$$\frac{I}{I_0} = e^{-\sigma_e L} \quad 2.14$$

where I and I_0 are the light intensities before and after passing through the dust cloud, respectively, σ_e is the extinction coefficient, and L is the path length of the light passing through the dust cloud.

In most cases, to calculate the extinction of light, the particles suspended in the air are considered independently for light scattering and absorption. The particle in the air differed in composition, size, and shape. The differences have to be considered when calculating the extinction of light. The particle arrangement in the air is described as:

$$\sigma_e = \sum_{\alpha} n_{\alpha} \sigma_e^{\alpha} \quad 2.15$$

where n_{α} is the number of each type of particles in a unit volume of the air and σ_e^{α} is the extinction efficiency of particle α . This approach is called independent scattering approximation, and has been used to study a small concentration of dust. Dick and Ivanov (1999) also found that this approach can be used for calculating the extinction coefficient of the dense particle with relatively small particle size.

The extinction efficiency is highly dependent on the particle size and materials, as the scattering process depends on particle size (Figure 2.5), and the absorption is mostly dependent on the chemical composition. Similar types of particles have the same extinction efficiency, and the light extinction coefficient is the sum of all the extinction efficiency of all the types of particles

(Equation 2.15). When particles are suspended in the air, the extinction coefficient of the light will be affected by the change in the number of particles in the light path. Therefore, the relationship between the number of suspended particles and the extinction coefficient can be used to measure the concentration of suspended dust in the air.

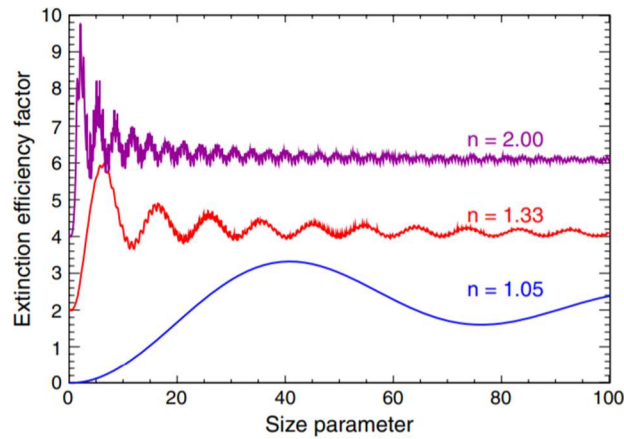


Figure 2.6 Relation between extinction efficiency and particle size (Source: Louedec and Urban, 2012)

The studies mentioned above explain how suspended particles affect the light intensity and the theory behind particle scattering and extinction. Dust dispersion is dependent on the processing conditions and studying the dispersion of dust is needed to develop an appropriate dust explosion prevention strategy. Therefore, the aim of this dissertation is to develop a model to simulate dust dispersion and to study the relationship between light extinction and suspended dust concentration.

2.4 References

- Addai, E. K., Gabel, D., & Krause, U. (2016). Experimental investigations of the minimum ignition energy and the minimum ignition temperature of inert and combustible dust cloud mixtures. *Journal of Hazardous Materials*, 307, 302-311.
- Amyotte, P. R., Chippett, S., & Pegg, M. J. (1988). Effects of turbulence on dust explosions. *Progress in Energy and Combustion Science*, 14(4), 293-310.

- ASTM (1987) ASTM Test E789-86 Standard test method for pressure and rate of pressure rise for dust explosions in a 1.2-litre closed cylindrical vessel (3rd Edn), Annual Book of ASTM Standards 14.02, American Society for Testing and Materials, Philadelphia , 680-699
- Bagaria, P., Prasad, S., Sun, J., Bellair, R., & Mashuga, C. (2019). Effect of particle morphology on dust minimum ignition energy. *Powder Technology*, 355, 1-6.
- Bartknecht, W. (1979). *Explosionen - Ablaut und Schutzmaßnahmen*. Von. Chemie Ingenieur Technik, Springer-V.
- Bernard, S., Lebecki, K., Gillard, P., Youinou, L., & Baudry, G. (2010). Statistical method for the determination of the ignition energy of dust cloud-experimental validation. *Journal of Loss Prevention in the Process Industries*, 23(3), 404-411.
- Boac, J. M., Maghirang, R. G., Casada, M. E., Wilson, J. D., & Jung, Y. S., (2009). Size distribution and rate of dust generated during grain elevator handling. *Applied Engineering in Agriculture*. 25(4), 533-541.
- Bohren, C. F., & Huffman, D. R. (2008). *Absorption and scattering of light by small particles*. John Wiley & Sons. New York, NY.
- Bouillard, J., Vignes, A., Dufaud, O., Perrin, L., & Thomas, D. (2010). Ignition and explosion risks of nanopowders. *Journal of Hazardous Materials*, 181(1-3), 873-880.
- Calvert, G., Ghadiri, M., & Tweedie, R., (2009). Aerodynamic dispersion of cohesive powders: a review of understanding and technology. *Advanced Powder Technology* 20(1), 4-16.
- Cao, W., Huang, L., Zhang, J., Xu, S., Qiu, S., & Pan, F. (2012). Research on characteristic parameters of coal-dust explosion. *Procedia Engineering*, 45, 442-447.
- Cashdollar, K. L. (1994). Flammability of metals and other elemental dust clouds. *Process Safety Progress*, 13(3), 139-145.
- Cashdollar, K. L. (2000). Overview of dust explosibility characteristics. *Journal of Loss Prevention in the Process Industries*, 13(3-5), 183-199.
- Cashdollar, K. L., & Chatrathi, K. (1993). Minimum explosible dust concentrations measured in 20-L and 1-m³ chambers. *Combustion Science and Technology*, 87(1-6), 157-171.
- Cesana, C., & Siwek, R. (2001). MIKE 3. Minimum Ignition Energy, B021_033, Adolf Kühner AG, Birsfelden, Switzerland.
- Cheng, N. S. (2009). Comparison of formulas for drag coefficient and settling velocity of spherical particles. *Powder Technology*, 189(3), 395-398.

- Conti, M., Geremia, R., Adamo, S., & Stefanini, M. (1981). Regulation of Sertoli cell cyclic adenosine 3': 5' monophosphate phosphodiesterase activity by follicle stimulating hormone and dibutyryl cyclic AMP. *Biochemical and Biophysical Research Communications*, 98(4), 1044-1050.
- Crowl, D. A., & Louvar, J. F. (2001). *Chemical process safety: fundamentals with applications*. Pearson Education.
- CSB. (2017). CSB dust incident 2006-2017 U.S. Chemical Safety and Hazard Investigation Board, Washington, DC. Retrieved from: https://www.csb.gov/assets/1/6/csb_dust_incidents.pdf
- CSB, (2006). CSB Investigation report – Combustible dust hazard study, Report No. 2006-H-1 U.S. Chemical Safety and Hazard Investigation Board, Washington, DC. Retrieved from: <https://www.csb.gov/file.aspx?DocumentId=5733>
- CSB. (2005). CSB Investigation report - Combustible dust fire and explosions, Report No. 2003-09-I-KY. Chemical Safety and Hazard Investigation Board, Washington, DC. Retrieved from: <https://www.csb.gov/file.aspx?DocumentId=5588>
- Cuervo, N., CM, O. D., Bardin, N., Monnier, S. S. L., Rémy, J. F., Auzolle, P., & Perrin, L. (2014). Combining CFD simulations and PIV measurements to optimize the conditions for dust explosion tests. *Chemical Engineering*, 36.
- Di Benedetto, A., Di Sarli, V., & Russo, P. (2010). On the determination of the minimum ignition temperature for dust/air mixtures. *Chemical Engineering Transactions*, 19, 189-194.
- Di Sarli, V., Russo, P., Sanchirico, R., & Di Benedetto, A. (2014). CFD simulations of dust dispersion in the 20 L vessel: Effect of nominal dust concentration. *Journal of Loss Prevention in the Process Industries*, 27, 8-12.
- Di Sarli, V., Russo, P., Sanchirico, R., & Di Benedetto, A. (2013). CFD simulations of the effect of dust diameter on the dispersion in the 20 L bomb. *Chemical Engineering*, 31.
- Dick, V. P., & Ivanov, A. P. (1999). Extinction of light in dispersive media with high particle concentrations: applicability limits of the interference approximation. *Journal of the Optical Society of America A*, 16(5), 1034-1039.
- Dobashi, R. (2009). Risk of dust explosions of combustible nanomaterials. In *Journal of Physics: Conference Series* (Vol. 170, No. 1, p. 012029). IOP Publishing.
- Eckhoff, R. K. (2005). Current status and expected future trends in dust explosion research. *Journal of Loss Prevention in the Process Industries*, 18(4-6), 225-237.

- Eckhoff, R. K. (2012). Does the dust explosion risk increase when moving from μm -particle powders to powders of nm-particles?. *Journal of Loss Prevention in the Process Industries*, 25(3), 448-459.
- Eckhoff, R. K., Fuhre, K., & Pedersen, G. H. (1987). Dust explosion experiments in a vented 236 m³ silo cell. *Journal of Occupational Accidents*, 9(3), 161-175.
- Edri, I., Savir, Z., Feldgun, V. R., Karinski, Y. S., & Yankelevsky, D. Z. (2011). On blast pressure analysis due to a partially confined explosion: I. Experimental studies. *International Journal of Protective Structures*, 2(1), 1-20.
- EN 13821: 2002. (2002). Explosion prevention and protection determination of minimum ignition energy of dust/air mixtures. European Standard 11–21.
- Fan, X., Zheng, W., & Singh, D. J. (2014). Light scattering and surface plasmons on small spherical particles. *Light: Science & Applications*, 3(6), e179-e179.
- Geldart, D. (1973). Types of gas fluidization. *Powder technology*, 7(5), 285-292.
- Glarner, T. (1984). Mindestzündenergie-Einfluss der Temperatur. *VDI-Berichte*, 494, 109-118.
- Hauert, F., Vogl, A., & Radandt, S. (1996). Dust cloud characterization and its influence on the pressure-time-history in silos. *Process Safety Progress*, 15(3), 178-184.
- Hinds, W. C. (1999). *Aerosol technology: properties, behavior, and measurement of airborne particles*. John Wiley & Sons. New York, NY.
- Holbrow, P., Andrews, S., & Lunn, G. A. (1996). Dust explosions in interconnected vented vessels. *Journal of Loss Prevention in the Process Industries*, 9(1), 91-103.
- Holbrow, P., Lunn, G. A., & Tyldesley, A. (1999). Dust explosion protection in linked vessels: guidance for containment and venting. *Journal of Loss Prevention in the Process Industries*, 12(3), 227-234.
- Hosseinzadeh, S., Berghmans, J., Degreve, J., & Verplaetsen, F. (2019). A model for the minimum ignition energy of dust clouds. *Process Safety and Environmental Protection*, 121, 43-49.
- Huang, Y., Risha, G., Yang, V., & Yetter, R. (2006, January). Flame propagation in bimodal nano/micro-sized aluminum particles/air mixtures. In *44th AIAA Aerospace Sciences Meeting and Exhibit*. American Institute of Aeronautics and Astronautics Inc, Reston, VA, 1155.

- Janes, A., Chaineaux, J., Carson, D., & Le Lore, P. A. (2008). MIKE 3 versus HARTMANN apparatus: Comparison of measured minimum ignition energy (MIE). *Journal of Hazardous Materials*, 152(1), 32-39.
- Jange, C. G., & Ambrose, R. K. (2019). Effect of surface compositional difference on powder flow properties. *Powder Technology*, 344, 363-372.
- Kauffman, C. W., Srinath, S. R., Tezok, F. I., Nicholls, J. A., & Sichel, M. (1985, January). Turbulent and accelerating dust flames. In *Symposium (International) on Combustion*. The Combustion Institute, Pittsburgh, PA, 20(1), 1701-1708.
- Kaushal, H., & Kaddoum, G. (2016). Optical communication in space: challenges and mitigation techniques. *IEEE Communications Surveys & Tutorials*, 19(1), 57-96.
- Kosinski, P., & Hoffmann, A. C. (2007). An Eulerian–Lagrangian model for dense particle clouds. *Computers & Fluids*, 36(4), 714-723.
- Kuai, N., Huang, W., Du, B., Yuan, J., Li, Z., Gan, Y., & Tan, J. (2013). Experiment-based investigations on the effect of ignition energy on dust explosion behaviors. *Journal of Loss Prevention in the Process Industries*, 26(4), 869-877.
- Leith, D. (1987). Drag on nonspherical objects. *Aerosol science and technology*, 6(2), 153-161.
- Liu, Q., Bai, C., Li, X., Jiang, L., & Dai, W. (2010). Coal dust/air explosions in a large-scale tube. *Fuel*, 89(2), 329-335.
- Liu, D., Bu, C., & Chen, X. (2013). Development and test of CFD–DEM model for complex geometry: A coupling algorithm for Fluent and DEM. *Computers & Chemical Engineering*, 58, 260-268.
- Louedec, K., & Urban, M. (2012). Ramsauer approach for light scattering on nonabsorbing spherical particles and application to the Henyey–Greenstein phase function. *Applied Optics*, 51(32), 7842-7852.
- Maremonti, M., Russo, G., Salzano, E., & Tufano, V. (1999). Numerical simulation of gas explosions in linked vessels. *Journal of Loss Prevention in the Process Industries*, 12(3), 189-194.
- Marmo, L., & Cavallero, D. (2008). Minimum ignition energy of nylon fibres. *Journal of Loss Prevention in the Process Industries*, 21(5), 512-517.
- Maxey, M. R. (1987). The motion of small spherical particles in a cellular flow field. *The Physics of fluids*, 30(7), 1915-1928.

- Mintz, K. J. (1993). Upper explosive limit of dusts: experimental evidence for its existence under certain circumstances. *Combustion and Flame*, 94(1-2), 125-130.
- Murillo, C., Dufaud, O., Bardin-Monnier, N., López, O., Munoz, F., & Perrin, L. (2013). Dust explosions: CFD modeling as a tool to characterize the relevant parameters of the dust dispersion. *Chemical Engineering Science*, 104, 103-116.
- National Fire Protection Association. (2002). NFPA 484: Standard for Combustible Metals, Metal Powders and Metal Dusts. National Fire Protection Association. Quincy, MA
- National Fire Protection Association. (2005). NFPA 654: Standard for the Prevention of Fire and Dust Explosions from the Manufacturing, Processing, and Handling of Combustible Particulate Solids. National Fire Protection Association. Quincy, MA.
- National Fire Protection Association. (2007). NFPA 68: Standard on explosion protection by deflagration venting. National Fire Protection Association. Quincy, MA
- National Fire Protection Association. NFPA 850. Recommended Practice for Fire Protection for Electric Generating Plants and High Voltage Direct Current Converter Stations. National Fire Protection Association. Quincy, MA.
- National Fire Protection Association. (2008). NFPA 61. Standard for the Prevention of Fires and Dust Explosions in Agricultural and Food Processing Facilities. National Fire Protection Association. Quincy, MA.
- Omar, A. H., Biegalski, S., Larson, S. M., & Landsberger, S. (1999). Particulate contributions to light extinction and local forcing at a rural Illinois site. *Atmospheric Environment*, 33(17), 2637-2646.
- Occupational Safety and Health Administration. (2009) OSHA Standard 29 CFR Part 1910, Combustible Dust, Department of Labor, Washington D.C.
- Occupational Safety and Health Administration. (2003) OSHA Standard 29 CFR 1910.272, Grain Handling Facilities, Department of Labor, Washington D.C.
- Occupational Safety and Health Administration. (2005). Safety and Health Information Bulletin. Combustible Dust in Industry: Preventing and Mitigating the Effects of Fire and Explosion. Department of Labor, Washington D.C.
- Phylaktou, H., & Andrews, G. E. (1993). Gas explosions in linked vessels. *Journal of Loss Prevention in the Process Industries*, 6(1), 15-19.

- Pilão, R., Ramalho, E., & Pinho, C. (2006). Overall characterization of cork dust explosion. *Journal of Hazardous Materials*, 133(1-3), 183-195.
- Portarapillo, M., Di Sarli, V., Sanchirico, R., & Di Benedetto, A. (2020). CFD Simulation of the Dispersion of Binary Dust Mixtures in the 20 L Vessel. *Journal of Loss Prevention in the Process Industries*, 104231.
- Radney, J. G., You, R., Ma, X., Conny, J. M., Zachariah, M. R., Hodges, J. T., & Zangmeister, C. D. (2014). Dependence of soot optical properties on particle morphology: measurements and model comparisons. *Environmental Science & Technology*, 48(6), 3169-3176.
- Razus, D., Oancea, D., Chirila, F., & Ionescu, N. I. (2003). Transmission of an explosion between linked vessels. *Fire Safety Journal*, 38(2), 147-163.
- Rumpf, H. (1958). Grundlagen und methoden des granulierens. *Chemie Ingenieur Technik*, 30(3), 144-158.
- Salamonowicz, Z., Kotowski, M., Półka, M., & Barnat, W. (2015). Numerical simulation of dust explosion in the spherical 20l vessel. *Bulletin of the Polish Academy of Sciences. Technical Sciences*, 63(1).
- Sapko, M. J., Weiss, E. S., Cashdollar, K. L., & Zlochower, I. A. (2000). Experimental mine and laboratory dust explosion research at NIOSH. *Journal of Loss Prevention in the Process Industries*, 13(3-5), 229-242.
- Shimura, K., & Matsuo, A. (2019). Using an extended CFD-DEM for the two-dimensional simulation of shock-induced layered coal-dust combustion in a narrow channel. *Proceedings of the Combustion Institute, Pittsburgh, PA*. 37(3), 3677-3684.
- Siwek, R. (1977). 20-L Laborapparatur für die Bestimmung der Explosionskenngrößen brennbarer Stäube. In *Diploma Dissert. Technikum Winterthur, Switzerland*.
- Snyder, W. H., & Lumley, J. L. (1971). Some measurements of particle velocity autocorrelation functions in a turbulent flow. *Journal of Fluid Mechanics*, 48(1), 41-71.
- Sun, J. H., Dobashi, R., & Hirano, T. (2001). Temperature profile across the combustion zone propagating through an iron particle cloud. *Journal of Loss Prevention in the Process Industries*, 14(6), 463-467.
- Switzer, P., & Ott, W. (1992). Derivation of an indoor air averaging time model from the mass balance equation for the case of independent source inputs and fixed air exchange rates. *Journal of Exposure Analysis and Environmental Epidemiology*, 2(Suppl 2), 113-135.

- Tamanini, F., & Valiulis, J. V. (1996). Improved guidelines for the sizing of vents in dust explosions. *Journal of Loss Prevention in the Process Industries*, 9(1), 105-118.
- Thomas, G. O., Oakley, G., & Brenton, J. (1991). Influence of the morphology of lycopodium dust on its minimum ignition energy. *Combustion and Flame*, 85(3), 526.
- Tong, Z. B., Yang, R. Y., Chu, K. W., Yu, A. B., Adi, S., & Chan, H. K. (2010). Numerical study of the effects of particle size and polydispersity on the agglomerate dispersion in a cyclonic flow. *Chemical Engineering Journal*, 164(2-3), 432-441.
- Wang, L. P., & Stock, D. E. (1993). Dispersion of heavy particles by turbulent motion. *Journal of the Atmospheric Sciences*, 50(13), 1897-1913.
- Wells, A.C. and Chamberlain, A.C., (1967). Transport of small particles to vertical surfaces. *British Journal of Applied Physics*, 18(12), 1793.
- Wells, M. R., & Stock, D. E. (1983). The effects of crossing trajectories on the dispersion of particles in a turbulent flow. *Journal of fluid mechanics*, 136, 31-62.
- Weiler, C., Wolkenhauer, M., Trunk, M., & Langguth, P. (2010). New model describing the total dispersion of dry powder agglomerates. *Powder Technology*, 203(2), 248-253.
- Wilson, J. D. (2000). Trajectory models for heavy particles in atmospheric turbulence: comparison with observations. *Journal of Applied Meteorology*, 39(11), 1894-1912.
- Yuan, C., Amyotte, P. R., Hossain, M. N., & Li, C. (2014). Minimum ignition temperature of nano and micro Ti powder clouds in the presence of inert nano TiO₂ powder. *Journal of Hazardous Materials*, 275, 1-9.
- Yuan, Z., Khakzad, N., Khan, F., & Amyotte, P. (2016). Domino effect analysis of dust explosions using Bayesian networks. *Process Safety and Environmental Protection*, 100, 108-116.
- Zhang, Z., & Chen, Q. (2007). Comparison of the Eulerian and Lagrangian methods for predicting particle transport in enclosed spaces. *Atmospheric Environment*, 41(25), 5236-5248.

3. MODELING DUST DISPERSION AND SUSPENSION PATTERN UNDER TURBULENCE

This chapter was published in *Journal of Loss Prevention in the Process Industries*, Vol 62, Yumeng Zhao and R.P. Kingsly Ambrose, Modeling dust dispersion and suspension pattern under turbulence, 103934, Copyright Elsevier (Nov 2019)

Abstract

Controlling dust generation and minimizing volumetric dust concentration, within confined spaces, is key to the prevention of dust explosions. Dust dispersion patterns under pressure, such as a primary explosion or dust leakage from equipment, can be simulated using unsteady state computational fluid dynamics – discrete phase models (CFD-DPMs). Although they offer computational efficiency, DPM simulations do not incorporate particle-wall or particle-particle interactions. In this paper, we, therefore, adopt the model to include particle-wall interaction based on energy conservation. In a confined volume, to experimentally observe the dust dispersion pattern, theoretical concentrations of 0.05 and 0.10 kg/m³ were generated and the turbulence was created with airflows of 2 and 10 m/s using an air compressor. Similar conditions were used to model the dust dispersion pattern. Our findings show that the dust concentration inside the confined chamber is not evenly distributed throughout its entirety and that explosive dust cloud concentration only takes up to 37.8% of a chamber's volume for a 0.10 kg/m³ injected dust concentration at 10 m/s air velocity. With a decrease in the dust injection rate and air velocity, the dust cloud volume decreased due to a fewer number of particles and low kinetic energy. This study presents an efficient dust dispersion modeling method, and the result shows the dust cloud volume is highly dependent on the dispersion velocity. The predicted dust concentration and the experimental results indicate that this boundary corrected CFD-DPM modeling approach is suitable for dilute particle dispersion flow, where the volume fraction of particles is lower and the adhered particles only form a single particle layer on the wall boundary.

3.1 Introduction

A dust explosion is a rapid increase in pressure in a confined space that occurs when suspended particles are ignited resulting in sudden release of energy. Most industries that produce finely-divided combustible materials, including food powders, chemicals (aluminum, fertilizers, plastics, etc.), coal, and pharmaceutical powders, carry the risk of a dust explosion. The severity of the explosion is highly dependent upon the generation and turbulence of the dust and its morphological properties (Wypych et al., 2005; Benedetto et al., 2010). Understanding the parameters that can help with assessing the explosiveness of powders is an important part of helping people to control processing environments and reduce the risk of an explosion (Eckhoff, 2003; Dorsett and Jacobson, 1960).

When dust ignites, the explosions occur in two phases: a primary explosion; and a secondary explosion. A primary explosion is usually a small overpressure that propagates a pressure of approximately 2 psi (Jones, 1990; Parnell et al., 2013). Secondary explosions occur when settled dust particles are suspended and ignited by the primary explosion. These have been found to be far more damaging because of the rapid rise in pressure they can generate (Field, 2012). The U.S. Occupational Safety and Health Administration (OSHA) regulations have addressed dust safety issues and indicate ways to properly design and locate dust collection systems that could minimize explosion hazards (OSHA, 2011). However, because of the enormous variability in industrial processes where dust might be dispersed and the range of potential equipment involved, such as bucket elevators, pneumatic transport systems, fluidized beds, silos, etc., dust collection systems can be difficult to design in ways that will best offset the risk of dust explosions (Eckhoff, 2003). A fundamental understanding of airflow patterns and how particles will behave during any corresponding turbulence is essential to the installation of dust explosion suppression systems that are properly aligned with a wide variety of possible processing and/or handling conditions.

Dust particle size and shape, as the factors that contribute to the dust explosion, have been extensively studied during the past few decades (Calle et al., 2005). Eckhoff (2009) suggested that the degree of particle agglomeration, dust concentration in the cloud, and degree of turbulence in the suspended dust are some of the most important factors influencing dust explosions. Eckhoff (2009) argued that these elements should always be included when assessing dust explosion safety parameters. Building upon this, Carlos et al. (2013) indicated that the current standards do not always provide appropriate safety parameters for industrial environments, because they fail to

incorporate the key factors proposed by Eckhoff. The differences in dust explosion testing methods led to disagreement in safety parameters, due to the differences in dust dispersion pattern. When testing using the ASTM standards (American Society for Testing and Materials, E1515-07) and Center for Agricultural Air Quality Engineering and Science (CAAQES) methods, Parnell et al. (2013) obtained different minimum explosion concentration (MEC) values for corn starch and cotton gin dust. With many practical challenges, quantification of the parameters proposed by Eckhoff (2009) through experimental measurements remains problematic. So, there is a need for a mathematical model to predict dust dispersion under confined conditions by including the factors listed by Eckhoff in ways that will help to reveal the behavior of dust under complicated industrial process conditions.

The aerodynamic properties of particles and particle-particle/particle-wall interactions influence the dust dispersion characteristics. The nature of explosive dust cloud generation is determined by both the dust particles' physical properties and the dispersion process (Calvert et al., 2009). This makes the simulation of the dust dispersed by primary explosions or conveyor leaks complicated. Particle dispersion is currently simulated primarily by means of either the Discrete Element Method (DEM) or Discrete Particle Model (DPM) approaches. DEM is an accurate simulation method for particle-air two-phase conditions because it takes into account every single particle's movement and the force relating to both the discrete and fluid phases. DEM simulation detects the contact between every two particles, which is very time consuming and computationally intensive for a large number of aerosol particles that form a dust cloud (Mezhericher et al., 2011). By contrast, DPM tracks particles as a group, which reduces the computational time. Therefore, to simulate the large number of suspended particles that might exceed the minimum explosion concentration (MEC), the time and cost associated with DEM would render it completely impractical. The computational fluid dynamics (CFD) approach has been used by many researchers to study particle dispersion (Zhang and Chen, 2007; Mezhericher et al., 2011; Klippel, et al., 2014; Di Benedetto et al., 2013). CFD-DPM is able to provide a robust model for analyzing particle travel along with the airflow during dispersion (Zhang and Chen, 2007). A DPM model is capable of tracking the trajectory of particles using the conservation of force, thus significantly reducing the computational time. However, particle-wall interaction and inter-particle bonding affect the particle dispersion and settling pattern. Therefore, for DPMs to provide a reasonable prediction, particle-particle and particle-wall interactions need to be

introduced (Deen et al., 2007). This study investigates the usefulness of the CFD-DPM modeling approach for simulating dust dispersion patterns, under turbulence, with a specific interest in providing a robust model for quantifying a dust cloud suspension pattern and its concentration after a primary explosion or from dust leakage.

The objectives of this Chapter are to i) develop a coupled CFD-DPM model that can predict dust dispersion in confined conditions, under turbulence; and ii) validate the model experimentally in a confined condition. To achieve intended results, particle-wall interactions were built into the CFD-DPM model by using the conservation of energy approach when a particle collides with the wall. This allows the particles to either rebound or stick to the walls after the collision. The specific model developed here is referred to as a stick-rebound model.

3.2 Materials and Methods

3.2.1 CFD-DPM model development

CFD-DPM modeling, adopting Eulerian and Lagrangian approaches for the fluid and particle phases, respectively, was undertaken using ANSYS FLUENT (Ansys Inc., PA, USA).

3.2.1.1 Modeling fluid turbulence

To determine the effect of fluid turbulence on dust dispersion, the airflow inside the chamber was simulated by solving the Navier-Stokes (RANS) equation with a standard k- ϵ turbulence model. The RANS model offers a good compromise between accuracy and computational efficiency and is widely used for engineering applications (Zhang et al., 2007). In addition, because a low flow velocity was used in this study, the Reynolds number for the fluid phase was low as well. So, a standard k- ϵ turbulence model was able to provide a better prediction of the airflow inside the confined space (Zhang et al., 2007).

For an incompressible Newtonian fluid, momentum (Equation 3.1) and mass conservation (Equation 3.2) are used to characterize the fluid phase movement:

$$\frac{\partial \rho u}{\partial t} + \nabla \rho u u = -\nabla p + \nabla \tau + F \quad 3.1$$

$$\frac{\partial \rho}{\partial t} + \nabla \rho u = 0 \quad 3.2$$

where t is the time step, ρ is the air density, u is the airflow velocity, p is the static pressure, τ is the stress tensor, and F presents all the external body forces, where the total external body force includes the gravitational force. With two-way coupling, both the effect of the airflow on the particle and the momentums exchange from particle to continuous phase are computed.

The kinetic energy from turbulence (k), which describes the fluctuations in velocity, and the dissipation rate of k (ϵ), can be obtained using the following transport equations:

$$\frac{\partial \rho k}{\partial t} + \frac{\partial \rho k u_i}{\partial x_i} = \frac{\partial}{\partial x_i} \left[\left(\mu + \frac{\mu_t}{\sigma_k} \right) \frac{\partial k}{\partial x_i} \right] + G_k + G_b - \rho \epsilon - Y_m \quad 3.3$$

$$\frac{\partial \rho \epsilon}{\partial t} + \frac{\partial \rho \epsilon u_i}{\partial x_i} = \frac{\partial}{\partial x_i} \left[\left(\mu + \frac{\mu_t}{\sigma_\epsilon} \right) \frac{\partial \epsilon}{\partial x_i} \right] + C_{1\epsilon} \frac{\epsilon}{k} (G_k + C_{3\epsilon} G_b) - C_{2\epsilon} \rho \epsilon * \frac{\epsilon}{k} \quad 3.4$$

where, G_k represents the generation of turbulence kinetic energy due to the mean velocity gradients; G_b is the generation of turbulence kinetic energy due to buoyancy; $C_{1\epsilon}$, $C_{2\epsilon}$, and $C_{3\epsilon}$ are constants; σ_k and σ_ϵ are the turbulent Prandtl numbers for k and ϵ , respectively; Y_m is the contribution of the fluctuating dilatation incompressible turbulence to the overall dissipation rate; ρ is the air density; u_i is the air velocity and x_i is the position vector; t is the time step; μ is the molecular viscosity of the fluid and μ_t is the turbulent viscosity. Turbulence intensity was set as 3% and the turbulent length scale as 0.005 m based on the actual inlet nozzle diameter of 0.005 m. The initial gauge pressure was set at 1 atm.

3.2.1.2 Wall boundary conditions

The standard RANS model usually fails to predict the turbulence in the near-wall region. So, the built-in Enhanced-Wall treatment available from ANSYS FLUENT is used in this model development. The Reynolds number near the wall is defined as (ANSYS, 2015):

$$Re_y = \frac{\rho y \sqrt{k}}{\mu} \quad 3.5$$

where y is the wall-normal distance calculated from cell centers.

3.2.1.3 Particle tracking model

A discrete phase model can be constructed from the force balance on a particle using the following equation:

$$-\frac{du_p}{dt} = F_D(u - u_p) + \frac{g(\rho_p - \rho)}{\rho_p} + F_x \quad 3.6$$

where, F_x is an additional acceleration term, such as Brownian force, virtual mass, or lift force. According to ANSYS (2015), these forces are much smaller than the drag force for a dense particle

over 10 μm in size, so they can be neglected in order to simplify the model. u_p is the particle velocity, ρ_p is the particle density, g is the gravitational force, and F_D is the drag force per unit of particle mass which can be calculated using equation 3.5 below:

$$F_D = \frac{18\mu}{\rho_p d_p^2} \frac{C_D R_{ep}}{24} \quad 3.7$$

$$R_{ep} \equiv \frac{\rho d_p |u_p - u|}{\mu} \quad 3.8$$

where, d_p is the particle diameter, C_D is the drag coefficient and R_{ep} is the particle's Reynolds number.

The model treats a group of particles as a parcel and calculates the parcel's trajectory based on single-particle physical characteristics. The parcels are injected from the nozzle face from 1000 streams, and the initial velocity of the particle is 0 m/s. The time step of the DPM model was kept the same as the fluid phase simulation. The turbulent dispersion of particles was modeled by stochastic tracking, where the particle drag force was calculated using the instantaneous fluid velocity.

3.2.1.4 *Stick-rebound model*

The particle-wall stick-rebound model was implemented using user-defined functions (UDF). When a particle hits the wall, the particle-wall adhesion force results in energy dissipation because of the particle-wall contact. Thus, the principle of conservation of energy for an incoming particle that rebounds from or adheres to a wall can be expressed as (Wang and Kasper, 1991):

$$Ke_i = Ke_r + E_{ad} + E_L \quad 3.9$$

where, Ke_i and Ke_r are the kinetic energy for the arriving and rebounding stages, respectively, which depend on the particle velocity, $Ke = \frac{1}{2} m u_p^2$, where m is a single particle's mass; E_{ad} is the particle-wall adhesion energy; and E_L is the energy lost due to elastic deformation. The rebound energy, Ke_r , will be equal to 0 when a rebound does not occur. Thus, the critical particle velocity for a rebound can be determined by the energy balance, where $Ke_i = E_{ad} + E_L$. E_{ad} is the energy dissipated by the adhesion force from the wall to the particle. During the particle-wall interaction, the Van der Waals force is considered to be the main adhesion force (F_{ad}):

$$F_{ad} = \frac{A d_p}{Z^2 12} \quad 3.10$$

where A is the Hamaker constant. The Hamaker constant between two dissimilar materials with their own Hamaker constants A_1 and A_2 is given as, $A = \sqrt{A_1 * A_2}$. Z is the distance of the closest approach between the surfaces, commonly set to 0.4 nm (Wang and Kasper, 1991). In this study, A for the interaction between a cornstarch particle and a silicon wafer equals 1.31×10^{-19} J (Hein, et al. 2002). The cornstarch particles have high elasticity (Ilić et al., 2013). The single particle's plastic deformation yield strength is rarely studied, so the plastic deformation of the particle was not considered in this study.

The critical particle rebound velocity, when $Ke_r = 0$, can be calculated using the particle's kinetic energy and adhesion force:

$$V_{cr} = \left(\frac{A}{\pi \rho Z d^2} \right)^{0.5} \quad 3.11$$

A particle rebounding after a wall impact will have a rebound velocity, V_r , that is normal to the wall and can be calculated from the rebound kinetic energy:

$$V_r = \sqrt{\frac{Ke - E_{ad}}{\frac{1}{2} * m}} \quad 3.12$$

The particle volume fraction was high at the dust injection inlet (*section 3.2.1.5*) due to the high concentration of dust during the injection. Under these conditions, the effect of the particles on the turbulent flow needs to be taken into account. Thus, the interaction between the particles and the airflow was treated as being 2-way coupled in this simulation (Elghobashi, 1994). Figure 3.1 shows the schematic representation of the simulation approach used in this study. The models used in the study are described in the subsequent sections. The assumptions used in this model development are:

- i) The particles are uniform in size (12 μm). This assumption was made based on the measured average particle size.
- ii) There is no inter-particulate interaction during dispersion.
- iii) The electrostatic force between the particles does not affect the dispersion
- iv) Plastic deformation of particles does not occur during the dispersion process.
- v) The tangential energy loss through static friction does not influence the dispersion process with an assumption that the tangential velocity remains the same after rebounding.

The mathematical model was used to predict the dust dispersion and suspension in a confined chamber, made of 1/8 inch thick plexiglass, with a geometry of 0.30 m×0.30 m×0.45 m to which was attached with a dust dispersion unit consisting of an inlet nozzle diameter of 0.01 m (Figure 3.2). The powder was fed into the chamber through the funnel and dispersed by the airflow from the nozzle. The dispersion was stopped after all dust particles were dispersed, which took 0.5 s.

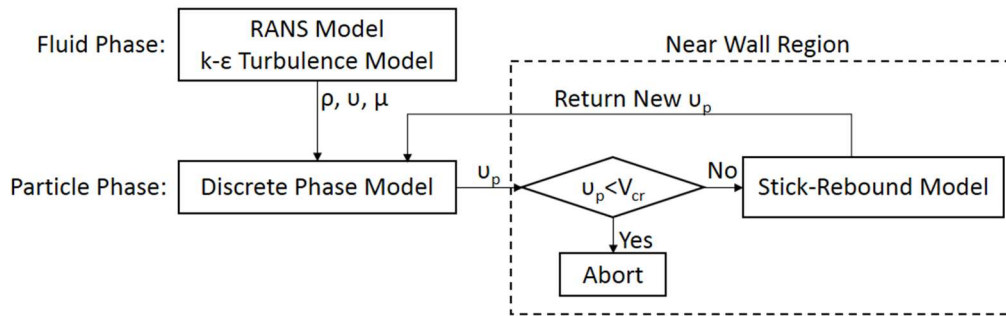


Figure 3.1 Schematic representation of the simulation approach

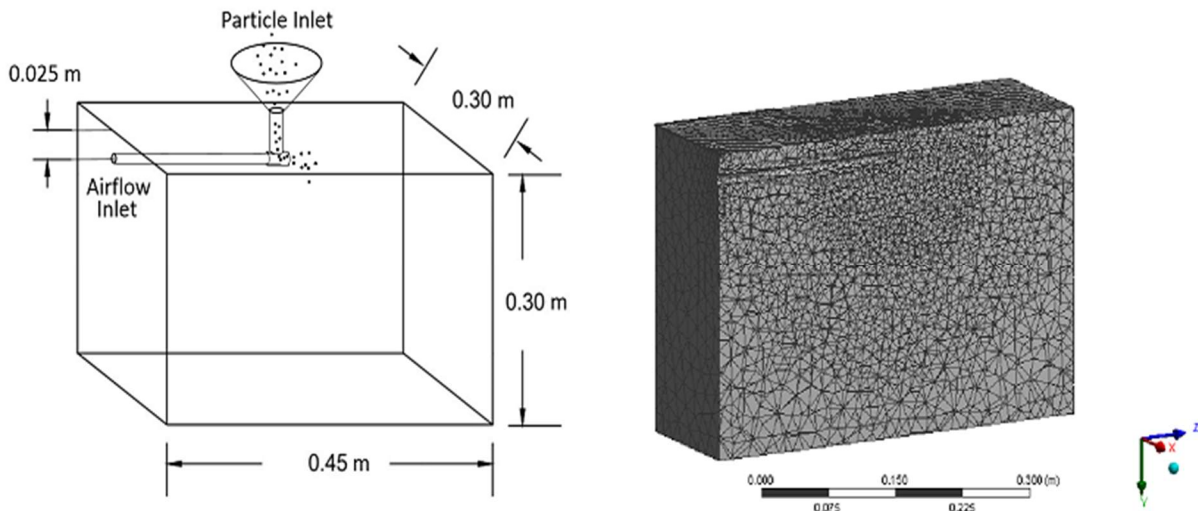


Figure 3.2 Dust dispersion chamber and mesh construction

3.2.1.5 Particle properties and other parameters used in the model development

Cornstarch was used as the dust medium in this study. The dispersion nozzle consisted of a tube and a plastic funnel. The tube with diameter of 0.005 m was connected to the air compressor,

and it was located 0.005 m below the top surface of the chamber. The dust particles were injected into the chamber through the funnel in the center of the top of the chamber. The particle density, ρ_p , was determined using an AccuPyc ii 1340 (Micromeritics Instrument Corp., Norcross, GA, USA). The particle size was measured using Morphologi G3-ID (Malvern Panalytical, Malvern, UK). Every single particle on the sample plate was scanned, and CE (circularity equivalent) diameter was obtained to obtain the cornstarch particle size number distribution. The average particle size was obtained based on number distribution. The terminal velocity, V_T , of a particle was calculated using Stoke's law given below:

$$V_T = \frac{\rho_p d_p^2 g}{18\mu} \quad 3.11$$

The physical properties of the corn starch particles used in this study are listed in Table 3.1. As the MEC of cornstarch is 0.04 kg/m³, the mass of cornstarch fed into the chamber (Figure 3.2) through the dispenser, was calculated on the basis of the chamber's volume. Theoretical dust concentrations of 0.05 and 0.10 kg/m³, where all the injected dust is fully suspended, were chosen based on the MEC of cornstarch. For a chamber volume of 4.05×10⁻² m³, the calculated mass dispersion rates were 0.0405 and 0.081 g/s, so that the dust inside the chamber after 0.5 s dispersion can reach concentration of 0.05 and 0.10 kg/m³, respectively.

The pressure rise during dust explosions happens in about 0.16 s (Maremonti et al., 1999). The flow velocity generated by the primary explosion depends not only on the pressure rise, but also upon the geometry. According to Kumar et al. (1992), the maximum overpressure from a corn starch explosion can reach up to 800 kPa. In this work, due to the limitations of the compressor used for experimental validation, a maximum pressure of 750 kPa was used. At this pressure, the measured dispersion velocity was 10 m/s. This value was obtained from the video recording of the dust dispersion process (described in section 3.2.2.3). A primary explosion will result in a lower overpressure. In this work, a lower pressure condition of 250 kPa was also tested, giving a dispersion velocity of 2 m/s.

For this simulation, the time step size was set at 0.001 s with 70 iterations per time step to achieve convergence at each repetition. Using the procedure described in the manual for the software, the time-step size was determined using the minimum cell size and the air velocity. It was set in an large value that met the requirement in order to keep the computational time as short as possible. Thus, in this study, the time step used was 0.001s. The unstructured and non-uniform

mesh was used in the simulation, which consisted of 127,822 cells (Figure 3.2). The size of the element for the fluid phase ranged from 9 mm near the nozzle to 15 mm in the rest of the dispersion chamber. The mesh has a minor effect on the DPM model (Zhang and Chen, 2007; Tarpagkou and Pantokratoras, 2013) since the particle trajectory was simulated by the force balance on particles. Inthavong et al., (2016) found that for particles larger than 20 nm, the diffusion effect caused by Brownian motion was relatively small, and the deposition rate is independent from mesh and timesteps. The simulation was conducted using an Intel Core I5-2400 CPU computer with 8G installed memory. The total computational time was 32 h to simulate 8 s of dust dispersion.

Table 3.1. Summary of particle properties and simulation parameters used in this study

Particle property/Parameter	Symbol	Value
Density of cornstarch particles (kg/m ³)	ρ_p	1491.9 (\pm 2.3)
Average diameter of a cornstarch particle (μ m)	d_p	11.49 (\pm 6.24)
Dust flow rate (kg/s)		0.0405, 0.0810 (corresponding to 0.05 and 0.10 kg/m ³ , respectively)
Airflow velocity (m/s)	u	2, 10
Gravitational acceleration (m/s ²)	g	9.81
Viscosity of air (Pa·s)	μ	$1.82 \cdot 10^{-5}$
Density of air (kg/m ³)	ρ_f	1.2047
Terminal velocity (m/s)	V_T	0.0058
Moisture content (% wet basis)	MC	9.1 ± 0.003
Ambient relative humidity (%)	RH	49.1 ± 1.1
Ambient temperature ($^{\circ}$ C)	T	20.6 ± 0.3

The dust concentration C in kg/m³ was calculated based on particle mass (g) in cell (M_c), particle residual time in cell Res (s), total particle flow rate Rf (kg/s), mesh cell volume V_m , (m³), and a single particle mass m (kg).

$$C = \frac{M_c * Res * Rf}{V_m m} \quad 3.12$$

The percent explosive dust volume was calculated from the cell volume with concentration exceeding the MEC of cornstarch, divided by the whole chamber volume (0.00405 m³).

3.2.2 Experimental validation

3.2.2.1 Dust sample and experimental chamber

The confined chamber described in section 3.2.1.5 was used to conduct the dust dispersion experiments (Figure 3.2). An air compressor was connected to the dispenser nozzle to produce airflow at the selected velocity (Table 3.1). During dispersion, the cornstarch was gradually fed into the chamber using the dispenser of radius 5 mm. For validation, similar to the simulation, the cornstarch was dispersed in 0.5 s.

3.2.2.2 Measuring the suspended dust concentration in the confined chamber

To measure the settled and/or the suspended dust, the dust dispersion chamber was placed on a weighing scale (Mettler Toledo SB8001, METTLER TOLEDO, Columbus, OH) with a sensitivity of 0.1 g. Four and eight grams of dust were dispersed in order to reach the theoretical concentrations of 0.05 and 0.10 kg/m³, respectively. The dust was fed into the chamber through the funnel and within 0.5 s it was dispersed by the air from the air compressor. The dispersion velocity was adjusted to either 2 or 10 m/s by changing the air pressure. After all the dust was dispersed, the compressed air was immediately shut down. The settled dust was weighed during the dispersion process. The amount of dust that settled 0.1, 0.2, 0.3, 0.4, and 0.5 s after dispersion was obtained from weigh scale readings, and the detailed data from the experiments are presented in Appendix A. The suspended dust was calculated by subtracting the mass of the settled dust from the dispersed dust. The 10 m/s airflow had a significant effect on the weighing scale measurements because of the airflow pressure on the chamber wall. The 2 m/s flow caused only minor changes in relation to the mass of the dust. Thus, just for the 10 m/s dispersion, the result was normalized by subtracting the scale reading error due to airflow. The scale reading due to airflow, without dust, was first obtained as a baseline. The settled dust weight was then calculated by subtracting the baseline value from the weighing scale readings.

3.2.2.3 Dust cloud distribution within the chamber

The dust cloud within the chamber was examined using image analysis. For this, a transparent chamber of the same size as described in Figure 3.2 was used. One face of the transparent chamber was fully covered using black paper as a background for imaging purposes. It was established in a preliminary experiment that cornstarch could be easily segmented from a black background because it scatters light and the photos of cornstarch has high intensity value. According to Beer-Lambert's law, the light intensity is linearly related to the suspended particle concentration (Ogle, 2016). Therefore, the intensity value distribution is representative of a dust cloud's suspension pattern and can help with the observation of the location of dust concentration

within the confined chamber. The dust dispersion process was video recorded using an iPhone 7 at 1080p resolution at a rate of 60 frames per second (fps). Individual frames were extracted from the recorded video to analyze the dust dispersion, suspension, and settling pattern. The frame before initiating the dust dispersion was treated as the background frame. Frames were chosen at 0.2, 0.4, and 0.6 s to assess the dispersion of the dust particles, their suspension, and the settling pattern. The extracted frames were converted to a hue, saturation, value (HSV) format, and the background was subtracted using MATLAB (The MathWorks, Inc., Natick, MA), to obtain the light intensity from the photos corresponding to the cornstarch. A contour plot of the intensity was then obtained for each frame. The suspended dust cloud location was then visualized from the contour plots and these plots were compared with the simulation results.

3.2.3 Data analysis

Each experiment was replicate three times for each air velocity and theoretical concentration.

The mean relative percent deviation (P%) and standard error (S. E.) were used to compare the predicted and experimental values.

$$P = \frac{100}{N} * \sum \frac{Y - Y_d}{Y_d} \quad 3.13$$

$$S. E. = \sqrt{\frac{\sum(Y - Y_d)^2}{df}} \quad 3.14$$

where Y is the measured concentration value, Y_d is the predicted concentration, df is the degrees of freedom, and N is the number of data points. The prediction error and standard error were calculated from dispersion times between 0.2 s to 0.5 s in order to exclude the error caused by the airflow at the start of the experiments at 0.1 s.

3.3 Results and Discussion

3.3.1 Simulated dust concentration

A dispersed dust concentration that reaches the MEC increases the probability of a secondary explosion. The dust cloud concentration is also one of the most important factors influencing an explosion's severity. The concentration during dust dispersion was therefore one of

the main parameters focused upon in the simulation. Figure 3.3 shows the simulated and experimental dust concentration as influenced by the air inlet velocity.

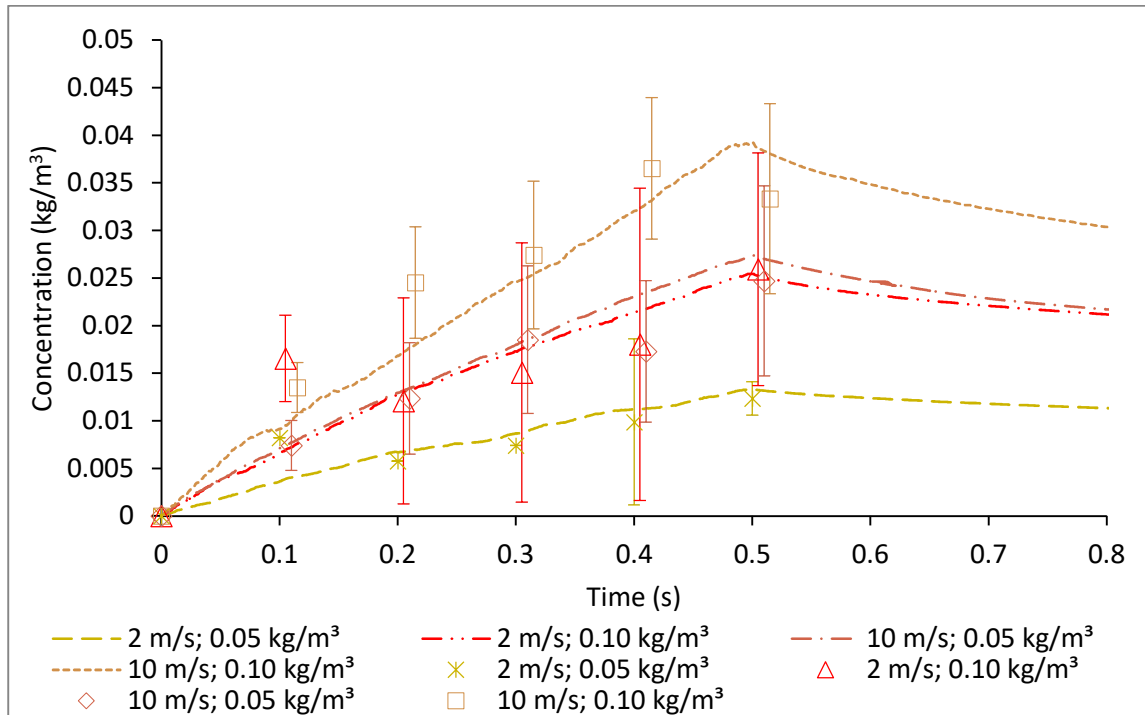


Figure 3.3 Simulated dust concentration using the stick-rebound model at various air velocities (the dashed lines represent the simulated concentration and the dots represent the experimental values. The experiment data is obtained at 0.1, 0.2, 0.3, 0.4, 0.5 s, data points are offset for better readability)

The cornstarch's terminal velocity calculated using equation 3.11, was 0.0058 m/s. So, without turbulence, the dust would have needed 52 s to settle from nozzle to the bottom of the chamber with distance of 0.3 m, theoretically. Thus, under ideal conditions and without taking wall-particle interaction or particle-particle interaction into account, after 0.5 s dispersion, the concentration should have reached the theoretical maximum concentrations of 0.05 or 0.10 kg/m³. However, the concentration inside the chamber did not reach the maximum theoretical concentration because of turbulence and particle-wall interaction effects.

The dust concentration during the experimental trials reached a peak value after all the dust had been dispersed, then decreased as the dust particles settled (Figure 3.3). At a 2 m/s dispersion velocity, the theoretical concentration of 0.05 kg/m³ of injected dust resulted in a real concentration of 0.0136 kg/m³, at its maximum. For 0.10 kg/m³ at 2 m/s, the real peak concentration was 0.0259

kg/m³. Doubling the injected dust mass led to a doubling of the peak concentration, as expected. However, doubling the injected dust mass, at a 10 m/s dispersion velocity did not double the peak concentration. For the theoretical concentration of 0.05 kg/m³, the real peak concentration was 0.0247 kg/m³. This value is only around 0.013 kg/m³ less than the 0.10 kg/m³ injection. The peak value at 10 m/s for the 0.10 kg/m³ injection was at 0.4 s instead of 0.5 s, which indicates that the particles were settling more quickly under this condition. Vreman et al. (2009) have shown that inter-particle effects can play an important role when the volume fractions are greater than 1.5% in a two-phase flow. When the particles were injected through the 5 mm radius dispenser, the particle injection rate was considered constant during dispersion. The volume fraction was calculated as the volume of particles injected divided by the volume of air per second. The calculated maximum volume fraction of the particles (during injection) was 1.58% at the volumetric dust concentration of 0.10 kg/m³. When there is a high particle volume fraction, inter-particle collisions will increase, so the kinetic energy will tend to decay faster due to particle-particle collisions. A 10 m/s injection also generates more turbulence than a 2 m/s injection, so this may also cause more inter-particle collisions. Thus, it can be concluded that the 0.10 kg/m³ concentration injected at 10 m/s would have had more inter-particle interactions and that this is one reason why the dust concentration was only slightly higher than the 0.05 kg/m³ injection.

When the dust concentration is compared for the same injection rate, the 0.05 kg/m³ injection had a peak concentration of 0.0132 kg/m³ at a 2 m/s dispersion velocity while the 10 m/s dispersion velocity gave a peak concentration of 0.0247 kg/m³. The same trend was noticed for the 0.10 kg/m³ volumetric dust injection. For the 2 m/s dispersion velocity experiments, the initial kinetic impulse given to the dust particles was lower than at the 10 m/s dispersion velocity, so the particles lost their kinetic energy and settled at a faster rate (Figure 3.3). As the dispersion velocity increased, the drag force from the fluid phase upon the dust particles increased, so the particles dispersed at 10 m/s had a better dispersion. This indicates that a primary explosion generates more turbulence, which could result in a stable dispersed dust cloud in the air when compared with minor turbulence such as created by sweeping the floor.

As the dust particles were very small and were subjected to higher magnitude surface forces, they tended to adhere to the wall and to the dispersion inlet. Thus, they did not always rebound after colliding with the wall and the stick-rebound-wall model is needed to generate more reliable simulation of dust dispersion. As can be seen in Figure 3.3, after all of the dust particles had been

dispersed inside the chamber, the maximum dispersed concentration was obtained at 0.5 s, then it decreased. This was the case because the injection rate was much higher than the dust settling rate.

Overall, the simulation using the stick-rebound model gave a good prediction of the dust dispersion process (Table 3.2). All simulations gave a good prediction of dispersed dust with relative percent deviation (P) under 10% except for 0.10 kg/m³ theoretical dust concentration at 10 m/s, where the simulation resulting in a P-value of 19.26. From Figure 3.3, it can be seen that the experimental concentration reached a peak value of 0.4 s. This could be because, when more particles were injected at a higher velocity, the probability of particle collisions increased, as did the particle settling rate because of the high energy loss caused by inter-particle collisions. At a high dust dispersion velocity and concentration, the particle collision and disintegration of agglomerates resulted in a larger prediction error. The DPM model simulates the particle movement in groups of particles, so tracking the inter-particle effect from the individual particle is not possible. Furthermore, some researchers developed a collision model using DPM for agglomeration of powders (Nichols, et al., 2002). And, these models use the agglomerate size as the input parameter, which is hard to measure for bulk powders and is not applicable in this current simulation of dispersion of dust that is highly influenced by individual particle characteristics.

Table 3.2 Comparison criteria between the predicted and experimental dust concentrations at 0.5, 5 and 10 s after dispersion

	2 m/s		10 m/s	
	0.05 kg/m ³	0.10 kg/m ³	0.05 kg/m ³	0.10 kg/m ³
P%	9.93	9.68	1.82	19.26
S.E.	0.001	0.0024	0.0037	0.0064

(Note: The P-value was calculated from 0.2 to 0.5 s dispersion time)

During the experiments, most of the dust settled within 2 s, while the simulated dust settling rate was slower. This could be because that after injection of all the dust, a higher number of particles tend to stick to the chamber wall, forming a layer of dust on the wall, as noticed during experimental trials. This layer of starch has a different roughness and friction from the chamber wall, and this affected the rebound conditions. Particle collisions after dispersion may also lead to a faster settling rate, as the terminal velocity increases with the particle size. In summary, the developed model can predict dust suspension for a dilute particle flow, where the particle adhesion

on the wall is not influenced by the adhesion force between the wall and the particle and where there are negligible particle collisions.

3.3.2 Dust cloud spread and distribution pattern

The dust cloud spread and dust distribution during the experiments and as predicted by the CFD-DPM-based simulation are presented in Figures 3.4 and 3.5. The dust cloud expanded after the completion of dust dispersion and then started settling. During experiments, based on visual observation, some of the dust particles settled as agglomerates, as the particles did not fully separate from each other during the fluid phase. With a lower terminal velocity, suspended small particles tend to form a stable dust cloud. As reported by Hinds (2012), the dust cloud suspension is highly dependent on the particle size. It has been observed that at higher dispersion velocities, the drag force upon the particles was larger and had a higher probability of separating the single particles out from the cluster to form a dust cloud (Nichols, et al., 2002), thus extending the duration of the suspension. This means that, a primary explosion or a leak from a pneumatic handling system, could produce a cloud that is suspended for much longer than a cloud formed through dust spillage.

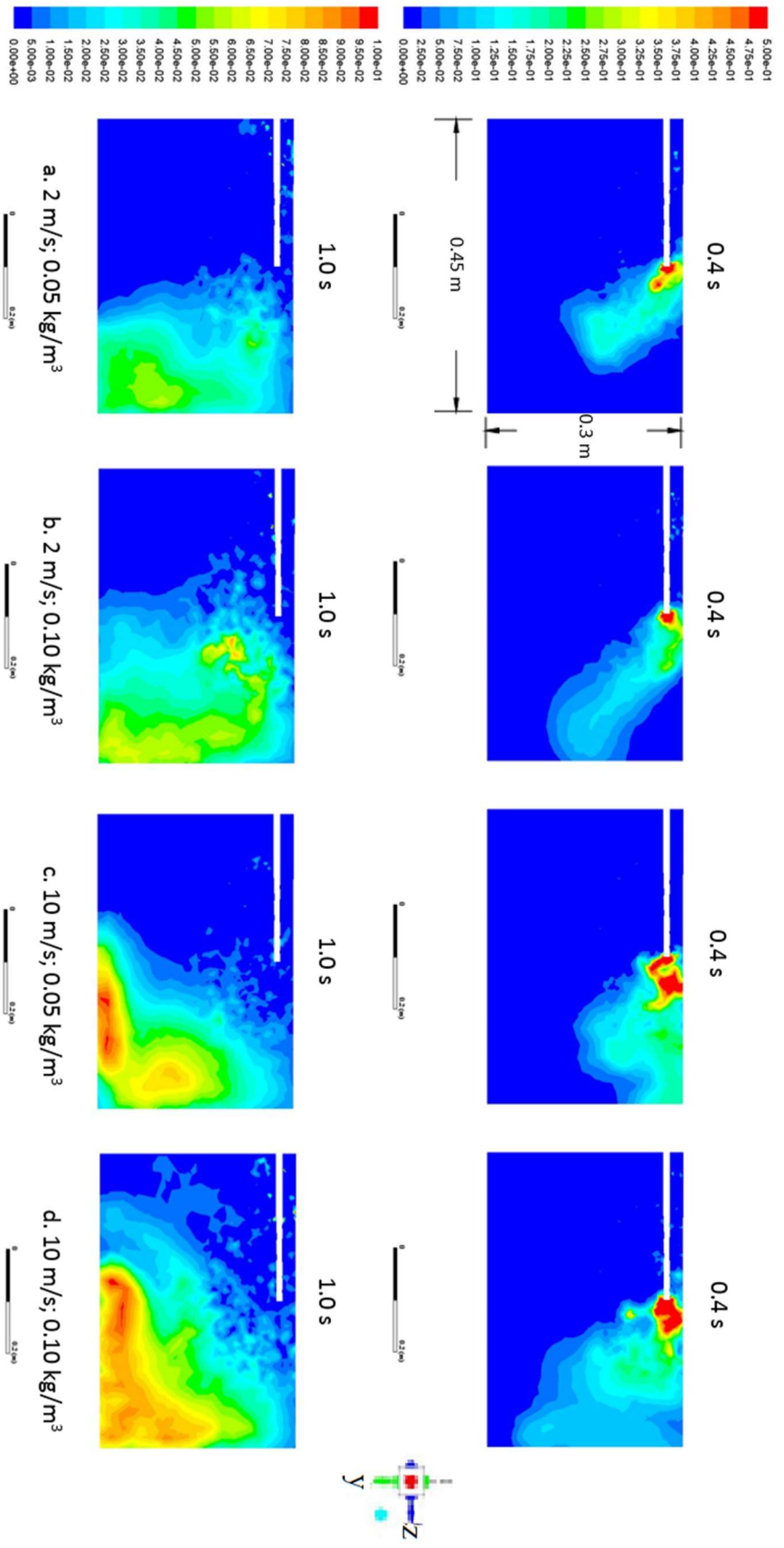


Figure 3.4 Simulated dust cloud spread and distribution pattern during dispersion (scale bar in kg/m³)

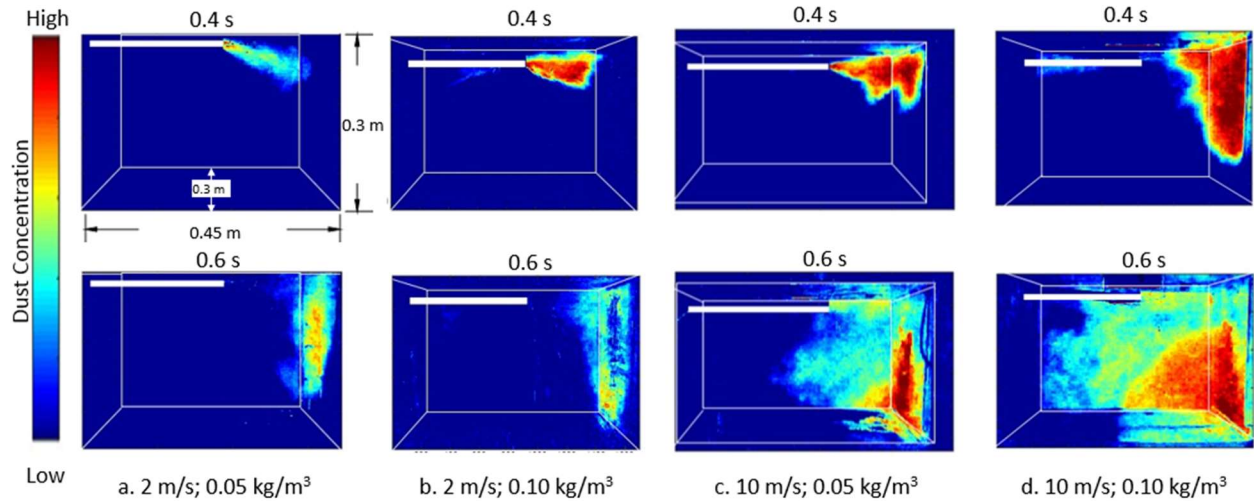


Figure 3.5 Experimental dust cloud spread and distribution pattern during dispersion

The experimental results showed the same trend as the simulation. As the dispersion velocity increased, the dust tended to spread out and settle at the center of the chamber (Figures 3.4 and 3.5). At a lower dispersion velocity, the dust cloud was less spread out and only concentrated in half of the chamber's volume, with most of the dust settling on the chamber wall or at the bottom, near the wall. As the quantity of injected dust particles increased, the dust cloud generated under the same velocity did not change much in terms of volume, but its concentration increased. From the simulation, it was observed that there will always be a higher dust concentration in some areas that exceed MEC, which is shown in Figure 3.4.

To summarize, the injection velocity has more of an effect upon the distance dust particles travel and the spread of a dust cloud's volume. The mass of the injected dust has more of an effect upon the dust concentration. Irrespective of the initial conditions, any amount of dispersed dust is a hazard and will have larger implications during an explosion, as the regional concentration can always be higher than MEC during dispersion. Di et al., (2014) also found that dust dispersion will form a non-uniform distributed dust cloud, which could affect the evaluation of MEC.

The kinetic energy resulting from the inlet air velocity during the experiments at dispersion rates of 10 m/s and 2 m/s is shown (at 0.3 s time step) in Fig 3.6. Higher kinetic energy was found throughout the chamber at the dust dispersion velocity of 10 m/s than at 2 m/s. As the particles moved along with the fluid, the dust cloud also moved in a negative Z-axis direction during the dispersion at 10 m/s. This explains the reason behind a higher dust cloud dispersion at 10 m/s than at 2 m/s. Another possible reason is that with 2 m/s dispersion, the dust particles do not have

enough kinetic energy to overcome the adhesion force between particle and wall. Therefore, those particles were not able to rebound from the wall or slide down the wall to the bottom of the chamber.

Boac et al. (2009) reported a similar result from a study at a grain elevator, that the upper collection duct with a higher velocity has more dust emission than at the lower duct. Pu and Jarosinski (1991) have shown that, under conditions of high turbulence, there is a rapid rise in pressure during dust explosions. The results for dust cloud formation under turbulence shown in Figures 3.4 and 3.5 can be one explanation for the fact that turbulence can affect a dust explosion. A higher velocity will create a larger and more uniform dust cloud containing a larger number of dust particles with a potential to release energy that is of higher magnitude during an explosion.

3.3.3 Dust particle transport

The dust particle transport is a particularly important parameter in dust explosion research because explosions can be especially severe for expanded dust clouds (Eckhoff, 2003). The traveling distance of a particle at 10 m/s dispersion velocity was greater than it was for a particle dispersed at 2 m/s. This corresponds to the kinetic energy as shown in Figure 3.6. It can also be seen from Figure 3.6 that the spread of kinetic energy at 10 m/s dispersion was higher when compared with 2 m/s dispersion velocity. This higher kinetic energy increased particle transport and resulted in a larger dust cloud.

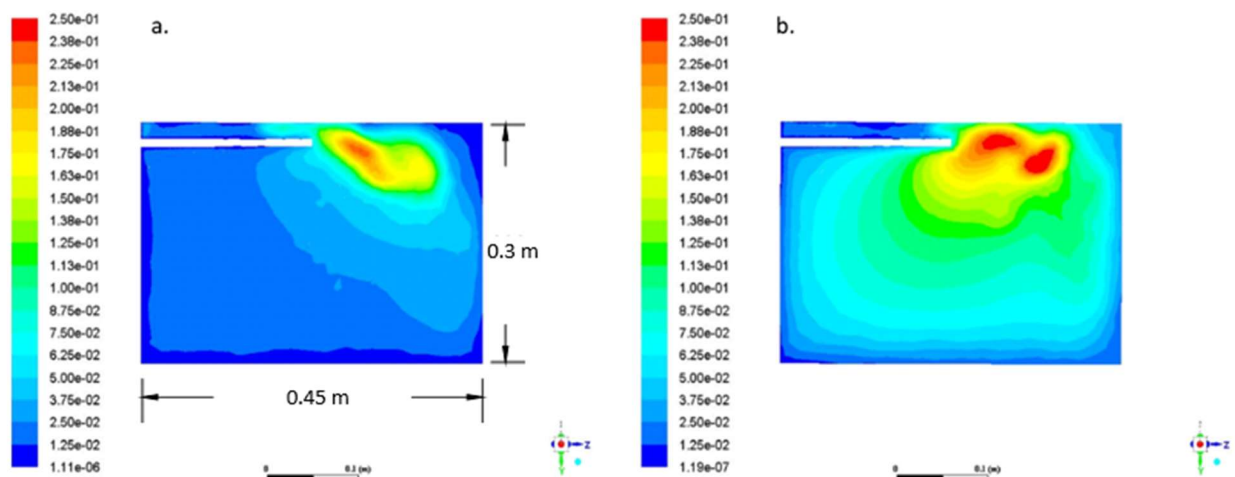


Figure 3.6 Model prediction of kinetic energy of dust particles at (a) 2 m/s and (b) 10 m/s inlet air velocity (scale bar in m^2/s^2)

To study the spread of the dust cloud, in addition to the 0.05 and 0.10 kg/m³ concentrations, a lower theoretical dust cloud concentration of 0.03 kg/m³ was also simulated for 2 m/s and 10 m/s dispersion velocity (Figure 3.7). At the theoretical concentration of 0.03 kg/m³, after all the dust had dispersed (~ 0.5 s), less than half of the entire chamber's volume had a dust concentration of over 0.03 kg/m³. In comparison, a 2 m/s inlet air velocity with a 0.05 kg/m³ dust concentration produced a dust cloud that occupied about 15.8% of the entire chamber volume. A 10 m/s dispersion velocity resulted in a 26.0% dust spread within the chamber. Similarly, at 10 m/s and 0.10 kg/m³, the explosive dust cloud spread to about 37.8% of the chamber volume, while at 2 m/s with the same injection mass it occupied about 25.7% of the chamber. These findings agree with the dust concentration and distribution results discussed in section 3.3.2, which suggest that a higher dispersion velocity will lead to greater expansion and a larger and more uniform dust cloud. The dispersion velocity and mass of dust can both have a large effect on the size of a dust cloud. Increasing the injected particle mass increased the size of the explosive dust cloud as can be seen in Figure 7 (a) as compared to Figure 7 (c) and Figure 7 (b) compared to 7 (d).

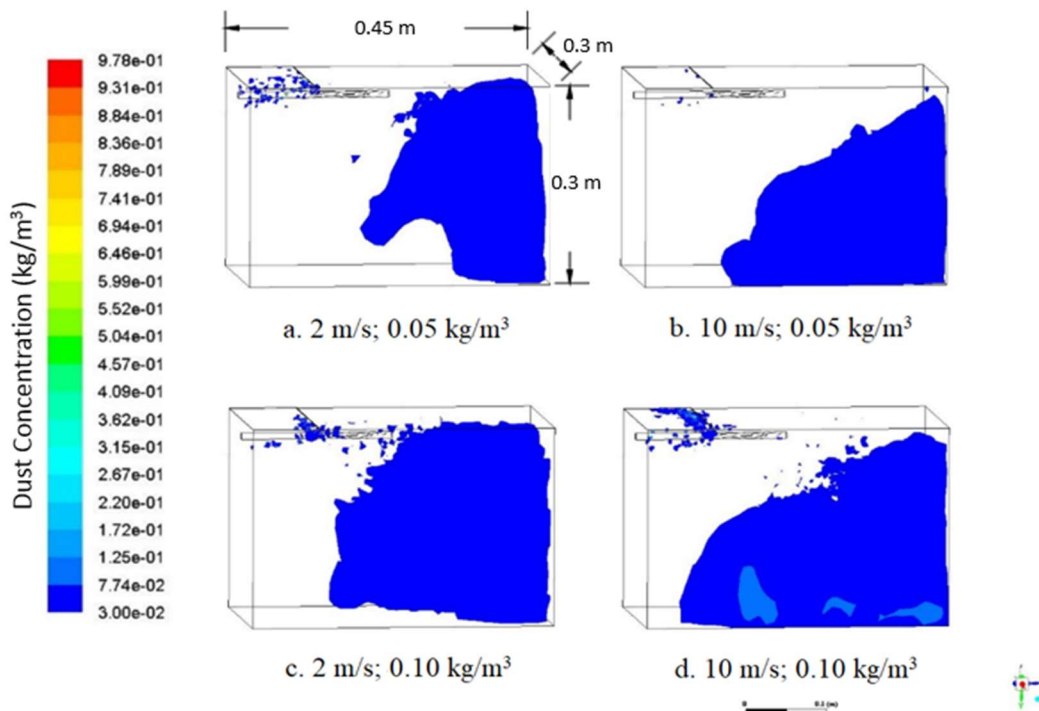


Figure 3.7 Model predictions for explosive dust cloud at 1.0s of (a) 2 m/s 0.05 kg/m³, (b) 10 m/s 0.05 kg/m³, (c) 2 m/s 0.10 kg/m³ and (d) 10 m/s 0.10 kg/m³

Most dust explosion studies make the assumption that a dust cloud will be evenly distributed and that a vessel's entire volume will be equivalent to the volume of the explosive cloud. Barton (2002) noted that the volume of an explosive dust cloud should be taken into account, instead of assuming that dust will be evenly distributed throughout a vessel. It is clear from Figure 3.7 that knowing the exact distribution of an explosive dust cloud is essential to prevent overestimation of the dust cloud minimum explosive concentration limit. Dust clouds and their concentration could affect the release of explosive energy and the rate at which the pressure might rise. In addition, knowledge of the distribution pattern and volume distribution would help with the accurate positioning of dust explosion suppression systems.

3.4 Conclusions

Dust dispersion under confined conditions was simulated using a CFD-DPM approach and experimental studies were used to validate the simulation results. The results indicated that a CFD-DPM simulation approach could predict the dust dispersion and concentration in confined spaces, with reasonable accuracy, irrespective of turbulent conditions. The prediction error was especially low for a dilute phase flow where there are fewer inter-particle interactions. The simulation results showed that, at a higher velocity, dispersed dust would form a larger and more uniform explosive cloud. This explains why high turbulence can lead to more severe dust explosions, with greater energy and a more rapid pressure release. In view of the variety of possible processing environments, the boundaries of different kinds of equipment and constructions will have an important role to play. The stick-rebound model offers the advantage of being able to account for the energy lost when a particle collides with a wall. By using this model, it will be possible to understand the dust dispersion pattern as influenced by process conditions.

Despite these encouraging outcomes, when the simulation results were compared to the actual experiment, it was found that the lack of particle-particle interaction remains a problem that will continue to affect the accuracy of the proposed CFD-DPM model, especially when there are high dust concentrations. The cohesiveness of particles can also affect the results by changing the size of agglomerates. So, the model may not be applicable for two-phase flow with a high-volume fraction of particles and in cases where particle de-agglomeration and particle collision significantly affect the dust dispersion process. Introducing particle-wall interaction is an important improvement to existing CFD-DPM approaches because it enables better prediction for

powder dispersion that does not contain large agglomerates. However, in the case of powders with a higher moisture content or fat, the powder is likely to agglomerate and cannot fully disperse, so the particle-particle interaction is going to be an essential part of providing an accurate prediction.

3.5 References

- ANSYS, (2015). ANSYS user's Manuals 16.0, ANSYS Inc., Canonsburg, Pennsylvania, USA
- Barton, K., (2002). Dust explosion prevention and protection: A practical guide, Institution of Chemical Engineers, Warwickshire, UK.
- Boac, J. M., Maghirang, R. G., Casada, M. E., Wilson, J. D., & Jung, Y. S., (2009). Size distribution and rate of dust generated during grain elevator handling. *Applied Engineering in Agriculture*. 25(4), 533-541.
- Calle, S., Klabá, L., Thomas, D., Perrin, L., & Dufaud, O., 2005. Influence of the size distribution and concentration on wood dust explosion: Experiments and reaction modelling. *Powder Technology* 157(1-3), 144-148.
- Calvert, G., Ghadiri, M., & Tweedie, R., (2009). Aerodynamic dispersion of cohesive powders: a review of understanding and technology. *Advanced Powder Technology* 20(1), 4-16.
- Deen, N. G., Annaland, M. V. S., Van der Hoef, M. A., & Kuipers, J. A. M., (2007). Review of discrete particle modeling of fluidized beds. *Chemical Engineering Science* 62(1-2), 28-44.
- Di Benedetto, A., Russo, P., Sanchirico, R., & Di Sarli, V., (2013). CFD simulations of turbulent fluid flow and dust dispersion in the 20-liter explosion vessel. *AIChE Journal* 59(7), 2485-2496.
- Di Sarli, V., Russo, P., Sanchirico, R., & Di Benedetto, A. (2014). CFD simulations of dust dispersion in the 20 L vessel: effect of nominal dust concentration. *Journal of Loss Prevention in the Processing Industries*, 27, 8-12.
- Dorsett, H. G., & Jacobson, M., (1960). Laboratory equipment and test procedures for evaluating explosibility of dusts (Vol. 5624). US Department of the Interior, Bureau of Mines, Washington, DC
- Eckhoff, R. K. (1983). Dust Explosions, Handbook of Powder Technology, Volume 4: by Peter Field, Elsevier, Netherlands.

- Eckhoff, R. K., (1996). Prevention and mitigation of dust explosions in the process industries: A survey of recent research and development. *Journal of Loss Prevention in the Processing Industries*, 9(1), 3-20.
- Eckhoff, R. K., (2003). *Dust explosions in the process industries: identification, assessment and control of dust hazards*. Oxford: Butterworth Heinemann, UK
- Eckhoff, R. K., (2009). Understanding dust explosions. The role of powder science and technology. *Journal of Loss Prevention in the Processing Industries*, 22(1), 105-116.
- Elghobashi, S. (1994). On predicting particle-laden turbulent flows. *Applied Scientific Research*, 52(4), 309-329.
- Hein, K., Hucke, T., Stintz, M., & Ripperger, S., (2002). Analysis of adhesion forces between particles and wall based on the vibration method. *Particle & Particle Systems Characterization: Measurement and Description of Particle Properties and Behavior in Powders and Other Disperse Systems*. *Particle & Particle Systems Characterization*, 19(4), 269-276.
- Hinds, W. C., (2012). *Aerosol technology: properties, behavior, and measurement of airborne particles*. Chapter 17. John Wiley & Sons. New York, NY. 379-385
- Ilić, I., Govedarica, B., & Srčić, S., (2013). Deformation properties of pharmaceutical excipients determined using an in-die and out-die method. *International Journal of Pharmaceutical*. 446(1-2), 6-15.
- Inthavong, K., Tian, L., & Tu, J. (2016). Lagrangian particle modelling of spherical nanoparticle dispersion and deposition in confined flows. *Journal of Aerosol Science*, 96, 56-68.
- Jones, S. C. (1990). Effects of population density on tunneling by Formosan subterranean termite (*Isoptera: Rhinotermitidae*) through treated soil. *Journal of Economic Entomology*, 83(3), 875-878.
- Klippel, A., Schmidt, M., Muecke, O., & Krause, U., (2014). Dust concentration measurements during filling of a silo and CFD modeling of filling processes regarding exceeding the lower explosion limit. *Journal of Loss Prevention in the Processing Industries*, 29, 122-137.
- Kumar, R. K., Bowles, E. M., & Mintz, K. J., (1992). Large-scale dust explosion experiments to determine the effects of scaling on explosion parameters. *Combustion and Flame*, 89(3-4), 320-332.

- Maremonti, M., Russo, G., Salzano, E., & Tufano, V., (1999). Numerical simulation of gas explosions in linked vessels. *Journal of Loss Prevention in the Processing Industries*, 12(3), 189-194.
- Mezhericher, M., Brosh, T., & Levy, A., (2011). Modeling of particle pneumatic conveying using DEM and DPM methods. *Particulate Science and Technology*, 29(2), 197-208.
- Nichols, G., Byard, S., Bloxham, M. J., Botterill, J., Dawson, N. J., Dennis, A., & Sherwood, J. D., (2002). A review of the terms agglomerate and aggregate with a recommendation for nomenclature used in powder and particle characterization. *Journal of Pharmaceutical Science*, 91(10), 2103-2109.
- Occupational Safety and Health Administration. (2003) OSHA Standard 29 CFR 1910.272, Grain Handling Facilities, Department of Labor, Washington D.C.
- Pan, S. Y., Wang, P., Chen, Q., Jiang, W., Chu, Y. H., & Chiang, P. C., (2017). Development of high-gravity technology for removing particulate and gaseous pollutant emissions: Principles and applications. *Journal of Cleaner Production*, 149, 540-556.
- Parnell Jr, C. B., McGee, R. O., Ganesan, B., Vanderlick, F. J., Hughs, S. E., & Green, K., (2013). A critical evaluation of combustible/explosible dust testing methods—Part 1. *Journal of Loss Prevention in the Processing Industries*, 26(3), 427-433.
- Proust, C. H., & Veysièrè, B., (1988). Fundamental properties of flames propagating in starch dust-air mixtures. *Combustion Science and Technology*, 62(4-6), 149-172.
- Pu, Y. K., Jarosinski, J., Johnson, V. G., & Kauffman, C. W., (1991), January. Turbulence effects on dust explosions in the 20-liter spherical vessel. In *Symposium (International) on Combustion (Vol. 23)*, The Combustion Institute, Pittsburgh, PA. 843-849.
- Rani, S. I., Gimbun, J., & Aziz, B. A., (2014). Prediction of particles-air movement in silo during filling operation. *Open Journal of Inorganic Non-metallic Materials*, 4(3), 21.
- Tarpagkou, R., & Pantokratoras, A. (2013). CFD methodology for sedimentation tanks: The effect of secondary phase on fluid phase using DPM coupled calculations. *Applied Mathematical Modelling*, 37(5), 3478-3494.
- Vreman, B., Geurts, B. J., Deen, N. G., Kuipers, J. A. M., & Kuerten, J. G., (2009). Two-and four-way coupled Euler–Lagrangian large-eddy simulation of turbulent particle-laden channel flow. *Flow, Turbulence and Combustion*, 82(1), 47-71.

- Wang, H. C., & Kasper, G., (1991). Filtration efficiency of nanometer-size aerosol particles. *Journal of Aerosol Science*, 22(1), 31-41.
- Zhang, Z., & Chen, Q., (2007). Comparison of the Eulerian and Lagrangian methods for predicting particle transport in enclosed spaces. *Atmospheric Environment*, 41(25), 5236-5248.
- Zhang, Z., Zhang, W., Zhai, Z. J., & Chen, Q. Y., (2007). Evaluation of various turbulence models in predicting airflow and turbulence in enclosed environments by CFD: Part 2-Comparison with experimental data from literature. *HVAC&R Research*. 13(6), 871-886.

4. SIMULATION OF CONTINUOUS DUST DISPERSION

Abstract

Dust dispersion and deposition are of great concern for the design of a dust control system. In this study, dust deposition was simulated in an enclosed chamber under continuous dispersion using a computational fluid dynamics (CFD)-discrete phase model (DPM) with a particle-wall sticky-rebound feature. Dispersions of 2, 4, and 6 g/min, corresponding to 15, 30, and 45 g/m³ suspended dust concentration, after 30 s of dispersion were simulated. The settled dust patterns were obtained from the simulation. The dust-deposition rate and particle-size distribution were obtained from select locations within the chamber. The results showed that the larger particles tend to settle closer to the dispersion nozzle than the smaller particles. The suspended dust concentration increased at a constant rate regardless of the particle dispersion rate. The validation experiments showed that the model developed predicts the dust-deposition rate and locations with mean standard prediction error of 5.6, 0.9 and 4.4 corresponding to 2, 3 and 6 g/min dust dispersion rate.

4.1 Introduction

Dust deposition in indoor environments is inevitable and is considered a complex process in the particulate material handling and processing industry. The accumulated dust layer can be dispersed by air pressure or an explosion shockwave, both of which have the potential risk of leading to secondary explosions (Eckhoff, 2003). Thus, to prevent explosion hazards, it is essential to study the mechanisms of dust dispersion and deposition.

To prevent secondary dust explosions, Occupational Safety and Health Administration (OSHA) and National Fire Protection Association (NFPA) have regulated the thickness of the dust layer that is allowed to accumulate on any surface (OSHA, 2005; NFPA, 2020). The NFPA standard 654 suggests that the thickness of the dust layer should be maintained below 0.8 mm. When a dust layer covers more than 5% of the building area or up to 93 m², this could lead to the potential risk of dust explosion (NFPA 654, Standard for the Prevention of Fire and Dust Explosions from the Manufacturing, Processing, and Handling of Combustible Particulate Solids). In addition, if the dust accumulates on hot surfaces, the dust particles can be ignited directly, eventually causing fire or explosions (Eckhoff, 2005). To prevent dust explosion, all surfaces

where the dust may accumulate should be designed and constructed to minimize dust accumulations, and the appropriate dust collection systems are needed to limit dust migration. Therefore, it is important to know how and where the dust particles will be deposited.

Researchers have found that the accumulated dust on ventilation surfaces can range from less than 1 g/m² to over 100 g/m², and from 0.1 to 1 g/m² on hard floored surfaces (Boor et al., 2013). Tovey and Ferro (2012) reported that dust deposition on a surface can take the form of monolayer or multilayer deposits, depending on the amount of dust that is settled. Particle deposition is highly affected by the number of suspended particles, particle size, particle composition, properties and position of surface materials, and air-flow characteristics (Braaten 1994; Jiang et al. 2008; Ibrahim et al. 2003; Ibrahim et al. 2004). Owing to the various factors affecting particle deposition, a mathematical model could help predict the particle deposition. Although many researchers have focused on the suspension of dust clouds, studies on the mechanisms of dust deposition and dust-layer formation are lacking in the literature.

Particle movement mainly depends on the drag force from the fluid phase and the gravitational force (Hinds, 1999). As the airflow pattern decides the movement of particles, computational fluid dynamics (CFD) is mostly used to predict the fluid phase (Murillo et al., 2013). The published studies mainly use two models for predicting particle movement: the Lagrangian and Eulerian methods. The Lagrangian method calculates the particle trajectory based on their dynamic forces, whereas the Eulerian methods treat particles as a continuous phase. A drift-flux model based on the Euler method was reported to predict the particle dispersion and deposition (Lai and Nazaroff, 2000; Chen et al. 2006; Gao and Niu, 2007). This method restricts the particle size and number of particles deposited in computational cells (Holmberg and Li, 1998). In addition, the particle size should be significantly smaller than the Kolmogorov microscale, which is at the magnitude of 1 mm for a normally ventilated room (Etheridge and Sandberg, 1996). In contrast, the Lagrangian method does not restrict particle size and the number of suspended particles but can be computationally intensive. In addition, the particle-particle and particle-wall interactions, and particle-fluid interactions can be implemented in Lagrangian method of simulations (Kosinski et al., 2005). Based on the Lagrangian method, a DPM model was developed by Zhao and Ambrose (2019) to track particles as a group to reduce computational time. This model successfully predicted the dust dispersion and concentration in confined spaces by incorporating with a particle wall stick-rebound model.

In particulate material-based manufacturing facilities, the dust is mostly continuously released from processing equipment and conveying systems. In this study, the authors used the CFD-DPM with particle rebounding developed by Zhao and Ambrose (2019) to simulate the continuous dispersion of dust in a confined environment. The objectives of this study to i) predict the continuous dispersion of dust using the CFD-DPM model, ii) model and determine the rate of dust deposition, and iii) experimentally validate the model predictions.

4.2 Materials and Methods

4.2.1 CFD-DPM model development

Indoor airflow can be considered to be turbulent (Etheridge and Sandberg, 1996). Thus, simulating the airflow field is essential for understanding the particle transport process. A turbulent airflow was characterized using the Navier-Stokes (RANS) equation with a standard $k-\varepsilon$ turbulence model. Two-way coupling was used in order to calculate the effect of particles on the airflow. The CFD-DPM model was implemented using ANSYS FLUENT (Ansys Inc. Pa, USA).

4.2.1.1 Modeling airflow

Turbulence was simulated using a standard $k-\varepsilon$ turbulence model. A detailed explanation of this approach is available in Chapter 3 and Zhao and Ambrose (2019). The initial gauge pressure was set at 1 atm. ANSYS FLUENT requires that turbulent transport quantities be specified: hydraulic diameter and intensity. The turbulence intensity is defined as the ratio of the root-mean-square of the velocity fluctuations and the mean velocity. The dust was dispersed from a tube with a diameter of 0.05 m at a velocity of 2 m/s; therefore, the turbulence intensity (I) was set at 7% and the turbulent length scale was 0.002 m (Ansys, 2015):

$$I = 0.16Re^{-1/8} \quad 4.3$$

where Re is the Reynolds number of airflows at the inlet.

4.2.1.2 Particle phase modeling

The particles were tracked based on corresponding force balances (Hinds, 1999):

$$-\frac{du_p}{dt} = F_D(u - u_p) + \frac{g(\rho_p - \rho)}{\rho_p} \quad 4.4$$

where, u_p is the particle velocity, ρ_p is the particle density, g is the gravitational acceleration constant, and F_D is the drag force per unit of the particle mass caused by differences in velocities of the air and particles.

The particles not only settled on the bottom of the chamber but also deposited on the vertical walls (Wells and Chamberlain, 1967). The particle–wall stick-rebound model (Zhao and Ambrose, 2019) was applied to the chamber wall:

$$Ke_i = Ke_r + E_{ad} + E_L \quad 4.5$$

where Ke_i and Ke_r are the kinetic energies for the incident and rebounding stages, E_{ad} is the energy dissipated by the adhesion force between the wall and the particle, and E_L is the energy lost due to elastic deformation.

The Rosin–Rammler distribution has been widely used to represent the particle size distribution (Steiner et al., 1974; Rani et al., 2015). Particle size distribution of dust using the Rosin–Rammler distribution is expressed as equation 5.6:

$$Y_d = e^{-(dp/\bar{d})^n} \quad 5.6$$

where, Y_d is the mass fraction with diameter greater than d , \bar{d} is the mean particle diameter, and n is the spread parameter. In this study, cornstarch was used as the dust material. Particle size distribution was obtained using a Morphologi G3-ID instrument (Malvern Instruments, Malvern, UK). The particle size of cornstarch ranged from 2.2 to 46 μm . \bar{d} was obtained from the measured particle size distribution, with a value of 19 μm , and then the spread parameter was chosen to fit the Rosin–Rammler model. A spread parameter of 3.5, gave the best fit of the Rosin–Rammler distribution with the measured particle size distribution was found (Figure 4.1).

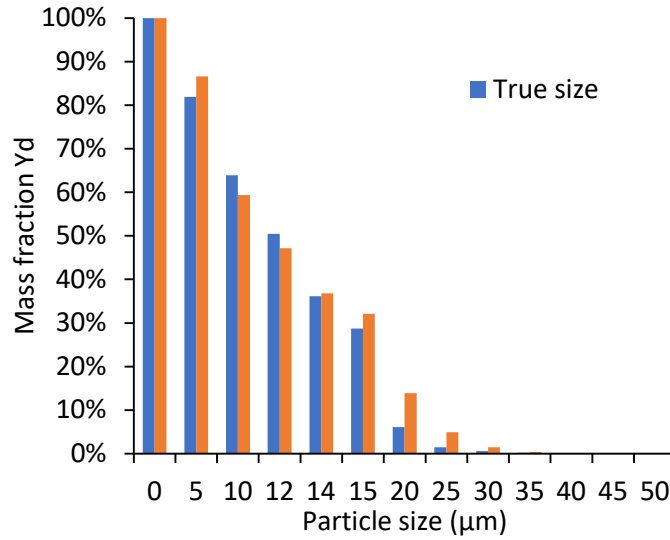


Figure 4.1 Cumulative particle size distribution

The dust was dispersed from the nozzle at 2, 4, 6 g/min dispersion rate for 30 s. During dispersion, the particle was suspended until sticking on the wall or settling on the chamber floor. The suspended particles in the chamber can be monitored during the simulation and the weight of particles that settled on the sampling stage on the chamber bottom was also monitored during dispersion.

The particle deposition primarily depends on the airflow pattern, and the particle size affects particle deposition. The simulation predicted the particles moving trajectories. Thus the number of particles of each size that settled on the bottom of chamber at different locations was predicted. The information of every particles at the three locations where sampling was conducted was obtained from the simulation, and this information was used to determine the particle size distribution at each location.

4.2.1.3 Geometry and meshing of chamber

A 0.30 m × 0.30 m × 0.45 m chamber with an inlet nozzle diameter of 0.05 m was used for simulation and validation (Figure 4.2). The mesh independence was achieved by conducting a sensitivity analysis of the effect of mesh size on the suspended dust concentration. Based on the results, the grid with the largest element size of 0.08 mm was used in this study. Three locations with dimension of 75 mm × 26 mm were chosen inside the chamber where the rate of dust deposition.

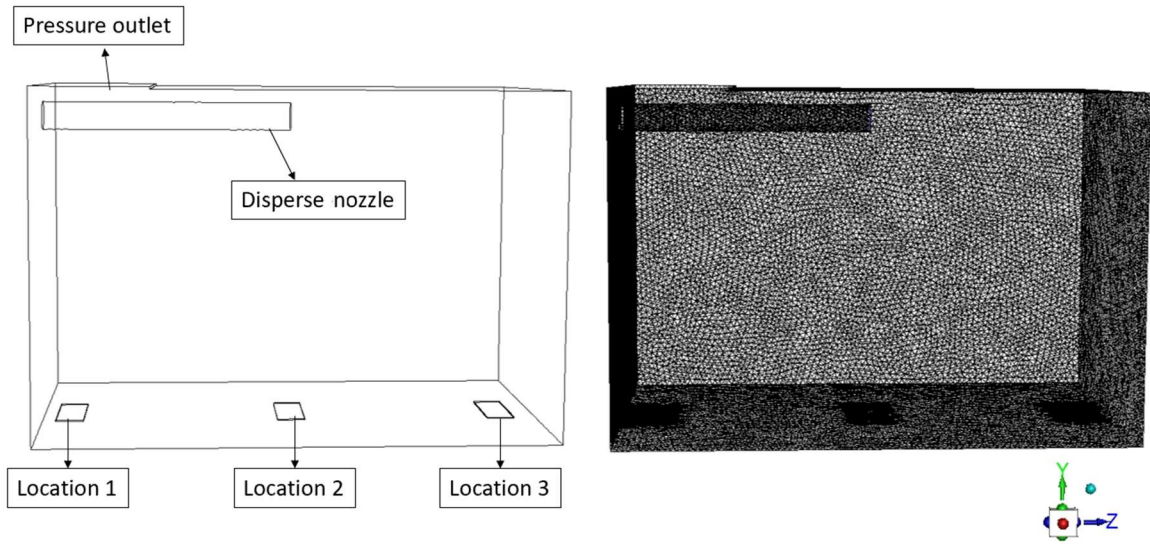


Figure 4.2 The dust chamber and mesh constructed for the simulation

4.2.1.4 Simulation parameters

The time step for the particle phase model was set at 0.001 s, while the time steps for the fluid phase was adaptive with 65 iterations per time step to achieve convergence. The dust dispersion was simulated for 30 s, and the mass settled on three locations was monitored during the simulation. The simulation was conducted using an Intel Core I5-2400 CPU computer with 8G installed memory. The dust properties and simulation parameters are presented in Table 4.1.

Table 4.1 Summary of particle properties and simulation parameters used in this study

Particle property/parameter	Symbol	Value*
Density of cornstarch particles (kg/m ³)	ρ_p	1491.9 (\pm 2.3)
Dust dispersion rate (g/min)	-	2, 4, 6 (values obtained from the experiments)
Airflow velocity (m/s)	u	2
Viscosity of air (Pa·s)	μ	$1.82 \cdot 10^{-5}$
Density of air (kg/m ³)	ρ_f	1.2047
Moisture content (% wet basis)	MC	9.1 (\pm 0.003)
Ambient relative humidity (%)	RH	49.1 (\pm 1.1)
Ambient temperature (°C)	T	20.6 (\pm 0.3)

* Values in parenthesis are standard deviations.

4.2.2 Experiment validation

The chamber in used in the validation of the experiment was the same size and shape as the chamber mentioned in section 4.2.1.3 was used in experimental validation (Figure 4.2). The cornstarch was put placed into the nozzle (funnel), and it was then dispersed through the nozzle for 30 s using compressed air supplied by the compressor with an airflow velocity of approximately 2 m/s. The dust inside the nozzle before and after dispersion was weighted weighed and the weight of particles dispersed during the 30 s was used to calculate the dispersion rate. The dust dispersion rates of 2, 4, and 6 g/min were used by controlling the weight of dust dispersed through the nozzle. These dispersion rates correspond to the dust concentrations of 15, 30, and 45 g/m³, which covers the MEC of cornstarch of 30 g/m³. To determine the amount of settled dust, pre-weighed glass slides with a size of 75 mm × 26 mm were placed on the bottom of the chamber, as indicated in locations 1, 2, and 3 indicated in Figure 4.2. The distance from the tip of the nozzle to the center point of the location 2 (glass slide) was 0.25 m. A long plastic belt was placed at the bottom of the chamber to serve as a conveyor belt to carry the glass slides in and out of the chamber. After every 10 s of dispersion, the glass slides were conveyed out of the chamber and new glass slides were conveyed into the chamber using the same conveyor set-up. The glass slides were always kept at the same location as in the simulation when they were conveyed into the chamber. Thereafter, the deposited dust weight was obtained by weighing the glass slides. The total settled dust was obtained by weighing the plastic belt before and after dispersion, in order to calculate the theoretical values after 30 s dispersion. Three replicate measurements were conducted for each dispersion rate.

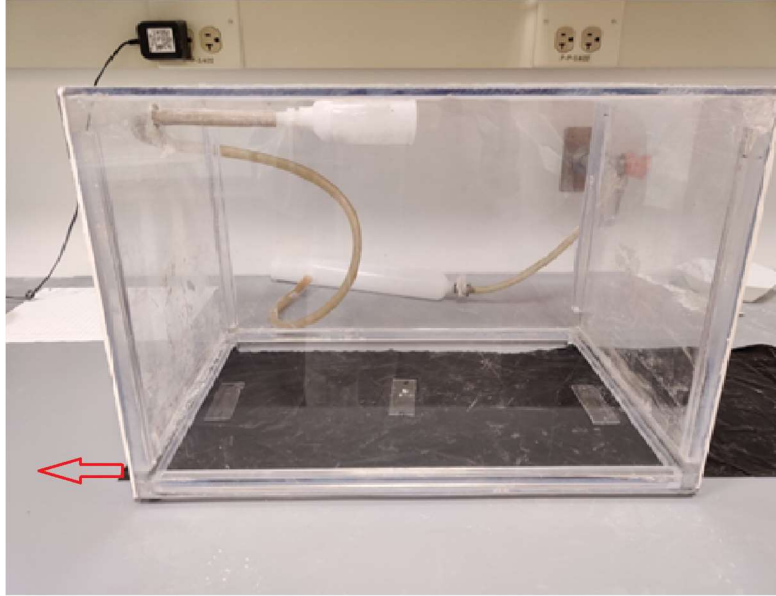


Figure 4.3 Picture of experimental set-up

4.2.3 Statistical analysis

The simulation was done once at each dispersion condition, and all experiments were done in three replicates. To compare the predicted and experimental values, mean squared prediction error (MSPE) was calculated for each dispersion rate and for each location using the following equation:

$$MSPE = E[(Y - Y_d)^2] \quad (6)$$

where, E is the expectation, Y is the measured value and Y_d is the predicted value.

4.3 Results and Discussion

The suspended dust concentration increased rapidly at the beginning of dispersion, and the rate of concentration decreased after around 3 seconds of dispersion (Figure 4.4). The corresponding theoretical concentrations at 2, 4, and 6 g/s dispersion rate after 30 s of dispersion were 10, 23, and 34 g/m³. This was calculated from the experiments by subtracting the settled particles from the dispersed particles. A high rate of change in suspended dust concentration was observed when there were only a few dust particles settling. As time and concentration of injected

particles increased, dust concentration tended to increase at a constant rate. Even with a dispersion of 2 g/min, the dust concentration increased with prolonged dispersion. The simulated dust concentration in a confined chamber kept increasing regardless of the dust dispersion rate (2–6 g/min), which means that the dust concentration eventually reached the minimum explosive concentration. This means that it is essential to have a dust collection system to limit the concentration of suspended dust particles in a processing operation.

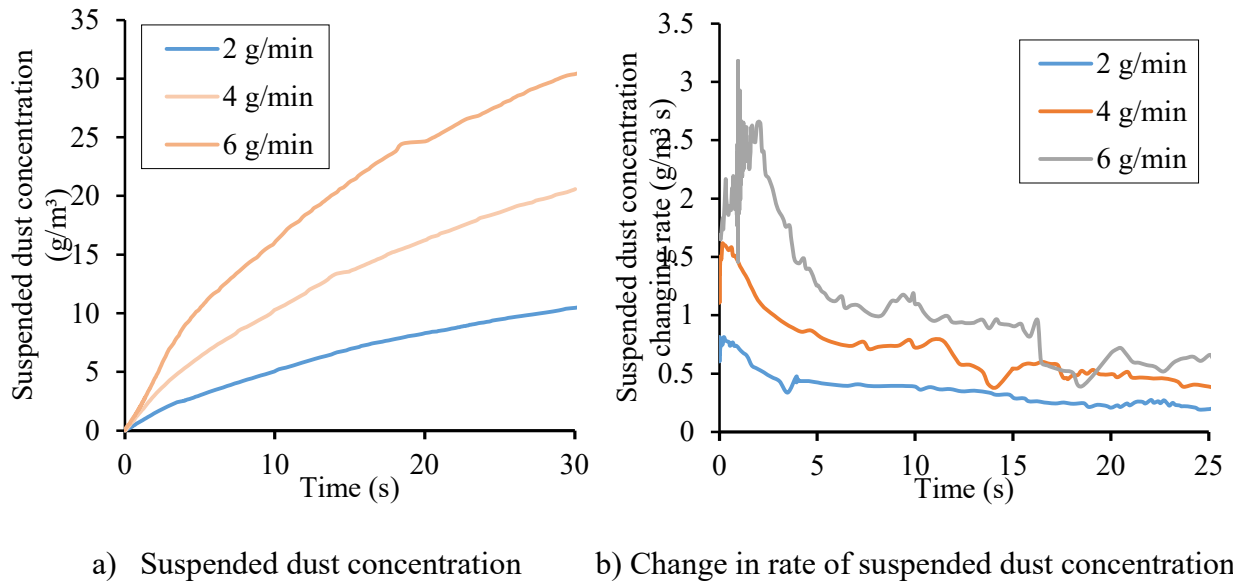


Figure 4.4 Predicted dust concentrations during continued dispersion

During dust dispersion, most particles settled onto the bottom of the chamber while some particles adhered to the chamber wall. Figure 4.5 shows the distributions of total settled dust at 3, 7, and 16 s at 2, 4, and 6 g/min dispersion rates. The settling of dust was highly influenced by the air movement. As indicated in Figure 4.5, most dust particles settled downstream of the nozzle while some particles were still suspended and traveling to the back of the nozzle due to turbulence. The deposition rate near location 3 is faster than the rate at locations 1 and 2, and a higher dispersion rate resulted in a faster dust accumulation on the bottom of the chamber.

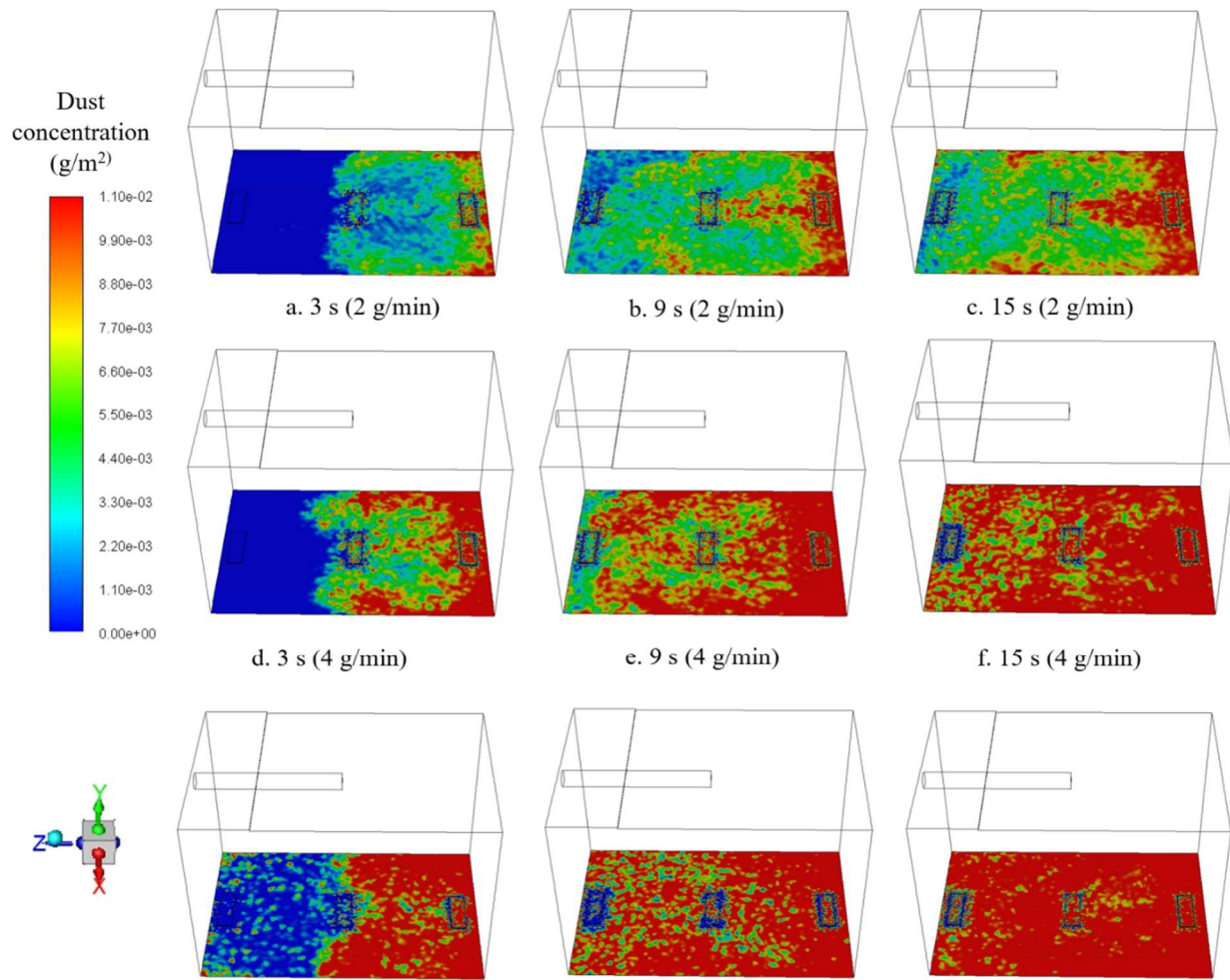


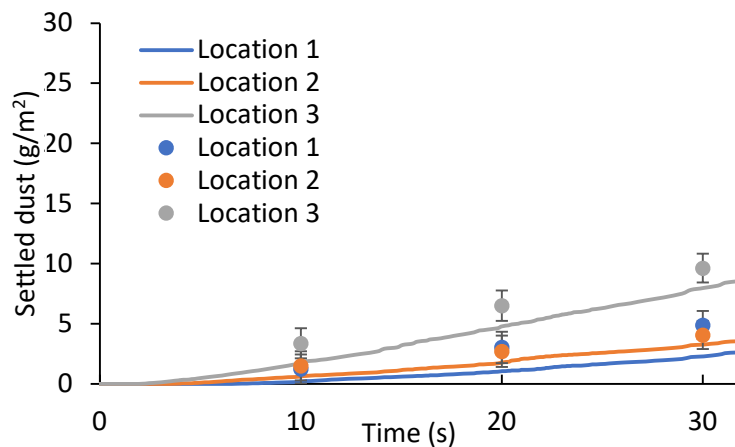
Figure 4.5 Total deposited dust at the bottom of the chamber

The weight of settled dust increased with the rate of dust dispersion. It was observed that location 3 had the highest dust deposition rate, both in the simulation and in the experiments. Locations 1 and 2, on the other hand, have similar deposition rates (Figure 4.6). The number of dust particles that settled at locations 1 and 2 was only half of which settled at location 3. The minimum explosion concentration for cornstarch is 30 g/m^3 , so the allowed dust that settled on the floor can be calculated based on the height of the enclosed space (NFPA, 2005). Based on the dimensions of the chamber, 9 g/m^2 of dust on the bottom would be able to explode if the dust layer was resuspended. The deposition rate was different from one location to another depending on the dust dispersion conditions. In other words, the dust layer thickness was not constant over the entire chamber floor. Thus, obtaining the deposition distribution is important to accurately calculating

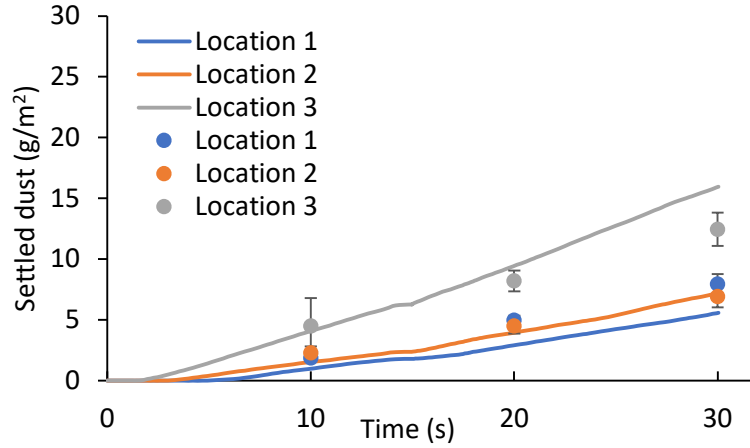
the weight of particles that can be deposited in an enclosed space. For practical applications, if the dust dispersion rate and velocity of air movement are available, through the simulation of dust deposition can predict the housekeeping interval can be determined to limit the explosion risks.

The rate of dust settling at each location is almost linear after 3 s of dispersion. Results presented in Chapter 3 showed that the dust cloud spreads after about 1 s of dispersion. Therefore, for the first 3 s of dispersion, the dust spreads out and reaches a relative equilibrium condition. After 3 s, the dust depositions rate is nearly constant.

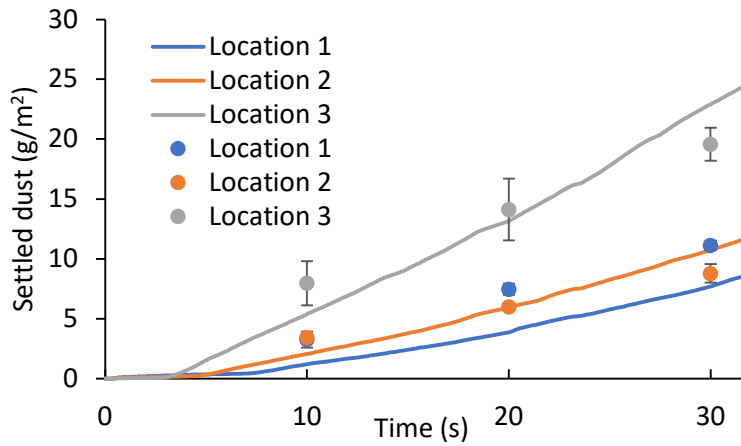
MSPE is a reference value to qualify the accuracy of the predictions; a smaller value of the MSPE indicates a better prediction. Location 1 had a higher MSPE than that of location 2, while the deposition rates of locations 1 and 2 are similar. The MSPE of location 2 had the lowest MSPE among all dispersion rates, which indicates that location 2 has the most accurate prediction (Table 4.2). The model underestimated the rate of dust settling in location 1 for all dispersion rates. A probable explanation is that the simulated turbulence dissipated slower than the real conditions. Particles settled slower when the turbulence dissipated slowly, which led to an underestimation of dust that settled at location 1. The high MSPE value at the dispersion rate of 6 g/min could be due to the larger settling rate of dust at this high rate of dust inflow. Therefore, an accurate simulation of turbulence within the confined space is needed to predict the dust deposition.



a) at dispersion rate of 2 g/min



b) at dispersion rate of 4 g/min



c) at dispersion rate of 6 g/min

Figure 4.6 Amount of dust settled at the selected three locations within the confined chamber (the solid lines represent the simulated results and the dots represent the experimental values)

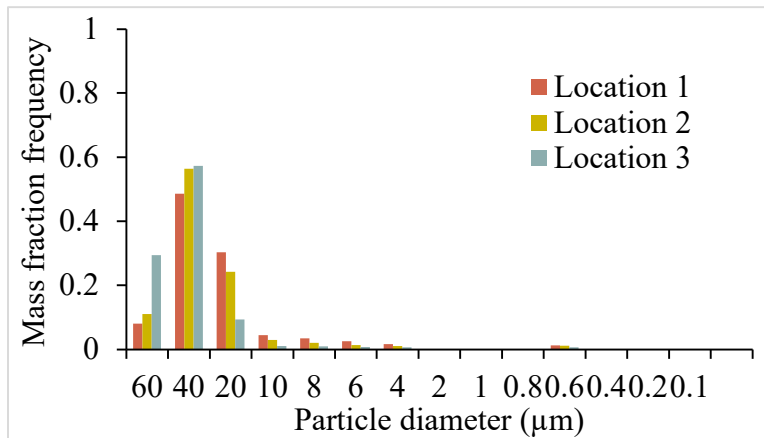
Table 4.2 Mean square prediction error (MSPE; $(g/m^2)^2$) of the settled dust within the confined chamber

Dispersion rate (g/min)	Location 1	Location 2	Location 3
2	4.84 ± 5.45	1.45 ± 1.10	7.80 ± 6.49
4	3.89 ± 4.30	1.59 ± 1.63	12.49 ± 15.11
6	10.09 ± 6.43	2.00 ± 2.34	10.56 ± 11.60

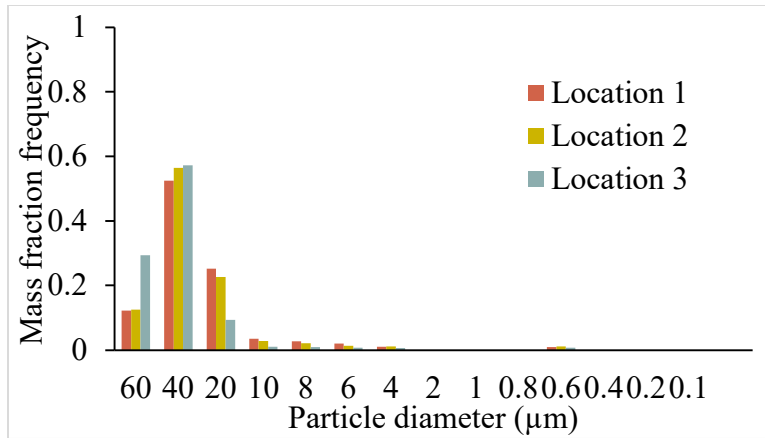
* Values after ± are standard deviations.

Though the particle deposition primarily depends on the airflow pattern, the particle size also has a major influence on the rate of settling.

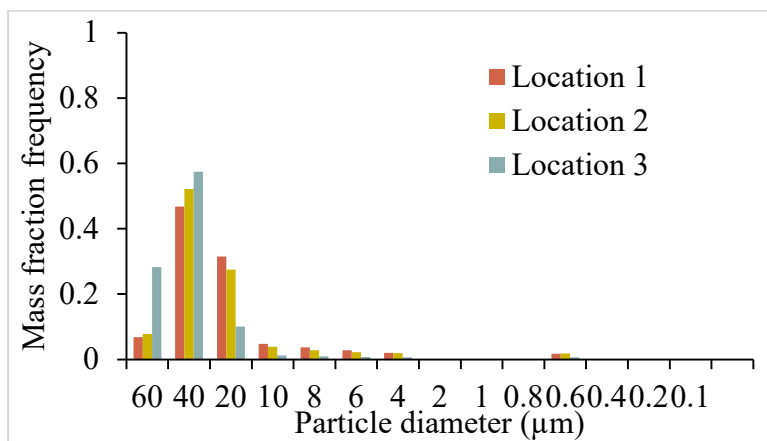
At location 3, the airflow moves downward to the bottom of the chamber. Similar to what happens in a particle impactor, once the airflow hits the wall, the flow direction changes. The particle moves with the airflow and gravitational force. Due to inertia, only small particles followed the airflow path, while the larger particles settled to the bottom (Sethi and John, 1993). Figure 4.7 clearly shows that location 3 has more particles with diameters over 20 μm , while the smaller particles settled at locations 1 and 2. For comparison purposes, an image of dust that settled on three glass slides captured after 10 s of 6 g/min dispersion is presented in Figure 4.8. It can be seen that location 3 (further right) has larger particles while location 2 shows a mix of particle sizes and location 1 has only one large agglomerate. The experimental results agree with the simulations. That is, large particles tend to settle at location 3, while smaller particles travel longer distances and settle at more distant locations.



a) at dispersion rate of 2 g/min



b) at dispersion rate of 4 g/min



c) at dispersion rate of 6 g/min

Figure 4.7 Simulated particle size distribution at three locations after 30 s of dispersion

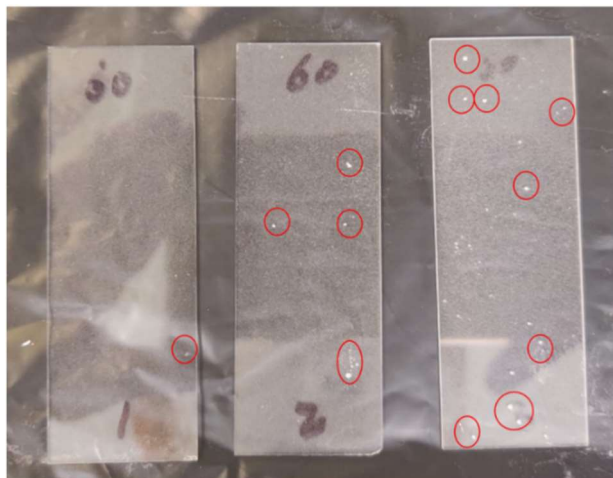


Figure 4.8 Cornstarch particles deposited on the glass slide after 10 s of dispersion at 4 g/min dispersion rate. (Slides were taken from location 1, 2 and 3 (left to right))

The particle size affects the explosion/burning velocity of dust (Cashdollar, 2000). Small particles with large specific surface areas have higher deflagration rates and result in a higher increase in explosion pressure (Di et al., 2010). In addition, the minimum explosive concentration decreases as the particle size decreases. The simulation shows that small particles travel long distances following the airflow pattern and are less likely to settle due to impacting on a surface. Thus, the smaller dust particles tend to suspend in the air for longer durations increasing dust explosion risks.

4.4 Conclusions

The objective of this study was to predict particle deposition with a reasonable accuracy, so that dust collection systems can be designed to target areas with high deposition rates. Using the CFD-DPM model developed, the particle deposition was predicted with sufficient accuracy. During continuous dispersion, suspended dust concentration increased regardless of the dust injection rate. The suspended particle concentration increased rapidly at the beginning of dispersion and then decreased to a relatively constant rate after the dust cloud fully spread in the chamber. Thus, dust collection systems are required in industries where dust emission occurs to ensure that suspended dust concentration is maintained below a minimum explosive concentration.

The major factor that affects particle dispersion and deposition is the airflow turbulence and movement. The particle size distribution also affects particle deposition patterns. A small particle with a low gravitational force and inertia tends to travel with the airflow, even with a sharp change in direction of the airflow. Special attention should be paid to such small particles even when there are low explosion concentrations because they have a faster burning rate and they are more likely to settle in a hidden area, such as, behind equipment.

To improve the accuracy of the prediction of particle deposition, an accurate turbulence condition is required. Small particle movements are more sensitive to airflow conditions. Thus, a comparison of CFD models to predict dust dispersion is needed for future work. Furthermore, deposition on vertical walls should be evaluated by conducting a study of particle-wall adhesion force such as Van der Waals force and the force produced by static electricity. Due to the limitations of

the DPM model, predicting dust layer thickness is not possible. When a monolayer formed, the force for particle deposition will change from particle-wall interaction to particle-particle interaction. For further improvement of the simulation, the particle-particle interaction should be included.

4.5 References

- ANSYS. (2015). ANSYS user's Manuals 16.0, ANSYS Inc., Canonsburg, Pennsylvania, USA
- Braaten, D. A. (1994). Wind tunnel experiments of large particle reentrainment-deposition and development of large particle scaling parameters. *Aerosol Science and Technology*, 21(2), 157-169.
- Cashdollar, K. L. (2000). Overview of dust explosibility characteristics. *Journal of Loss Prevention in the Process Industries*, 13(3-5), 183-199.
- Chen, F., Simon, C. M., & Lai, A. C. (2006). Modeling particle distribution and deposition in indoor environments with a new drift-flux model. *Atmospheric Environment*, 40(2), 357-367.
- Di Benedetto, A., Russo, P., Amyotte, P., & Marchand, N. (2010). Modelling the effect of particle size on dust explosions. *Chemical Engineering Science*, 65(2), 772-779.
- Eckhoff, R. K. (2005). Current status and expected future trends in dust explosion research. *Journal of Loss Prevention in the Process Industries*, 18(4-6), 225-237.
- Gao, N. P., & Niu, J. L. (2007). Modeling particle dispersion and deposition in indoor environments. *Atmospheric Environment*, 41(18), 3862-3876.
- Hinds, W. C. (1999). *Aerosol technology: properties, behavior, and measurement of airborne particles*. John Wiley & Sons. New York, NY
- Holmberg, S., & Li, Y. (1998). Modelling of the indoor environment-particle dispersion and deposition. *Indoor Air*, 8(2), 113-122.
- Ibrahim, A. H., Dunn, P. F., & Brach, R. M. (2003). Microparticle detachment from surfaces exposed to turbulent air flow: controlled experiments and modeling. *Journal of Aerosol Science*, 34(6), 765-782.

- Ibrahim, A. H., Dunn, P. F., & Brach, R. M. (2004). Microparticle detachment from surfaces exposed to turbulent air flow: Effects of flow and particle deposition characteristics. *Journal of Aerosol Science*, 35(7), 805-821.
- Jiang, Y., Matsusaka, S., Masuda, H., & Qian, Y. (2008). Characterizing the effect of substrate surface roughness on particle–wall interaction with the airflow method. *Powder Technology*, 186(3), 199-205.
- Kosinski, P., Hoffmann, A. C., & Klemens, R. (2005). Dust lifting behind shock waves: comparison of two modelling techniques. *Chemical Engineering Science*, 60(19), 5219-5230.
- Lai, A. C., & Nazaroff, W. W. (2000). Modeling indoor particle deposition from turbulent flow onto smooth surfaces. *Journal of Aerosol Science*, 31(4), 463-476.
- Murillo, C., Dufaud, O., Bardin-Monnier, N., López, O., Munoz, F., & Perrin, L. (2013). Dust explosions: CFD modeling as a tool to characterize the relevant parameters of the dust dispersion. *Chemical Engineering Science*, 104, 103-116.
- National Fire Protection Association. (2005). NFPA 654: Standard for the Prevention of Fire and Dust Explosions from the Manufacturing, Processing, and Handling of Combustible Particulate Solids. National Fire Protection Association, Quincy, MA
- Occupational Safety and Health Administration. (2005). Combustible Dust in Industry: Preventing and Mitigating the Effects of Fire and Explosion. Safety and Health Information Bulletin. OSHA, Washington, DC.
- Occupational Safety and Health Administration. (2016). Safety and health topics: Grain handling. OSHA, Washington D.C. Retrieved from <https://www.osha.gov/SLTC/grainhandling/>
- Rani, S. I., Aziz, B. A., & Gimbun, J. (2015). Analysis of dust distribution in silo during axial filling using computational fluid dynamics: Assessment on dust explosion likelihood. *Process Safety and Environmental Protection*, 96, 14-21.
- Sethi, V., & John, W. (1993). Particle impaction patterns from a circular jet. *Aerosol Science and Technology*, 18(1), 1-10.
- Steiner, G., Patel, M., & Carstensen, J. T. (1974). Effects of milling on granulation particle-size distribution. *Journal of Pharmaceutical Sciences*, 63(9), 1395-1398.
- Wells, A.C. and Chamberlain, A.C., (1967). Transport of small particles to vertical surfaces. *British Journal of Applied Physics*, 18(12), 1793.

Zhao, Y., & Ambrose, R. K. (2019). Modeling dust dispersion and suspension pattern under turbulence. *Journal of Loss Prevention in the Process Industries*, 62, 103934.

5. EFFECT OF SUSPENDED DUST CONCENTRATION ON THE LIGHT EXTINCTION COEFFICIENT

This chapter was published in *Journal of Loss Prevention in the Process Industries*, Yumeng Zhao and R.P. Kingsly Ambrose, A real-time method for sensing suspended dust concentration from the light extinction coefficient, 104242, Copyright Elsevier (2020)

Abstract

In the powder handling and processing industry, the location of dust emission can vary, with the suspended dust concentration assessment requiring the installation of immovable or wired equipment. For increased dust sensing, not limited by location within the facility, a portable suspended dust concentration measuring system is needed. The suspended dust concentration under daylight environment affects the light extinction coefficient. To develop a simple dust concentration measurement system, the relationship of suspended dust concentration and the light extinction coefficient is presented in this Chapter. Cornstarch, corn dust, and sawdust were used as test materials in this study. The light extinction coefficient was found to linearly correlate with the suspended dust concentration and the σ_e values depended on the dust properties. The mass extinction coefficients (K) was obtained for cornstarch, sawdust and corn dust, from known, suspended dust concentrations using image analysis. The mass extinction coefficient of the three sample materials tested in this study were in the range of 0.03 to 0.04. The light extinction coefficient can be used for the real-time measurement of suspended dust concentration in both open and confined spaces.

5.1 Introduction

Increasing production demands have exacerbated the health and safety risks to workers in particulate material processing and handling facilities. Over 70% of the dusts produced in the industry are explosive, and the suspended dust concentration is one of the most important factors that indicates the likelihood of to a major explosion (Abbasi and Abbasi, 2007). Suspended dust concentration, an indicator of explosion risk in industrial environments (Hinds, 2012; Zhao and Ambrose, 2019), is normally expressed as particle counts per unit volume or mass per unit of volume. However, the suspended dust concentration measurement to evaluate explosion risk, with

the minimum explosive concentration (MEC) that could be as low as 15 g/m³ (Laurent, 2011), is less developed.

To monitor the MEC within the industry, a highly mobile method with a large measurement area is required. In environmental science and occupational safety-related dust concerns, the well-developed gravimetric and light scattering methods are widely used for measuring airborne dust concentration. They form the basis of European and US standard methods for monitoring the outdoor concentration found in PM₁₀ and PM_{2.5} (Tasić et al., 2012). These methods are mostly used for respirable dust with a concentration of micro-grams per unit volume.

In order to prevent dust explosions, a method to measure the suspended grain dust in silos using the Lambert-Beer law is proposed by Hauert et al., (1996). But the probe that includes a laser and a photodiode must be calibrated before every use. Light scattering with a portable dust track aerosol monitor (Dacunto et al., 2015) or using an optical fiber method (Zhong and Li, 1988) are the other approaches used to measure MEC. However, the optical beam may be a potential ignition source for combustible dust. For example, a Nd-YAG laser can ignite the cornstarch cloud with 1.9W incident power on the suspended starch cloud (Proust, 2002). Other techniques use electrostatic interactions, including scanning mobility particle sizers such as the differential mobility analyzer. While electrostatic equipment can measure the number of aerosol particles per unit volume, these devices are generally very expensive and used more for testing particle-size distributions (Kousaka et al., 1985).

In the market today, nearly all methods for measuring dust concentration require the purchase and installation of new equipment in an industrial facility. However, suspended dust clouds are dynamic and move with air currents in the facility, and dust can be emitted from a variety of locations in a processing facility. So, there is a need for a portable and inexpensive dust concentration measurement method/probe.

Smoke and suspended dust particles can reduce visibility as the particles scatter and absorb light. The reduction in the intensity of light passing through a dust cloud is referred to as extinction. The effects of dust concentration on visibility through the atmosphere have been studied widely. Several empirical relationships between dust concentration and visibility have been proposed (Chepil and Woodruff, 1957; Patterson and Gillette, 1977; Chung et al., 2003; Wang et al., 2008; Baddock et al., 2014; Camino et al., 2015). These relationships are used widely in environmental science but have not been studied for use in industrial environments. Each empirical relationship

between visibility and dust concentration was developed for a different specific environment and type of dust. Therefore, to estimate the dust concentration from visibility in an indoor environment, new empirical relationships need to be developed. Atmospheric science generally classifies dust clouds by their cause, such as dust storms or fuel burning, so the materials making up the dust vary and are usually underspecified. However, industrial dust emissions are primarily from known products, so the components and size of dust will be consistent and known. Light will be affected predictably by such clouds of dust, which should make empirical relationships between dust concentration and light extinction relatively easy to establish. Changes in light intensity can be detected using the cameras' CCD/CMOS sensors to infer dust concentrations. This Chapter presents the relationship between dust concentration and extinction coefficient.

5.2 Theoretical Background

The extinction coefficient represents the rate of diminution of transmitted light via scattering and absorption for a medium. The particle concentration affects the extinction coefficient (σ_e) of the atmosphere (Ogle, 2016):

$$\sigma_e = \frac{\pi d_p^2 N q}{4} \quad 5.1$$

where d_p is the particle diameter, N is the number of particles per unit volume and q is the dimensionless extinction efficiency of a single particle. For the same dust sample, the aerosol particle-size distribution and q are considered constant at all mass concentrations.

Thus, mass concentration C can be calculated as follows:

$$C = \frac{2d_p \rho}{3q} \cdot \varepsilon \quad 5.2$$

where ρ is the particle density. To obtain the dust concentration, the value of the extinction coefficient ε is required, and to calculate this value a dimensionless mass extinction coefficient K (m^2/g) is introduced, where

$$\frac{1}{K} = \frac{2d_p \rho}{3q} \quad 5.3$$

As the particle diameter and chemical composition are constant for the same material in a dust cloud, so the dimensionless extinction efficiency and density are also considered as constant.

The extinction coefficient can be calculated based on atmospheric light scattering models which describe the observed light intensity of a target and a background, as that intensity is affected by the extinction coefficient at distance R (Graves and Newsam, 2011):

$$J_{0r} = J_0 e^{-\sigma_e R} + J_A (1 - e^{-\sigma_e R}) \quad 5.4$$

where, J_r is the observed target light intensity with R the distance from target to observed location, J_0 is the real target light intensity and J_A is the ambient light intensity.

The ambient light intensity highly depends on the environmental conditions; therefore the background reference J_g is introduced in order to calibrate the extinction coefficient:

$$\sigma_e = \frac{\ln\left(\frac{J_{0r} - J_{gr}}{J_0 - J_g}\right)}{R} \quad 5.5$$

where, J_{gr} is the observed background light intensity, J_g is the real background light intensity, and target and background reference are at distance R from the observed location.

The light intensity (J) can be obtained through a camera. J_0 and J_g are the intensities without particles between target and camera, and are affected by the ambient light conditions. However, obtaining the real-time J_0 and J_g when sensing the dust cloud concentration is impossible. Therefore, another target is required to calculate real-time σ_e . Using two targets with different distances from the observed location enable calculation of the σ_e without knowing J_0 and J_g value.

On the other hand, most cameras use a charge-coupled device (CCD) sensor, and there will be noise signals when sensing the light signal. Thus, a calibration to remove the noise signal is important before using the light intensity obtained from a CCD. J is linearly related to the intensity value obtained from a CCD sensor (G) (Healey and Kondepudy, 1994):

$$G = A(J + N_{DC} + N_S + N_R) \quad 5.6$$

where A is the amplifier to increase the signal power from a CCD sensor, N_{DC} is the dark current noise, N_S is the zero mean Poisson shot noise, and N_R is the readout noise. Noise is unstable in most cases and makes the result inconsistent, especially when a response intensity is less than the

noise. Then the intensity will not be accurate or even undetectable. The two-target method can also be used to overcome the noise effect.

The extinction coefficient calculated using the intensity value measured from two targets can be used to eliminate the effects of noise:

$$\sigma_e = \frac{\ln\left(\frac{G_{or1} - G_{gr1}}{G_{or2} - G_{gr2}}\right)}{R} \quad 5.7$$

where G_{or1} and G_{gr1} are the first target and its background intensity value calculated from the image by averaging the grey value of all pixels, respectively. G_{or2} and G_{gr2} are the second target and its background intensity value also calculated from the image, respectively. R is the distance between the two targets.

5.3 Materials and Methods

5.3.1 Experimental dust dispersion

A transparent $0.3 \times 0.3 \times 0.45$ m³ chamber, with two targets placed inside, was used for suspended dust concentration measurement tests. Cornstarch (Clabber Girl Corporation, IN, USA), sawdust (System Three Resins, Inc, WA, USA) and corn dust obtained from a local grain elevator were used in all experimental measurements. Dust samples of 0.5, 1.0, 1.5, 2.0, or 2.5 g were placed inside the chamber, in front of the nozzle, where the theoretical concentration corresponds to 17.5, 25, 42.5, 50, 67.5 g/m³ respectively, and then dispersed using 100 kPa compressed air from the bottom of the chamber. To test the measurement limit, cornstarch dust tests were conducted using up to 4 g of powder that corresponds to about 100 g/m³ concentration.

5.3.2 Measurement of the actual suspended dust concentration during dispersion

The actual suspended dust concentration during dispersion was measured using a 532-nm laser instrument (Besram Technology Inc, Wuhan, China). For these tests, the laser beam was placed in the center of the chamber and a photodiode was placed 0.225 m away, at the chamber wall. During dust dispersion, the photodiode voltage was measured every 0.5 s with a DM2 Compact Digital Multimeter (Wavetek, California, USA). According to Klippel et al. (2014), the change in laser intensity is exponentially related to the dispersed dust concentration. Therefore

prior to measurement, the laser system was calibrated by dispersing a known dust concentration in ethanol (Klippel et al., 2014). The change in intensity was recorded using the laser through a 30 and 60 g/m³ dust-ethanol suspension, and an exponential fit for the concentration and the change in intensity was obtained (Figure 5.1). Then, the dust cloud concentration in the chamber was calculated using this calibration curve, which is considered as the actual suspended dust concentration. The calibration measurements were replicated three times for each type of dust.

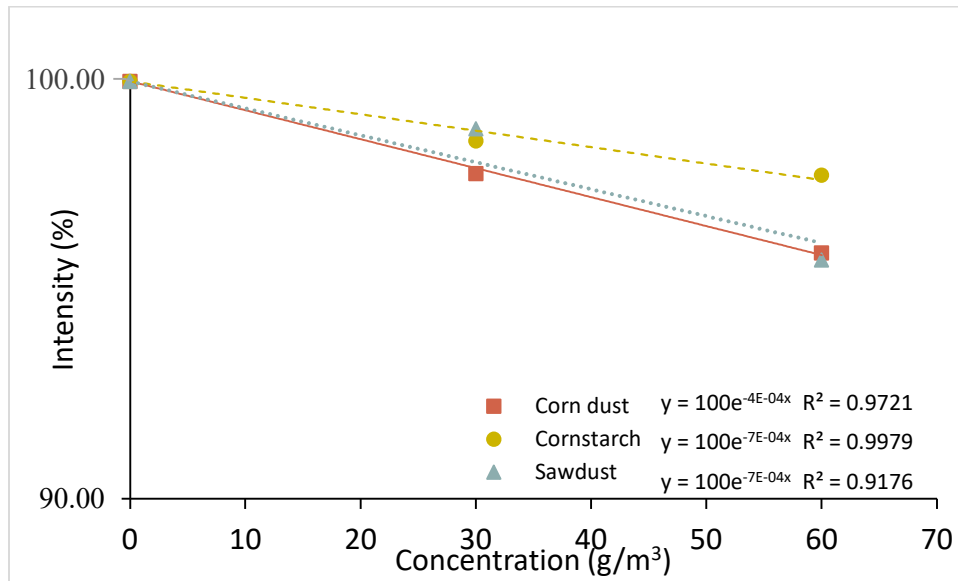


Figure 5.1 Calibration curve for measuring dust concentration using a laser. (▲ and dotted line represents sawdust, ● and dashed line represents cornstarch, and ■ and solid line represents corn dust)

5.3.3 Dust concentration measured using Two-target method

The suspended dust concentration in the chamber was analyzed using photos of two targets with black and white stripes (Figure 5.2).

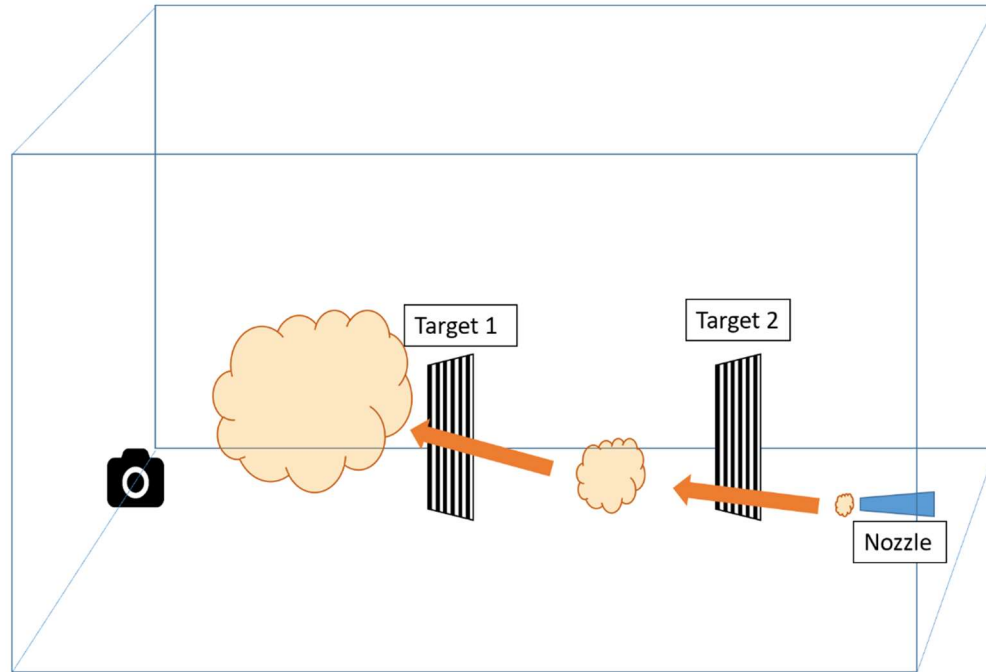


Figure 5.2 Schematic representation of measuring light extinction coefficient

An iPhone 7 (Apple Inc., USA) was placed inside the chamber to take a video of two targets during dust dispersion, with 1080p resolution at 60 fps. The distances between the lens and Target 1 and between Target 1 and Target 2 were both 0.22 m, respectively (Figure 5.2). Still, images were then extracted from the video, at every 0.1 s, using FFmpeg, an open-access video processing software. Custom-written scripts in Matlab 2015a (MathWorks, Inc., USA) were then used for image analysis. Each trial was repeated three times.

The targets in the experiment were paper printed with black and white strips, where the black strips are considered as the target and the white strips as the reference background. During image analysis, the two printed targets were first cropped from each photo, and then the black and white strips from the cropped target were separated using Otsu's method as implemented in Matlab. The separated black and white strips were then converted from RGB into HSV format using a built-in Matlab tool, and the intensity values of each pixel from black and white strips were obtained. The average intensity values of the black strips (B) and white background (G) were used to calculate the dust's extinction coefficient using Equation 5.7.

The extinction coefficient value was calculated for all the frames extracted from the video, at intervals of 0.1 s. The suspended dust concentration changes during dispersion, so the 0.5 s

interval peak extinction coefficients were averaged and considered as the extinction coefficient, ϵ . The peak concentration measured using the laser was considered as concentration (C) for calculation purposes. Using a linear relationship between σ_e and C, the mass extinction coefficient K was calculated (Equation 5.2).

5.3.4 Dust particle properties

The size and shape of the dust particles were measured with the Morphologi G3-ID instrument (Malvern Instruments, Malvern, UK) using a bottom light approach with light intensity set at 80. The light intensity calibration was performed automatically by the equipment. This analysis returns the circularity equivalent diameter (CE-diameter), and intensity values. The intensity value is the average greyscale of particle images obtained from microscope, ranging from 0 (black) to 255 (white). Since the Morphologi G3-ID uses a bottom-lit microscope, particle intensities are affected by light scattering and absorption, giving a qualitative indicator of the particles' extinction efficiency. Particle density was tested with an AccuPyc II 1340 Pycnometer (Micromeritics Instrument Corp., GA, USA).

5.3.5 Statistical analysis

For each trial, regression analyses on extinction coefficient values were conducted using the PROC REG function in SAS software (SAS Inc., NC, USA). The atmospheric air extinction coefficient is negligible at the short distance of 0.025 m with no suspended particulate matter (Hinds, 2012), so the intercept was set to 0 for the regression analysis.

5.4 Results and Discussion

5.4.1 Dust concentration and extinction coefficient during dispersion

Dust was dispersed fully within 3 s of introducing the compressed air. For dispersion of 2 g of dust, suspended dust concentrations measured using the laser and the extinction coefficient values are plotted in Figures 5.3 to 5.5. The peak concentration of suspended dust was observed around 0.5 to 1.5 s and then decreased as the particles settled. During the dust dispersion process,

particles are suspended by air movement, and only settle once they hit the chamber wall due to gravitational force and/or particle-wall interaction force. Regardless of the amount of dust dispersed in air, almost all suspended dust had settled after about 4 s, even through the air was continuously supplied during the experiments.

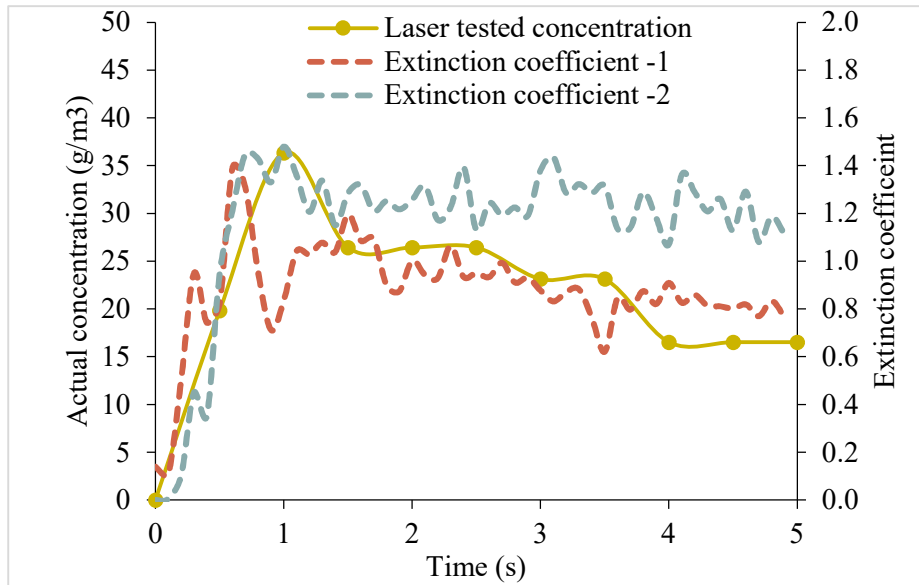


Figure 5.3 Extinction coefficient of cornstarch during dispersion. (Solid line is the actual, and dashed lines are the extinction coefficient of two replicate dispersion experiments)

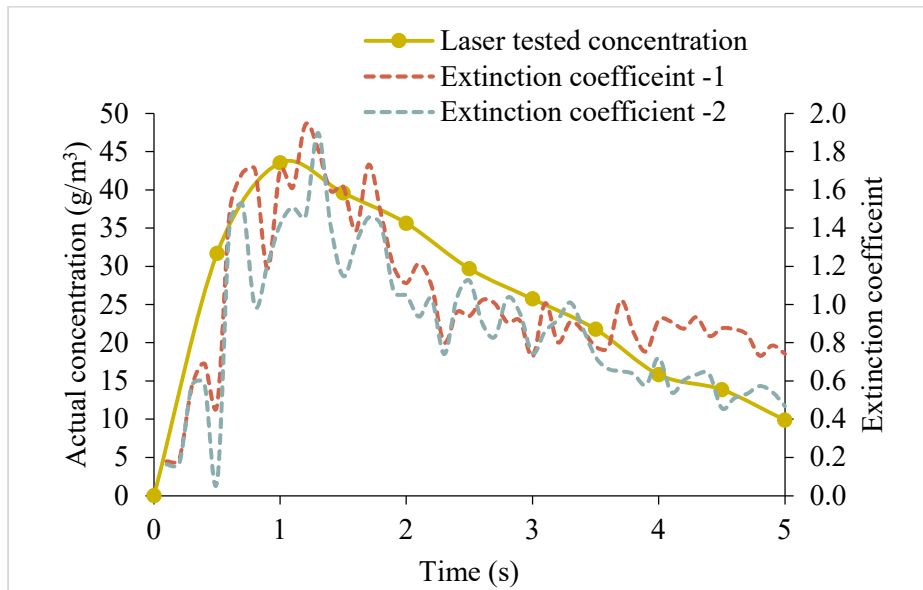


Figure 5.4 Extinction coefficient of sawdust during dispersion. (Solid line is the actual concentration, and dashed lines are the extinction coefficient of two replicate dispersion experiments)

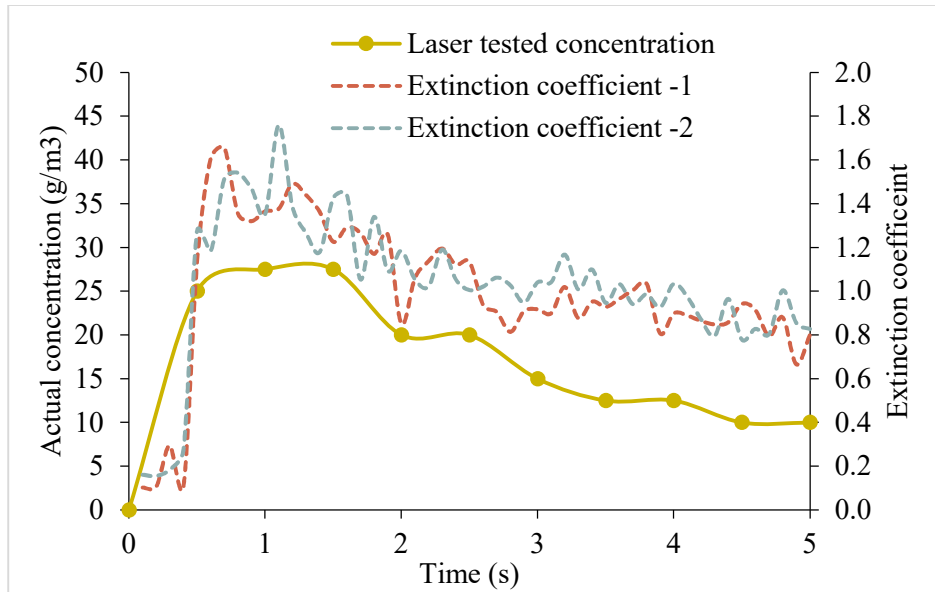


Figure 5.5 Extinction coefficient of corn dust during dispersion. (Solid line is the actual concentration, and dashed lines are the extinction coefficient of two replicate dispersion experiments)

The extinction coefficient values follow a similar trend as the dust concentration during dispersion. The peak concentration was reached around 0.5–1.5 s in both cases and then declined to suggest that the changing suspended dust concentration affects the extinction coefficient value (Figures 5.3 to 5.5). A small valley around 0.4 s, before the peak value, appears in all extinction coefficient measurements and indicates the heterogeneity of the dust cloud distribution at the beginning of dispersion. The pressurized airflow dispersed the dust from a single point near the nozzle, so most of the dust moves away from target 1 towards the camera at the beginning of the dispersion process (Figure 5.2). With the dust cloud movement, there was a moment that dust was concentrated between target 1 and the camera, while the concentration between the two targets was low. This is the moment where the valley was observed. Peak suspended dust concentration occurs once the dust is found uniformly spread throughout the chamber.

Because laser measurements were recorded at longer intervals of 0.5 s, no valley before the peak concentration was observed. Furthermore, since laser measurements only record information from the area that the laser beam passes through, the sampling size is small, and these measurements were highly dependent on location. The extinction coefficient shows fluctuation, which might be related to dust particle/cloud movement on the path of light between target and camera. The sawdust and corn dust extinction coefficients were reproducible. However, the

cornstarch suspension pattern was different after the peak suspended concentration, which can be explained by unstable and non-uniform dispersion of cornstarch agglomerates. Cornstarch tends to be more agglomerated than corn dust and sawdust and settled faster during dispersion. Thus, a steep decline after the peak value was observed during cornstarch dispersion.

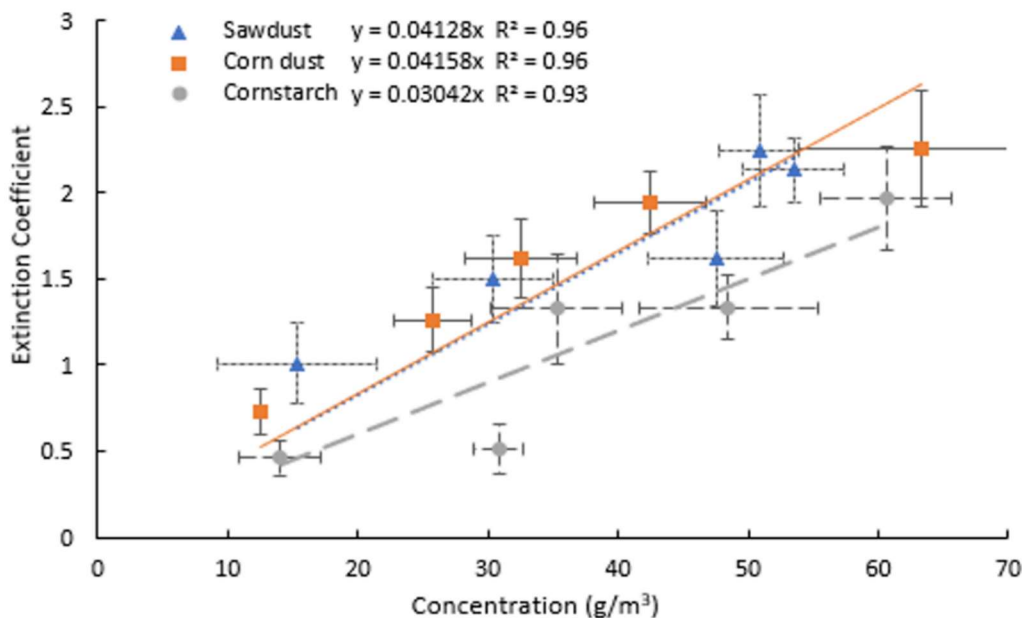


Figure 5.6 Extinction coefficient of dusts at different concentrations (▲ and dotted line represents sawdust, ● and dashed line represents cornstarch, and ■ and solid line represents corn dust)

5.4.2 Mass extinction coefficient

The mass extinction coefficient (K) clearly follows a linear relationship with dust concentration (Figure 5.6). The K value was obtained from the linear regression model between the extinction coefficient and concentration. The calculated K values for cornstarch, corn dust, and sawdust were 0.03042, 0.04158, and 0.04128 m²/g, respectively. The R² for sawdust and corn dust regression equations were 0.96, and R² for the cornstarch regression equation was 0.93.

The mass extinction coefficient of submicron urban/rural aerosol particles ranged from 1.1 to 9 m²/g (Lodge et al., 1981; Charlson et al., 1999; Myhre et al., 1998; Mallet et al., 2003). Pinnick et al. (1985) reported that the 9.5 μm sandy soil particles have a K value of 0.11 m²/g under infrared light. The results from Dillner et al., (2001) show that K values decrease with increasing particle

size, and that light wavelength has a smaller effect on K for larger particles. Due to particle size and particle property differences, the values we reported are much smaller than the published values for smaller particles.

To check the limit of the measurements, an additional trial was conducted with cornstarch particles suspended dust concentration of 100 g/m³ (Figure 5.7). The measured extinction coefficient value was higher than the expected value for this concentration, which could be due to the sensitivity limitations of the CCD/CMOS sensors in the imaging device. At a very low light intensity level, the CCD sensor noise is independent of the signal (Healey and Kondepudy, 1994). Therefore, when detecting the light intensity at 100 g/m³, the photocurrent signal could be weaker than the CCD sensor noise which could leads to this observed result.

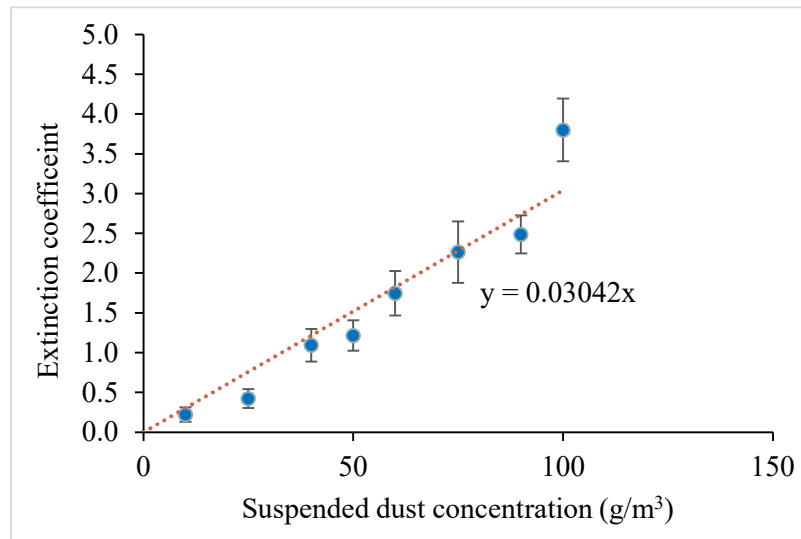


Figure 5.7 Extinction coefficient for cornstarch up to 100 g/m³ of suspended concentration

5.4.3 Dust particle properties and mass extinction coefficient (K)

Studies have shown that the mass extinction coefficient depends on particle properties such as particle size (Colangeli et al., 1995; Hand and Malm, 2007). Therefore, the effects of dust particle properties were evaluated for their effect on K values. The particle size, shape, and light intensity values of the dust particles tested by Morphologi G3-ID are shown in Table 5.1. CE-diameter and intensity values were different among the dust cloud types, with sawdust particles being smaller and more intense than those of corn dust and cornstarch.

Table 5.1 Dust particle properties

	CE Diameter (μm)	Intensity Mean	Density (kg/m^3)	K value (m^2/g)
Cornstarch	11.49 (13.07)	72.34 (37.24)	1491.8	0.03042
Sawdust	7.68 (6.24)	112.90 (17.77)	1491.9	0.04128
Corn dust	25.37 (23.02)	67.94 (10.96)	1484.8	0.04158

(Note: Values in parentheses are standard deviations.)

According to equation 5.3, the particle size, density, and dimensionless extinction efficiency affect the mass extinction coefficient. The dimensionless extinction efficiency of the particles is related to both light absorption efficiency and scattering efficiency (Hahn, 2009). Particle light absorption depends on their chemical composition, and the particles' scattering properties are related to size and refractive index (Hinds, 2012).

The intensity value of sawdust particles is 112.90, which is almost double that of corn dust when measured in the bottom light microscope. The higher intensity for sawdust over corn dust and cornstarch powder may be related to its brighter color, smaller size, more efficient light scattering ability, and lower light absorption. Thus, sawdust may have the lowest dimensionless extinction efficiency of the three samples. However, as mentioned above, sawdust also has the smallest particle size, which has a negative correlation with K (Equation 5.3). Therefore, because of the offsetting effects of small particle size and low dimensionless extinction efficiency, the sawdust K is similar to that of corn dust.

Conversely, when comparing cornstarch with corn dust, K value differences between these two powders could be due to size and density differences. Although cornstarch has a similar intensity value to corn dust, its particle size is smaller, and density is greater.

For the dust materials we tested, the K value were affected by particle size, dimensionless extinction efficiency, and density. Thus, for materials with consistent size, shape, and chemical components, the K value can be measured experimentally and used to back-calculate the concentration using the two-target sensing method. Therefore, the establishment of a K library for different dust materials is essential for application of this method.

5.5 Conclusions

The extinction coefficient is linearly related to the suspended dust concentration, and the mass extinction coefficient (K) is the key value that can be used to measure the suspended dust

concentration. Although the K value depends on the particle size, density and light absorption properties. A detailed relationship between mass extinction coefficient and particle properties is still a work in progress. For cornstarch, sawdust, and corn dust, the mass extinction coefficient ranged from 0.03-0.04. If the measured mass extinction coefficients are available for each material, the suspended dust concentration can be obtained from the light extinction properties. In order to use this method to measure the suspended dust concentration, a library of mass extinction coefficient values that cover a wide range of dust materials will be needed. The two-target method can be used with any imaging system thereby offering a low-cost and in-situ suspended dust concentration measurement technique with rapid response time.

5.6 References

- Abbasi, T., & Abbasi, S. A. (2007). Dust explosions—Cases, causes, consequences, and control. *Journal of Hazardous Materials*, 140(1-2), 7-44.
- Adachi, M., Okuyama, K., & Kousaka, Y. (1985). Electrostatic dispersion of aerosol particles carrying unipolar charge. *Journal of Chemical Engineering of Japan*, 18(6), 502-509.
- Baddock, M. C., Strong, C. L., Leys, J. F., Heidenreich, S. K., Tews, E. K., & McTainsh, G. H. (2014). A visibility and total suspended dust relationship. *Atmospheric Environment*, 89, 329-336
- Camino, C., Cuevas, E., Basart, S., Alonso-Pérez, S., Baldasano, J. M., Terradellas, E., & Berjón, A. (2015). An empirical equation to estimate mineral dust concentrations from visibility observations in Northern Africa. *Aeolian Research*, 16, 55-68.
- Charlson, R. J., Anderson, T. L., & Rodhe, H. (1999). Direct climate forcing by anthropogenic aerosols: Quantifying the link between atmospheric sulfate and radiation. *Beitrage zur Physik der Atmosphäre-Contributions to Atmospheric Physics*, 72(1), 79-94.
- Chepil, W. S., & Woodruff, N. P. (1957). Sedimentary characteristics of dust storms; Part II, Visibility and dust concentration. *American Journal of Science*, 255(2), 104-114.
- Chung, Y. S., Kim, H. S., Park, K. H., Jhun, J. G., & Chen, S. J. (2003). Atmospheric loadings, concentrations and visibility associated with sandstorms: Satellite and meteorological analysis. *Water, Air and Soil Pollution: Focus*, 3(2), 21-40.

- Colangeli, L., Mennella, V., Palumbo, P., Rotundi, A., & Bussoletti, E. (1995). Mass extinction coefficients of various submicron amorphous carbon grains: Tabulated values from 40 NM to 2 mm. *Astronomy and Astrophysics Supplement Series*, 113, 561.
- Dacunto, P. J., Klepeis, N. E., Cheng, K. C., Acevedo-Bolton, V., Jiang, R. T., Repace, J. L., & Hildemann, L. M. (2015). Determining PM 2.5 calibration curves for a low-cost particle monitor: common indoor residential aerosols. *Environmental Science: Processes & Impacts*, 17(11), 1959-1966.
- Dillner, A. M., Stein, C., Larson, S. M., & Hitzengerger, R. (2001). Measuring the mass extinction efficiency of elemental carbon in rural aerosol. *Aerosol Science & Technology*, 35(6), 1009-1021.
- Graves, N., Newsam, S., 2011. Using visibility cameras to estimate atmospheric light extinction. 2011 IEEE Workshop on Applications of Computer Vision (WACV), Kona, HI, 577–584.
- Hand, J. L., & Malm, W. C. (2007). Review of aerosol mass scattering efficiencies from ground-based measurements since 1990. *Journal of Geophysical Research: Atmospheres*, 112(D16).
- Hahn, D. W. (2009). Light scattering theory. Department of Mechanical and Aerospace Engineering, University of Florida.
- Hauert, F., Vogl, A., & Radandt, S. (1996). Dust cloud characterization and its influence on the pressure-time-history in silos. *Process Safety Progress*, 15(3), 178-184.
- Healey, G. E., & Kondepudy, R. (1994). Radiometric CCD camera calibration and noise estimation. *IEEE Transactions on Pattern Analysis and Machine Intelligence*, 16(3), 267-276.
- Hinds, W. C., (2012). Aerosol technology: properties, behavior, and measurement of airborne particles. Chapter 17. John Wiley & Sons, New York, NY. 379-385.
- Klippel, A., Schmidt, M., Muecke, O., & Krause, U. (2014). Dust concentration measurements during filling of a silo and CFD modeling of filling processes regarding exceeding the lower explosion limit. *Journal of Loss Prevention in the Process Industries*, 29, 122-137.
- Kousaka, Y., Okuyama, K., & Adachi, M. (1985). Determination of particle size distribution of ultra-fine aerosols using a differential mobility analyzer. *Aerosol Science and Technology*, 4(2), 209-225.

- Laurent, A., 2011. Sécurité des procédés chimiques. Connaissances et méthodes d'analyse des risques (2^o Éd.). Lavoisier. 267
- Lodge Jr, J. P., Waggoner, A. P., Klodt, D. T., & Crain, C. N. (1981). Non-health effects of airborne particulate matter. *Atmospheric Environment*, 15(4), 431-482.
- Mallet, M., Roger, J. C., Despiiau, S., Dubovik, O., & Putaud, J. P. (2003). Microphysical and optical properties of aerosol particles in urban zone during ESCOMPTE. *Atmospheric Research*, 69(1-2), 73-97.
- Myhre, G., Stordal, F., Restad, K., & Isaksen, I. S. (1998). Estimation of the direct radiative forcing due to sulfate and soot aerosols. *Tellus B*, 50(5), 463-477.
- Ogle, R. A. (2016). Dust explosion dynamics, Chapter 4. Radiative Properties of Dust Clouds. Butterworth-Heinemann, New York, NY, 169-173
- OSHA. (1997). Combustible Dust: Safety and Injury Prevention Awareness Training Program. OSHA, Washington D.C. Retrieved from https://www.osha.gov/sites/default/files/2018-12/fy08_sh-17797-08_cd_instructor_manual.pdf
- Patterson, E. M., & Gillette, D. A. (1977). Measurements of visibility vs mass-concentration for airborne soil particles. *Atmospheric Environment*, 11(2), 193-196.
- Pinnick, R. G., Fernandez, G., Hinds, B. D., Bruce, C. W., Schaefer, R. W., & Pendleton, J. D. (1985). Dust generated by vehicular traffic on unpaved roadways: Sizes and infrared extinction characteristics. *Aerosol Science and Technology*, 4(1), 99-121.
- Proust, C. Laser ignition of dust clouds. *Journal de Physique IV*, 2002, 12 (7), 79-88.
- Rusu-Zagar, G., Rusu-Zagar, C., Iorga, I., & Iorga, A. (2013). Air pollution particles PM10, PM2.5 and the tropospheric ozone effects on human health. *Procedia-Social and Behavioral Sciences*, 92, 826-831.
- Sun, X. B., Hong, J., & Qiao, Y. L. (2005). Investigation of measurements of polarized properties of atmospheric scattering radiation. *Chinese Journal of Quantum Electronics*, 22(1), 111-115.
- Tasić, V., Jovašević-Stojanović, M., Vardoulakis, S., Milošević, N., Kovačević, R., & Petrović, J. (2012). Comparative assessment of a real-time particle monitor against the reference gravimetric method for PM10 and PM2.5 in indoor air. *Atmospheric Environment*, 54, 358-364.

- Wang, Y. Q., Zhang, X. Y., Gong, S. L., Zhou, C. H., Hu, X. Q., Liu, H. L., & Yang, Y. Q. (2008). Surface observation of sand and dust storm in East Asia and its application in CUACE/Dust. *Atmospheric Chemistry and Physics*, 8(3), 545-553.
- Zhao, Y., & Ambrose, R. K. (2019). Modeling dust dispersion and suspension pattern under turbulence. *Journal of Loss Prevention in the Process Industries*, 62, 103934.
- Zhong, X. X. and Li, J. S., (1988). Optical fiber sensor for dust concentration measurement. *Proceedings SPIE 0838, Fiber Optic and Laser Sensors V*, San Diego, CA, 285-287.

6. SUMMARY OF CONCLUSIONS AND DISCUSSION

6.1 Restatement of Dissertation Goals

Suspended dust concentration during handling and processing of bulk solids is of great concern for both workers' health and explosion risk. Dust explosion can be prevented by controlling the suspended dust particles and accumulated dust layers on the floor. Owing to complex handling and processing conditions, the dust emission and deposition locations in industries can vary. As discussed in Section 1.1, the determination of dust dispersion and deposition parameters and the real-time measurement of suspended dust particle concentration are some of the challenges that must be solved to control the suspended dust particle concentration. This study aimed to develop a model to predict particle dispersion and deposition as well as study the light extinction properties of suspended dust to develop a real-time sensing method. The specific objectives of this study, as stated in Chapter 1, are as follows:

1. To develop a suspended particle–wall interaction model to predict the dust dispersion under turbulence;
2. Simulation of continuous dust dispersion with dust deposition using a discrete phase model;
3. To evaluate the change in light-extinction efficiency as influenced by suspended dust clouds.

This dissertation work addresses two main themes associated with dust dispersion and deposition: effect of turbulence on dust dispersion and disposition in an enclosed space, and the relationship between the suspended dust concentration and light extinction.

Section 6.2 describes the project overview, and Section 6.3 describes the CFD-DPM model of dust dispersion and deposition, along with the light extinction properties of suspended dust. In Section 6.4, the possible future work in this research area is presented.

6.2 Project Overview

The parameters of the dust explosion, the importance of studying dust dispersion and deposition for preventing dust explosion, and project objectives were discussed in Chapter 1. Chapter 2 provides an overview of the published studies and their results explaining the dust

explosion and dust dispersion mechanisms as well as the optical properties of dust particles. In addition, the five factors affecting a dust explosion, and the current preventive methods were discussed in detail. The available models to predict the dust dispersion were also explained. The review indicated that suspended dust concentration is an important factor to be considered in the prevention of dust explosion. Section 2.3 presents an overview of the light-extinction properties of dust, thus providing information on measuring the suspended dust concentration using optical properties. Chapter 3 elaborates on dust dispersion in an enclosed chamber and the development of the CFD-DPM model with a particle-wall sticky-rebound model. Furthermore, the experiments conducted to validate the simulation were described and the effect of turbulence and dispersion rate on the dust-dispersion pattern was discussed. In chapter 4, the continuous dispersion in an enclosed chamber as well as the effect of turbulence and particle size on dust deposition by using the developed CFD-DPM model was explained. In addition, chapter 4 describes the observations regarding suspended dust concentrations with different dispersion rates and the effect of particle size distribution on dust deposition.

Chapter 5 includes experimental observations on the relationships between suspended dust concentration and light-extinction. The relationship between suspended dust concentration with light extinction is compared with an existing laser method, and a good correlation was found between the two methods. Cornstarch, sawdust and corn dust were used to assess the correlation coefficient value of the proposed method of using light extinction to measure suspended dust concentration.

6.3 Discussion of Major Findings

A CFD-DPM with particle–wall interaction was developed to predict the dust dispersion and deposition. The effects of turbulence, dispersion rate, and particle-size distribution on dust dispersion and deposition were quantified. In addition, a method to measure the suspended dust concentrations was developed based on light extinction.

6.3.1 CFD-DPM model with particle–wall interaction to predict suspended dust concentration

Dust suspension and deposition patterns are important factors in the design of a dust-collection system and prevention of dust explosions. Despite the interaction between airflow and

particles, the particle–wall interaction plays an important role in dust dispersion and deposition. Thus, the particle–wall interaction model based on the particle–wall adhesion force was developed to predict dust dispersion. The simulation results showed that dust dispersed under high velocity formed a larger and more uniform dust cloud. Thus, high turbulence could result in more severe dust explosions owing to the faster spreading of the dust cloud. Regarding continuous dust dispersion, the dust concentration ultimately increases at a constant rate, irrespective of the dispersion rate.

The prediction error for dust concentration was especially low in the case of a dilute phase flow, with fewer interparticle interactions. However, in the prediction for high dust concentrations, the lack of particle-particle interaction apparently affects the accuracy of the proposed CFD-DPM. Another concern is the dispersion of cohesive powders, where the particle-particle interaction plays a major role in the deagglomeration process during dispersion. Accounting for particle-particle interaction is considered essential for providing an accurate prediction.

6.3.2 CFD-DPM with particle–wall interaction to predict continued dust dispersion and dust deposition

To prevent dust explosion, NPFA suggested that all surfaces, where dust might accumulate, must be designed and constructed in a way to minimize dust accumulations. The proposed model is used to predict dust deposition patterns with continuous dust dispersion. In addition, the turbulence and movement of the airflow and the particle-size distribution affect particle-deposition patterns. The mean size of the particle settled at the location close to the point of dust discharge is larger than that of the particle settled farther from the discharge point. A small particle with low gravitational force and inertia tends to change its direction of flow sharply along with the airflow. Therefore, special attention should be given to such small particles, because they are more likely to settle in a hidden area, for example, behind equipment.

6.3.3 Light extinction property of suspended dust

The measurement of the suspended concentration is important for preventing dust explosion and ensuring workers good health. A method of measuring the suspended dust concentration by testing the light-extinction coefficient of a dust cloud between two targets by using a digital camera was developed. A linear relationship was found between the extinction

coefficient and suspended dust concentration. For certain materials, the physical and chemical properties of the particles can be considered as constant, and thus, the mass extinction coefficient (the correlation coefficient value between the extinction coefficient and suspended-dust concentration) is considered as constant.

Costs for device installation and maintenance of the two-target image method of measuring the light-extinction coefficient are relatively low and the methods can measure the suspended dust in a much larger area than laser-based equipment.

6.4 Future Work

By using CFD-DPM, the particle dispersion and deposition pattern were studied in detail. In addition, a linear relationship between suspended dust concentration and light extinction coefficient was found. In this Section, two aspects of advance research that could help provide a greater understanding of the issues associated with predicting dust suspension and deposition and control the suspended dust concentration in the processing industry are presented.

6.4.1 Prediction of dust dispersion and deposition using CFD-DPM

To improve the prediction accuracy of particle deposition, accurate input of existing turbulent conditions is required. The airflow pattern is the main factor that affects particle movement. In particular, the movement of smaller particles is greatly affected by the airflow conditions. Therefore, comparison of the CFD models for their ability to predict dust dispersion is important.

Furthermore, deposition on vertical walls should be considered, and particle-wall interactions, such as static electricity forces, must be examined to obtain a better prediction of dust dispersion and deposition. Particle-particle interaction could be essential for predicting dust movement and deposition for cohesive powders or high concentration dispersion. When a monolayer is formed, the force of particle deposition will lead to interaction of dust particles with the particle layer instead of the wall material. The interaction force between materials depends on factors such as the chemical properties, surface roughness, and moisture content. Therefore, particle interaction with the wall boundary will change from particle-wall interaction to particle-particle interaction once the first layer of dust is settled.

6.4.2 Sensitivity analysis of particle properties used in the simulations

In this study, values from the literature and measured property values were used in simulations. A sensitivity analysis of property values is needed to improve the accuracy of the model. In this study, particle-wall interaction was modeled using Van der Waals force between particle and wall. However, other forces between particle and the wall that developed during contact, such as electrostatic force and solid bridge force, are not considered in this study. Furthermore, a contact model that includes plastic and elastic deformation of particles should be better able to predict the particle deposition. Experimental measurement of energy loss during particle and wall collision is difficult. Thus, sensitivity studies incorporating a rebound-stick model in DPM model are needed, in order to better understand the nature of particle-wall interaction for dust dispersion simulation.

6.4.3 Inclusion of particle properties in understanding light extinction coefficient of suspended dust

The chemical and physical properties of particles can change the light-extinction coefficient properties. Therefore, a detailed study of the relationships between light extinction and particle properties is required. For this, a standard method to obtain the mass extinction coefficient is essential. In addition, various ambient light conditions may affect the boundary (target) identification as well as the measured dust concentration. Thus, tests should be conducted at particulate material handling or processing facilities to validate the method at an industrial scale.

**APPENDIX A. SUSPENDED DUST CONCENTRATIONS AT 0.1S
INTERVALS FOR 0.5 S OF DISPERSION FOR VARIOUS
COMBINATION OF AIR VELOCITY AND DUST CONCENTRATION
(UNITS: g/m³)**

Time (s)	2 m/s-0.05kg/m ³	2 m/s-0.10 kg/m ³	10 m/s-0.05 kg/m ³	10 m/s-0.10 kg/m ³
0.1	0.007 ± 0.000	0.017 ± 0.005	0.007 ± 0.003	0.013 ± 0.011
0.2	0.006 ± 0.000	0.012 ± 0.011	0.012 ± 0.006	0.025 ± 0.007
0.3	0.007 ± 0.000	0.015 ± 0.014	0.019 ± 0.008	0.027 ± 0.007
0.4	0.011 ± 0.009	0.018 ± 0.016	0.017 ± 0.007	0.037 ± 0.011
0.5	0.013 ± 0.002	0.026 ± 0.012	0.025 ± 0.010	0.033 ± 0.005

* Values after ± are standard deviations from three replications. See section 3.2 for a description of the measurement procedure.

VITA

Yumeng Zhao was born in Zhengzhou, China. She earned her BS in Grain Science and Technology from Henan University of Technology, China in 2014. With a team of scientists at Henan University of Technology, she has applied for one patent on improving the flour quality. Yumeng Zhao earned her MS degree in Agricultural and Biological Engineering from Purdue University in 2016. She worked as a research assistant on grain milling. After MS, she started the PhD program on the dust explosion prevention at Purdue University from 2016. During her stay at Purdue University, Yumeng Zhao authored/co-authored eight peer-reviewed journal manuscripts, presented in six conferences, and has applied for one patent.